Journal of
Science & Technology in the Tropics Volume 3 Number 2 December 2007

JOSTT

DEDICATED TO THE ADVANCEMENT OF SCIENCE AND TECHNOLOGY RELATED TO THE TROPICS

Journal of Science & Technology in the Tropics

AKADEMI SAINS MALAYSIA

COSTAM

Volume 3 Number 2
December 2007
ISSN 1823-5034

Journal of Science & Technology in the Tropics Volume 3 Number 2 December 2007

CONTENTS

Table 1. Strains and plasmids used.

Strain or plasmid	Relevant characteristics	Reference or source
Escherichia coli		
JM109	recA1, endA1, gyrA96, thi, hsdR17, supE44, relA1,□ (lac-proAB)/F'[traD36, proAB+, lac I q, lacZ□M15]	Conserved in our lab
DH5α	F-,φ80d/lacZΔM15, Δ(lacZYA-argF) U169, deoR, recA1, endA1, hsdR17, phoA, supE44, λ-, thi-1, gyrA96, relA1	Conserved in our lab
BL21(DE3)	F-, ompT, gal (λcI 857, ind1, Sam7, nin5, lacUV5-T7gene1), dcm(DE3)	Conserved in our lab
Plasmids		
pHCV17	pUC19 containing the complete HCV genome	This laboratory
pMD18-T simple	A TA PCR cloning vector, Amp^r	TaKaRa Biotechnology (Dalian, China)
pET28a(+)	A six- histidine tag, a thrombin recognition site and a T7 tag at the N-terminus fusion expression vector	Conserved in our lab
pBV220	A PRPL promoter, Clts857 gene and two strong transcription terminators non-fusion expression vector	Conserved in our lab
pMDNS4E	pMD18-T simple containing HCV NS4 gene for subcloning into pET28a(+)	This study
pMDNS4B	pMD18-T simple containing HCV NS4 gene for subcloning into pBV220	This study
pETNS4	pET28a(+) containing HCV NS4 gene	This study
pBVNS4	pBV220 containing HCV NS4 gene	This study

Table 2. The primers used in this study.

External primers (5'-3')	
P1 TGGAAGTGTCTCATACGGCTG	
P2 CTAAAGTTCTGGACCGAGGT	
Internal primers (5'-3')	
E1 ATGCTAGC*ATG*AGCACTTGGGTGCTGGTAGG	For cloning into pET28a(+)
E2 CCAGAATTC*TTA*GCATGGCGTGGAGCAGT	
B1 AGAGGAATTC*ATG*AGCACTTGGGTGCTGGTAGG	For cloning into pBV220
B2 CCAGGATCC*TTA*GCATGGCGTGGAGCAGT	

DNA manipulation

Standard techniques for cloning and subcloning procedures, plasmid preparation, and agarose gel electrophoresis were used. Several HCV1b genomes were compared to obtain the conserved regions by using the ClustalW program (www.ebi.ac.uk). Primers based on the conserved regions from the 3' end of the NS3 region and the 5' end of the NS5 region of the representative strain were designed and synthesized. Nested-PCR was used to amplify the NS4 gene. The primers are listed in Table 2. All primers were synthesized by Shanghai Sangon (Shanghai, China).

PCR amplification was carried out in a final volume of 25 μL, containing 50 ng DNA, 1 μL of each primer (10μM), 12.5 μL 2×Taq PCR Master Mix (TIANGEN Biotech, China). The amplification conditions were the same for the outer and inner primers, as follows: an initial incubation at 94 °C for 10 min, followed by 5 cycles, each consisting of denaturing at 94 °C for 1 min, annealing at 42 °C for 1 min and extension at 72 °C for 1.5 min, followed by 25 cycles, each consisting of denaturing at 94 °C for 1

min, annealing at 58 °C for 1 min and extension at 72 °C for 1.5 min, a final step of extension at 72 °C for 10 min. After purification by gel electrophoresis and quantification, 50 ng of the primary product was used as the template for the second reaction. Amplification was examined by 1% agarose electrophoresis.

Cloning of the HCV NS4 gene in bacterial fusion and non-fusion expression vectors

The PCR product using E1 and E2 as internal primers was ligated into the pMD18-T simple vector, generating pMDNS4E. The target fragment that was digested with *Nhe*I and *EcoR*I from the pMDNS4E was inserted into pET28a (+), (digested by the same restriction enzymes), using T4 DNA ligase (TaKaRa Biotechnology, China) at 16°C over night. The PCR product using B1 and B2 as internal primers was cloned into the pMD18-T simple vector to obtain the recombinant plasmid of pMDNS4B. The *EcoR*I/ *Bam*HI fragment derived from the constructed TA clone pMDNS4B was then subcloned to the same restriction sites of pBV220 vector to form pBVNS4. *E. coli* BL21 (DE3) and *E. coli* DH5α competent cells were prepared by the calcium chloride method and were used for transformation of the pETNS4 and pBVNS4 plasmids, respectively. The transformed bacteria were selected by screening the colonies on media containing certain antibiotics: kanamycin for pETNS4 and ampicillin for pBVNS4. Potential positive colonies were further analyzed by restriction enzyme digestion, PCR and sequencing.

DNA sequencing and phylogenetic analysis

PCR products and the recombinant plasmids were sent to BGI Life Tech (Beijing, China) for sequencing (ABI3730). The results were compared with the NCBI database. Phylogenetic analysis was performed using the distant matrix method followed by neighbour joining to create an evolutionary dendrogram for illustration of genetic relatedness.

RESULTS

Primers designed from the conserved regions of HCV 1b were used to amplify the complete NS4 region from the plasmid pHCV17. A 968 bp PCR product was amplified using E1 and E2 primers. *Nhe*I and *EcoR*I restriction enzyme sites were introduced at the 5' end to facilitate cloning. These primers created a *Nhe*I site and start codon at the 5' end, and an *EcoR*I site and stop codon at the 3' end of the NS4 gene PCR product. After purifying the PCR products using a PCR Product Purification Kit (TaKaRa Biotechnology, China), the products were cloned into the pMD18-T vector. This recombinant plasmid was designated pMDNS4E and digested with *Nhe*I and *EcoR*I. The DNA fragment was then subcloned into pET28a (+) which had been previously digested with the same enzymes to generate pETNS4.

The DNA fragments containing the HCV NS4 coding sequence amplified using the B1 and B2 primers were inserted into the pMD18-T vector. Use of these primers resulted in an *EcoR*I site and start codon at the 5' end, and *Bam*HI site and stop codon at the 3' end of the PCR product This recombinant plasmid, designated pMDNSB, was digested with *EcoR*I and *Bam*HI, and then ligated into the pBV220 vector that had been previously digested with the same enzymes. This new recombinant non-fusion expression plasmid was designated pBVNS4.

The pETNS4 plasmid was introduced into *E.coli* BL21 (DE3). The pBVNS4 plasmid was introduced into E.coli DH5α. DNA sequence analysis indicated that the recombinant vectors had been constructed successfully (data not shown).

Maps of the two plasmids are shown in Figure 1.The results of restriction enzyme digestion and PCR identification are shown in Figures 2 and 3.

PCR products were sequenced directly. The results of sequencing were compared with NCBI database. The most similarity sequence was AY587016 (Hepatitis C virus polyprotein mRNA, partial cds.) giving 100% identity. A phylogenetic tree was constructed to estimate evolutionary relationships based on the NS4 sequence (Fig. 4).

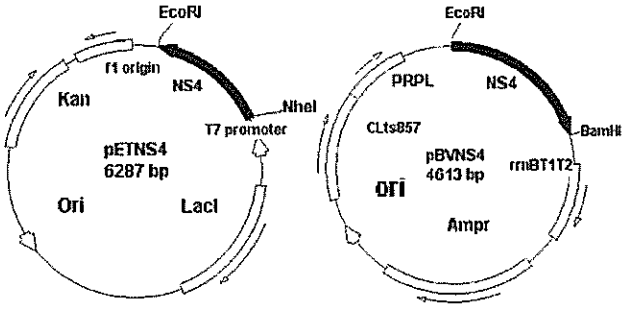

Figure 1. Construction of pETNS4 and pBVNS4.

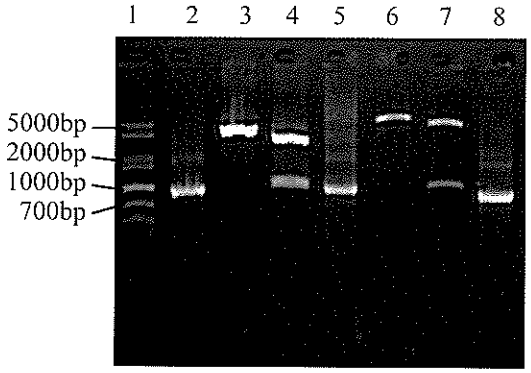

Figure 2. Restriction enzyme digestion and PCR analysis of recombinant plasmid pMDNS4E and pETNS4. Lane 1, 1 kb plus DNA marker; Lane 2, PCR product of pHCV17; Lane 3, pMDNS4E digested with *EcoR*I; Lane 4, pMDNS4E digested with *Nhe*I and *EcoR*I; Lane 5, PCR product of pMDNS4E; Lane 6, pETNS4 digested with *EcoR*I; Lane 7, pETNS4 digested with *Nhe*I and *EcoR*I; Lane 8, PCR product of pETNS4.

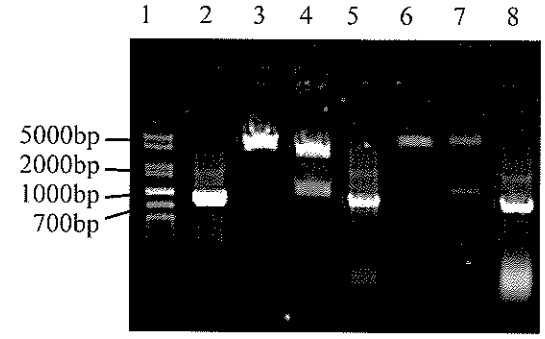

Figure 3. Restriction enzyme digestion and PCR analysis of recombinant plasmid pMDNS4B and pBVNS4. Lane 1, 1 kb plus DNA marker; Lane 2, PCR product of pHCV17; Lane 3, pMDNS4B digested with *EcoR*I; Lane 4, pMDNS4B digested with *EcoR*I and *Bam*HI; Lane 5, PCR product of pMDNS4B; Lane 6, pBVNS4 digested with *EcoR*I; Lane 7, pBVNS4 digested with *EcoR*I and *Bam*HI; Lane 8, PCR product of pBVNS4.

DISCUSSION

Hepatitis C was discovered in 1989. It is now thought to be the most common of the hepatitis viruses. About 3% of the world population is infected with this pathogen resulting in a large variety of clinical symptoms [12]. About 25% of hepatitis C cases develop chronic hepatitis, which may lead to cirrhosis and liver cancer [13]. Based on sequence heterogeneity, the HCV genome was classified into six major genotypes [14]: 1-6, four of these (genotype 1-4) containing distinct subtypes (a, b, c) [15]. In China, the main genotypes are HCV 1b and 2a. Immunological studies have shown that the most important epitopes lie within the putative core protein and in the non-structural protein 3 (NS3) and 4 (NS4) [16, 17]. The HCV NS4 protein, which is the focus of the present study, contains two strong antigenic regions. One region, which was originally designated region 5-1-1 [18], comprises the C-terminal part of NS4a and the N-terminal part of NS4b [19]. The other region, designated region 59, is located at the C-terminus of the NS4b protein [20, 21]. The NS4 protein has been used as an antigenic target in various commercial diagnostic tests for the detection of HCV antibodies in the serum of patients with HCV infection. A recombinant C-100-3 protein containing the 5-1-1 immunodominant region has major diagnostic relevance [22]. There is evidence suggesting the possibility of using NS4 as a viral replication marker [23, 24]. The correlation between the activity of anti-NS4 antibodies and the responses to interferon treatment [25, 26] suggests that detection of NS4 is useful in the evaluation of the effectiveness of antihepatitis C immunotherapy. Availability of the complete NS4 protein could provide clues for

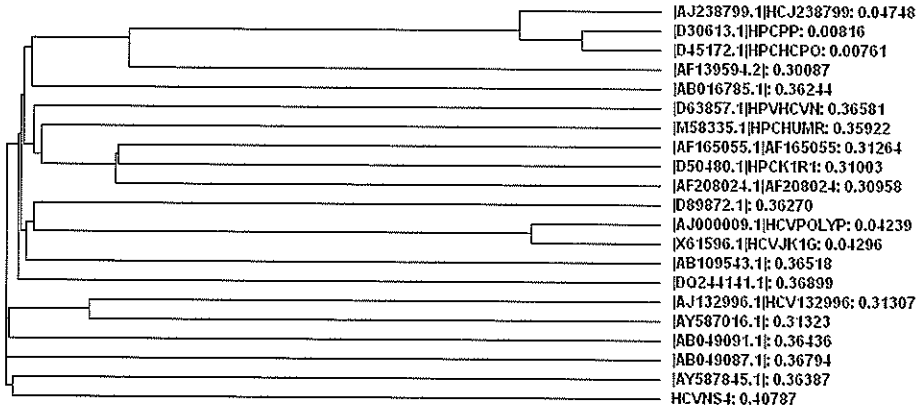

Figure 4. Phylogenetic tree based on the NS4 sequence.

developing an HCV DNA vaccine.

By using bacterial expression systems, target proteins can be easily modified and their expression can be controlled. The focus of this study was to insert the DNA sequence that encodes HCV NS4 into fusion and non-fusion vectors that will allow large amounts of expression and easy purification of the recombinant protein. Bacterial expression will facilitate future studies aimed at determining the efficacy of the NS4 protein as a vaccine and for studying its role in the immunology of the disease.

Acknowledgements – We are thankful to Dr. William Ruyechan (University at Buffalo, SUNY) for critically reviewing the manuscript.

REFERENCES

1. Choo Q.L., Kuo G. and Weiner A.J. (1989) Isolation of a cDNA clone derived from a blood-borne non-A, non-B viral hepatitis genome. *Science* **244**: 359–362.
2. Choo Q.L., Richman K.H. and Han J.H. (1991) Genetic organization and diversity of the hepatitis C virus. *Proc. Natl. Acad. Sci. USA* **88**: 2451-2455.
3. Kato N., Hijikata M. and Ootsuyama Y. (1990) Molecular cloning of the human hepatitis C virus genome from Japanese patients with non-A, non-B hepatitis. *Proc. Natl. Acad. Sci. USA* **87**: 9524-9528.
4. Takamizawa A., Mori C. and Fuke I. (1991) Structure and organization of the hepatitis C virus genome isolated from human carriers. *J. Virol.* **65**: 1105-1113.
5. Clarke B. (1997) Molecular virology of Hepatitis C virus. *J. Gen. Virol.* **78**: 2397-2410.
6. Miller R.H and Purcell R.H. (1990) Hepatitis C virus shares amino acid sequence similarity with pestiviruses and flaviviruses as well as members of two plant virus subgroups. *Proc. Natl. Acad. Sci. USA* **87**: 2059-2061.
7. Bartenschlager R. and Lohmann V. (2000) Replication of hepatitis C virus. *J. Gen. Virol.* **81**: 1631-1648.
8. Lin C., Pragai B.M. and Grakoui A. (1994) Hepatitis C virus NS3 serine proteinase: trans-cleavage requirements andprocessing kinetics. *J. Virol.* **68**: 8147-8157.
9. Wolk B., Sansonno D. and Krausslich H.G. (2000) Subcellular localization, stability, and trans-cleavage competenceof the hepatitis C virus NS3-NS4A complex expressed in tetracycline-regulated cell lines. *J. Virol.* **74**: 2293-2304.
10. Hijikata M., Mizushima H. and Tanji Y. (1993) Proteolytic processing and membrane association of putative nonstructural proteins of hepatitis C virus. *Proc. Natl. Acad. Sci. USA* **90**:10773-10777.
11. Egger D., Wolk B.and Gosert R. (2002) Expression of hepatitis C virus proteins induces distinct membrane alterations including a candidate viral replication complex. *J. Virol.* **76**: 5974-5984.
12. Cohen J. (1999) The scientific challenge of hepatitis C. *Science* **285**: 26–30.
13. Shimotohno K. (2000) Hepatitis C virus and its pathogenesis. *Semin. Cancer Biol.* **10**: 233-240.
14. Tomei L., Vitale R.L. and Incitti I. (2000) Biochemical characterization of a hepatitis C virus RNA-dependent RNA polymerase mutant lacking the C-terminal hydrophobic sequence. *J. Gen. Virol.* **81**: 759-767.
15. Simmonds P., Holmes E.C. and Cha T.A. (1993) Classification of hepatitis C virus into six major genotypes and a series of subtypes by phylogenetic analysis of the NS-5 region. *J. Gen. Virol.* **74**: 2391-2399.
16. Chien D.Y., Choo O.L. and Tabrizi A. (1992) Diagnosis of hepatitis C virus (HCV) infection using an immunodominant chimeric polyprotein to capture circulating antibodies: Reevaluation of the role of HCV in liver disease. *Proc. Natl. Acad. Sci. USA* **89**: 10011-10015.
17. Muraiso K., Hijikata M. and Ohkoshi S. (1990) A structural protein of hepatitis C virus expressed in E. coli facilitates accurate detection of hepatitis C virus. *Biochem. Biophys. Res. Commun.* **172**: 511-516.
18. Kuo G.., Choo Q.L. and Alter H.J. (1989) An assay for circulating antibodies to a major etiologic virus of human non-A, non-B hepatitis. *Science* **244**: 362-364.
19. Grakoui A., Wychowski C. and Lin C. (1993) Expression and identification of hepatitis C virus polyprotein cleavage products. *J. Virol.* **67**: 1385-1395.
20. Khudyakov Y.E., Khudyakova N.S. and Jue D.L. (1995) Linear B-cell epitopes of the NS3-NS4-NS5 proteins of the hepatitis C virus as modeled with synthetic peptides. *Virology* **206**: 666-672.
21. Wienhues U., Ihlenfeldt H.G. and Seidel C. (1998) Characterization of a linear epitope in the

nonstructural region 4 of hepatitis C virus with reactivity to seroconversion antibodies. *Virology* **245**: 281-288.

22. McOmish F., Chan S.W. and Dow B.C. (1993) Detection of three types of hepatitis C virus in blood donors: investigation of type-specific differences in serologic reactivity and rate of alanine aminotransferase abnormalities. *Transfusion* **33**(1): 7–13.
23. Sansonno D., Dammacco F. (1993) Hepatitis C virus c100 antigen in liver tissue from patients with acute and chronic infection. *Hepatology* **18**: 240-145.
24. Seidl S., Koenig B. and Reinhardt G. (1998) Higher detection rate of hepatitis G and C virus RNA in liver tissue than in serum of deceased injection drug users. *Int. J. legal Med.* **112**: 35-38.
25. Gonzalez-Peralta R.P., Fang J.W. and Davis G.L. (1995) Significance of hepatic expression of hepatitis C viral antigens in chronic hepatitis C. *Dig. Dis. Sci.* **40**(12): 2595-601.
26. Sakugawa H., Nakasone H. and Nakayoshi T. (1998) Relation between reactivity to the NS-4 region peptides of hepatitis C virus (HCV) and clinical features among patients infected with HCV genotype 1b. *Microbiol. Immunol.* **42**(4): 299-303.

Journal of Science and Technology in the Tropics (2007) **3**: 75-80

Colour genes of the ornamental guppies of Singapore

Gideon Khoo[1], Lim Tit Meng[2] and Violet P. E. Phang[2]
[1]Faculty of Engineering & Science, Universiti Tunku Abdul Rahman,
Setapak, 53300 Kuala Lumpur, Malaysia
[2]Department of Biological Sciences, National University of Singapore,
Kent Ridge, Singapore 117543
(Email: gideonkhoo@mail.utar.edu.my)

Received 28.09.2007; accepted 17.10.2007

Abstract Since the early 1950s, Singapore is internationally known as the guppy-breeding centre. At least 40 different colour varieties of guppies are cultured in Singapore, with each farm specialising in 10 to 15 varieties. These fancy varieties have been developed by skilful farmers through intensive and continual selective breeding. Genes controlling background body pigmentation such as albino (*a*), blond (*b*), gold (*g*) and blue (*r*) are autosomally inherited and recessive to their wild-type alleles which produce drab olive-brown background coloration. Colour patterns which are superimposed onto wild-type background coloration are due to genes located on the sex chromosomes. These sex-linked colour genes are dominant and sex-limited to males as their expression requires male hormones. Y-linked colour pattern genes are inherited only along the paternal line while X-linked genes are present in both sexes. Among the guppy varieties produced locally, only two Y-linked genes, *Ssb* and *Sst*, that control snakeskin tail and body patterns, respectively, have been found in varieties with snakeskin-like reticulations. Single colour genes that are both X- and Y-linked produce red (*Rdt*), blue (*Blt*), green (*Grt*), black (*Bt*) and variegated (*Var*) patterns on the caudal fin. The black caudal-peduncle of the Tuxedo variety is the result of *Bcp*, a gene that is both X- and Y-linked. Different combinations of colour pattern genes and background pigmentation genes as well as interactions among them give rise to various colour phenotypes. For instance, the inclusion of the *Bcp* gene in Snakeskin varieties causes black reticulations on the tail fin to be replaced by large, coarse black spots. The Neon variety, characterised by a metallic turquoise tail and black caudal-peduncle, is postulated to be produced through interactions between four colour pattern genes, i.e., *Ln* (light turquoise blue), *Blt* (navy blue tail), *Rdt* (red tail) and *Bcp* (black caudal-peduncle).

Keywords guppy – colour genes – sex-linked – autosomal – inheritance

INTRODUCTION

The guppy, *Poecilia reticulata*, collected from Venezuela, was first described and named by the German ichthyologist Wilhelm Peters in 1859. The species name means net-like or reticulate in Latin. Two years later, the Spanish zoologist, De Filippi, obtained some fishes from Barbados which he considered a new genus and species, and named them *Lebistes poeciloides*. In 1866, Robert J. Lachmere Guppy, who resided in Trinidad, sent some fishes to ichthyologist Albert Günther who named it as a new species, *Girardinus guppii*. Other synonyms have been given, e.g., *Poeciloides reticulatus* Jordan and Gilbert, 1883; *Heterandia guppii* Jordan, 1886; *Acanthophacelus reticulatus* Eigenmann, 1907; *Acanthophacelus guppii* Eigenmann, 1910; *Girardinus poeciloides* Boulenger, 1912; *Poecilia poeciloides* Langer 1913; *Lebistes reticulatus* Regan, 1913; and *Glaridichthys reticulata* Milewski, 1920 [1]. However, Rosen and Bailey [2] showed that the correct name for this species is *P. reticulata*. The common name guppy, named after R. J. Lachmere Guppy, was used from 1909 onwards because the German aquarist, J. P. Arnold, imported the fish from the British Museum under the name *Girardinus guppii*.

DISTRIBUTION AND HABITAT

The guppy is an inhabitant of fresh and brackish waters of tropical regions. Its native habitat includes Venezuela, Trinidad, Antilles, Windward and Leeward Islands, Barbados, Grenada, Antigua, Guyana as well as Central America [1]. They inhabit almost all waters – shallow ditches, canals, streams, lakes, rivers, pools and ponds. However, due to many man-made introductions, the guppy can now be found in tropical waters all over the world. It was introduced to Singapore, Malaysia and other parts of South-East Asia as a biological control agent of mosquitoes [3].

THE GUPPY AS AN ORNAMENTAL FISH

Since its discovery, the multi-coloured patterns on the body, tail and fins of male guppies have attracted the interests of fish hobbyists. It is commonly known as 'millions fish' or 'rainbow fish'. The guppy first appeared in Germany as an aquarium fish in 1905 [4]. Fish hobbyists and breeders in Europe, Britain and U.S.A. subsequently began to improve the guppy by selective breeding. The emphasis is towards larger finnage, intense and uniformly distributed colours, and new colour patterns or combinations particularly on the caudal fin. The ultimate goal is to establish homozygous strains of fixed colour phenotypes.

It was not until the late 1940s that the guppy was introduced to aquarists in Singapore. Commercial culture of the guppy in Singapore started in the early 1950s with some farmers switching from growing vegetables and fruits to the more lucrative culture of ornamental and freshwater fishes. Since then, ornamental fish culture and export have developed into a multi-million dollar business, and is now one of the primary industries in Singapore.

Many species of aquarium fishes are cultured locally, and Singapore has earned world renown as a guppy breeding centre. The wide range of brilliant

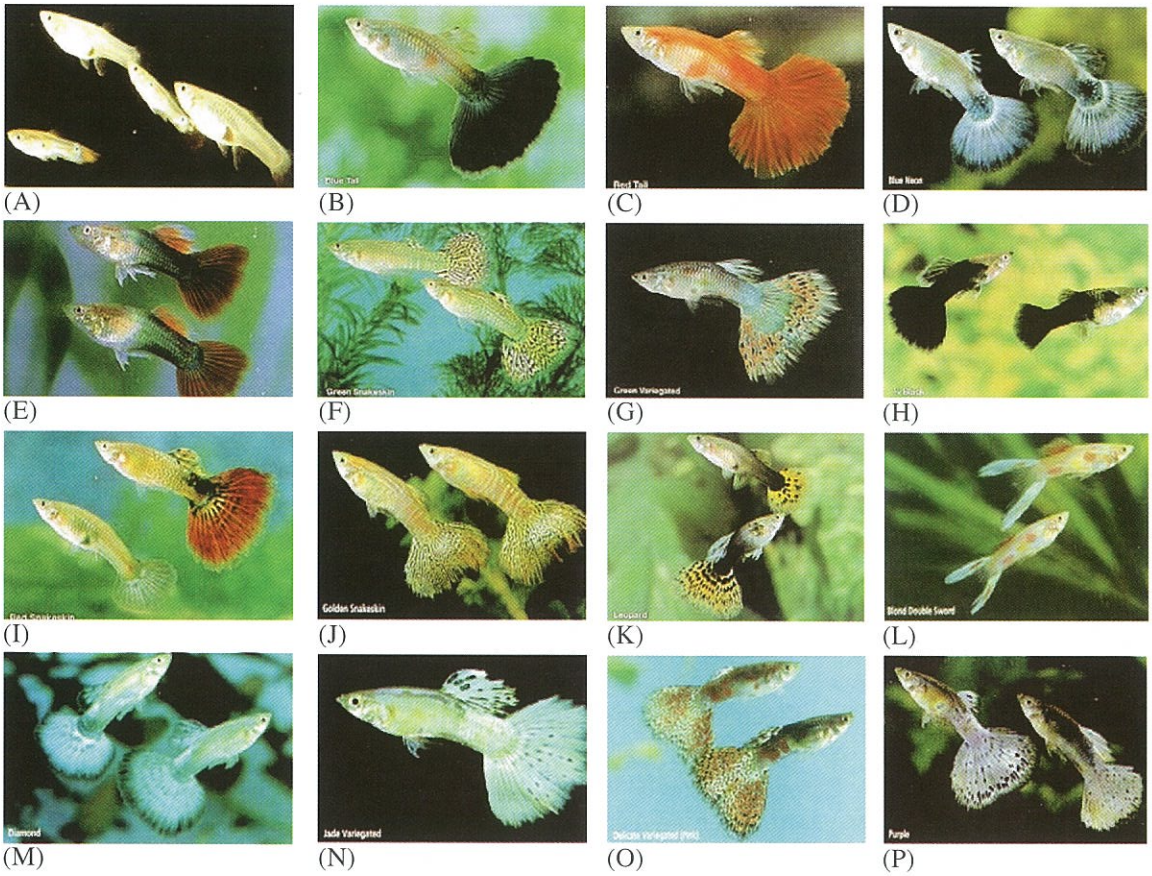

Figure 1. (A) Male and female wild-type guppies. Commercially cultured guppy varieties: (B) Blue Tail, (C) Red Tail, (D) Blue Neon, (E) Tuxedo, (F) Green Snakeskin, (G) Green Variegated, (H) 3/4 Black, (I) Red Snakeskin, (J) Golden Snakeskin with vertical bars on the caudal-peduncle, (K) Leopard, (L) Double Sword, (M) Diamond, (N) Jade Variegated, (O) Delicate Variegated, and (P) Purple.

and beautiful colours on the body, tail and dorsal fins of present day guppy varieties contribute to its popularity as an ornamental fish. The guppy is one of the most economically important ornamental fish species, accounting for about 30% of total ornamental fish exports from Singapore to international markets.

About 40-50 domesticated varieties of the guppy are produced by monoculture farms in Singapore. Each farm specialises in 10-15 varieties [5]. Guppy farmers strive continuously to improve the quality of the fish and to develop new strains with novel finnage and colour patterns (Fig. 1).

GENETIC CONTROL OF COLOUR PATTERNS

The guppy exhibits marked sexual dimorphism. Males possess bright colourful spots and patterns while females are uniformly olive-brown (Fig. 1A). An unusual characteristic of guppy genetics is that most of the genes responsible for colour patterns are dominant and sex-linked, i.e., present on both the X- and Y-chromosomes [6, 7]. Also, crossing-over of these colour genes could take place between the X- and Y-chromosomes [8]. Conversely, gene loci affecting background body coloration, e.g., albino (a), blond (b), gold (g) and blue (r) are recessive and autosomal [9, 10].

Gene control and inheritance of colour phenotypes in some established varieties were elucidated by performing single-pair reciprocal crosses between selected varieties and wild-type stock, and also between different varieties. Three- to four-week old fry of different varieties were sourced from farms in Singapore. Wild-type (WT) guppies were obtained from a stock maintained for several years in the Department of Biological Sciences, National University of Singapore. This wild-type stock was originally collected from an isolated hill-stream near the Bukit Timah nature reserve [11]. Six- to eight-week old mature virgin males and females were used for all crossing experiments. Single pairs were kept in 3.5-litre breeding tanks. Broods were produced 4-6 weeks after mating and reared in 8-litre grow-out tanks. F2 offspring were obtained from single-pair matings between full-sibling F1 fish. F1 and F2 progenies were segregated and scored according to their phenotypes and sex.

SOLID TAIL COLOURS

The Red Tail (RT) and Blue Tail (BT) phenotypes are two of the most common guppy strains. Blue Tail males are characterised by a navy blue tail while females have very weak expression of the tail colour (Fig. 1B). Red Tail males have an orange-red tail but females have faint red tails with tinges of opaque white towards the dorsal part of the tail (Fig. 1C). Androgen treatment of BT and RT females intensified their respective tail colours, indicating the presence of tail colour genes. Wild-type guppies have hyaline fins with males displaying highly polymorphic coloured spots and patches on the body and tail (Fig. 1A). Gene control of the tail colour of these two varieties was determined by carrying out the following reciprocal crosses: BT × WT, RT × WT and BT × RT [12].

Segregated colour phenotypes of F1 and F2 progenies showed that the blue tail colour was due to a single dominant X-linked gene (*Blt*). Similarly, a dominant X-linked gene (*Rdt*) is responsible for the red tail colour. However the *Rdt* gene could also be found on the Y-chromosome of some male guppy stocks [11]. Hence, the genotypes of BT and RT males are $X_{Blt}Y$ and $X_{Rdt}Y$, respectively, and those of homozygous BT and RT females are $X_{Blt}X_{Blt}$ and $X_{Rdt}X_{Rdt}$, respectively.

Reciprocal crosses between BT and RT varieties were conducted to test for allelism between the X-linked *Blt* and *Rdt* genes. The results showed that the two tail colour genes were allelic. Another possibility is that *Blt* and *Rdt* are closely linked. In the event of crossing-over of *Blt* and *Rdt* from the X-chromosome to the Y-chromosome, these two genes may be carried by male guppies on the Y-chromosome.

The blond Blue Tail and blond Red Tail varieties are similar to the corresponding BT and RT phenotypes except they possess overall pale yellow background body coloration and less intense tail colours. This is because they are homozygous for the recessive autosomal blond gene *(b)* which causes the melanophores on the scales and skin to be reduced from corolla or dendritic shapes to small punctuate ones [9, 13]. The genotypes of blond BT and RT males are $bbX_{Blt}Y$ and $bbX_{Rdt}Y$, respectively, while those of homozygous females are $bbX_{Blt}X_{Blt}$ and $bbX_{Rdt}X_{Rdt}$, respectively.

Other dominant X-linked tail colour genes are

the green tail gene (*Grt*) of the Green Snakeskin variety (Fig. 1F), the black tail gene (*Bt*) in the three-quarter black strain (Fig. 1H), and the green neon tail gene (*Gn*) of the Green Neon variety. *Blt* and *Grt* are not allelic and the distance between them is about 19.4 map units [14].

THE BLACK CAUDAL-PEDUNCLE

In the Tuxedo variety, males have a black caudal-peduncle and red tail (Fig. 1E), while females have slightly less intense black caudal-peduncle and hyaline tail with pinkish-white tinges. Their background body coloration is olive-brown due to the autosomal dominant *B* gene. Studies on the inheritance of this colour phenotype were carried out using reciprocal crosses between the Tuxedo variety and WT [11]. The red tail is determined by *Rdt* and the black caudal-peduncle by *Bcp*, both of which are X-linked dominant genes. The genotypes of Tuxedo males and females are $X_{Bcp,Rdt}Y$ and $X_{Bcp,Rdt}X_{Bcp,Rdt}$, respectively.

Tuxedo stocks of some farms, however, carry the *Bcp* and *Rdt* genes on both the X- and Y-chromosomes. The genotype of such males is therefore $X_{Bcp,Rdt}Y_{Bcp,Rdt}$. Reciprocal crosses also showed strong evidence that *Bcp* and *Rdt* are tightly linked, and are only 2.4 map units apart [11, 15]. This raises the possibility that the two genes are inherited as a single unit.

Blond Tuxedo guppies have identical sex-linked colour genes as Tuxedo but they are homozygous for blond *(b)*, the recessive allele of *B*. Interaction between the autosomal *b* and sex-linked *Bcp* and *Rdt* dilutes the intensities of the black caudal-peduncle and red tail.

SNAKESKIN BODY AND TAIL PATTERNS

Male Green Snakeskin (GSS) guppies have iridescent, snakeskin-like reticulations on the body and greenish-yellow tail with black snakeskin reticulations (Fig. 1F). GSS females have olive-brown wild-type coloration with grey and green tinges on the tail. Females do not manifest snakeskin patterns even after androgen treatment. Results from reciprocal crosses between GSS and WT showed that the snakeskin body and tail patterns of GSS males are determined by two dominant Y-linked genes, *Ssb* and *Sst*, respectively. *Ssb* and *Sst* are so tightly linked that their recombination frequency was reportedly only about 1% [13]. The greenish-yellow tail colour is mediated by the dominant X-linked *Grt* gene. The corresponding wild-type allele, Grt^+, produces a hyaline tail. The colour phenotype of male GSS is due to the presence of the X-linked *Grt* and Y-linked *Ssb* and *Sst* ($BBX_{Grt}Y_{Ssb,Sst}$), while GSS females carry only *Grt* ($BBX_{Grt}X_{Grt}$).

The Y-linked *Ssb* and *Sst* genes are present in the Red Snakeskin (RSS) (Fig. 1I), and Blue Snakeskin (BSS) varieties [16]. *Sst* is expressed as black reticulations on the red tail (*Rdt*) of the RSS but is masked by the navy blue tail (*Blt*) of the BSS. Genotypes of RSS and BSS males are $X_{Rdt}Y_{Ssb,Sst}$ and $X_{Blt}Y_{Ssb,Sst}$, respectively. RSS and BSS females possess the $X_{Rdt}X_{Rdt}$ and $X_{Blt}X_{Blt}$ genotypes, respectively, which are identical to RT and BT females. The corresponding Blond Red Snakeskin and Blond Blue Snakeskin varieties are homozygous for the blond gene (*bb*).

The Yellow (YSS) and Golden Snakeskin varieties are characterised by blond coloration and silvery snakeskin patterns on the body and tail (Fig. 1J). Reciprocal crosses between YSS and GSS gave identical results [13]. Among the F1 offspring, all males had GSS phenotype while the females had the green tail phenotype without snakeskin patterns on the body and tail. F2 males showed the typical Mendelian monohybrid segregation ratio of 3 GSS males : 1 YSS male. F2 females also conformed to the 3 Green Tail : 1 blond tail ratio. Thus, the YSS differs from GSS by having *bb* instead of BB genotype.

VARIEGATED TAIL PATTERNS

Variegated patterning on the caudal fin is currently a popular trait in many domesticated guppy strains (Fig. 1G, 1N-P). Gene control of this highly variable mosaic pattern of black spots and patches of different sizes on a brightly coloured tail fin was elucidated by reciprocal crosses between the Green Variegated (GV) strain and WT stock [17]. F1 and F2 offspring data showed that variegated tail patterning is due to a single locus, *Var*, on the X- and Y-chromosomes. The *Var* allele is dominant over the wild-type Var^+ which does not express these patterns. *Var* appears to be located very close to the *Ssb* and *Sst* genes [13, 15-17]. Genotypes of males and females of the GV strain are proposed to be $X_{Var}Y_{Var}$ and $X_{Var}X_{Var}$, respectively.

GENE INTERACTIONS

Sex-linked colour pattern genes that interact with autosomal background pigmentation genes give rise to additional colour phenotypes. For example, inclusion of the *Bcp* gene in Snakeskin varieties causes fine black reticulations on the tail fin to be replaced by large, coarse black spots (compare Fig. 1F, 1J with Fig. 1K). Neon and metallic-coloured variants (Fig. 1D, 1M, 1N, 1P), characterised by a metallic sheen on their tail and caudal-peduncle, are postulated to be produced by a complex interaction of four colour genes, namely, *Ln* (light turquoise blue), *Blt, Rdt* and *Bcp*.

About 90% of Yellow and Golden Snakeskin males have the typical snakeskin pattern on their bodies and tails. The remaining males are different in that the snakeskin body pattern has been modified into 4 or 5 vertical bars on the caudal-peduncle region (compare Fig. 1F with Fig. 1J). F1 and F2 results of single-pair reciprocal crosses of the YSS strain show that a single autosomal recessive gene, *bar*, is responsible for the vertical bar pattern [18]. In the homozygous condition, *bar/bar*, this gene interacts with the Y-linked *Ssb* gene to give vertical barring patterns on the caudal-peduncle of YSS males. This pattern is not expressed when the dominant allele, bar^{+}, is present [18].

CONCLUSION

The guppy is unique among teleosts in that genes coding for colour patterns are all dominant sex-linked and sex-limited, with males developing colour patterns after sexual maturity. Genes responsible for background body coloration are autosomal with all known mutant genes recessive to the wild-type olive-brown pigmentation. The brilliant coloration of domesticated farm-bred male guppies is due to the combined effects of major sex-linked genes, autosomal background colour genes and interacting genetic factors with colour-enhancing effects.

REFERENCES

1. Wischnath L. (1993) *Atlas of Livebearers of the World.* T.F.H. Publications Inc., USA.
2. Rosen D.E. and Bailey R.M. (1963) The poeciliid fishes (Cypriniodontiformes), their structure, zoogeography and systematics. *Bull. Amer. Mus. Nat. Hist.* **126:** 1-176.
3. Herre A.W.C.T. (1940) Additions to the fish fauna of Malaya and notes on rare or little known Malayan and Bornean fishes. *Bull. Raffles Mus.* **16:** 27-61.
4. Wichand B. (1906) Neuimportierte bezw. erstmalig nachgezuchtete Zahnkarpfen (Poeciliidae). *Bl. f. Aq. u. Terr. Kunde, Jahrg.* **17:** 495-496.
5. Fernando A.A. and Phang V.P.E. (1985) Culture of the guppy, *Poecilia reticulata,* in Singapore. *Aquaculture* **51:** 49-63.
6. Winge Ö. (1922) One-sided masculine and sex-linked inheritance in *Lebistes reticulatus. J. Genet.* **12:** 145-162.
7. Winge Ö. (1927) The location of eighteen genes in *Lebistes reticulatus. J. Genet.* **18:** 1-43.
8. Winge Ö. (1923) Crossing-over between the X- and the Y-chromosome in *Lebistes. J. Genet.* **13:** 201-219.
9. Goodrich H.B., Josephson N.D., Trinkaus J.P. and Slate J.M. (1944) The cellular expression and genetics of two new genes in *Lebistes reticulatus. Genetics* **29:** 584-592.
10. Kirpichnikov V.S. (1981) *Genetic Bases of Fish Selection.* Translated by G.G. Gause. Springer-Verlag, Germany.
11. Khoo G., Lim T.M., Chan W.K. and Phang V.P.E. (1999) Sex-linkage of the black caudal-peduncle and red tail genes in the Tuxedo strain of the guppy, *Poecilia reticulata. Zool. Sci.* **16:** 629-638.
12. Fernando A.A. and Phang V.P.E. (1990) Inheritance of red and blue caudal fin colorations in two domesticated varieties of the guppy, *Poecilia reticulata. J. Aqua. Trop.* **5:** 209-217.
13. Phang V.P.E., Ng L.N. and Fernando A.A. (1989) Inheritance of the snakeskin colour pattern in the guppy, *Poecilia reticulata. J. Hered.* **80:** 393-399.
14. Phang V.P.E. and Fernando A.A. (1991) Linkage analysis of the X-linked green tail and blue tail colour genes in the guppy, *Poecilia reticulata. Zool. Sci.* **8:** 975-981.
15. Khoo G., Lim T.M., Chan W.K. and Phang V.P.E. (1999) Linkage analysis and mapping of three sex-linked colour pattern genes in the guppy, *Poecilia reticulata. Zool. Sci.* **16:** 893-903.
16. Phang V.P.E., Fernando A.A. and Chia E.W.K. (1990) Inheritance of the colour patterns of the blue snakeskin and red snakeskin varieties of the guppy, *Poecilia reticulata. Zool. Sci.* **7:** 419-425.
17. Khoo G., Lim T.M., Chan W.K. and Phang V.P.E. (1999) Genetic basis of the variegated tail pattern

JOURNAL OF SCIENCE AND TECHNOLOGY IN THE TROPICS

NOTICE TO CONTRIBUTORS

JOSTT is a multi-disciplinary journal. It publishes original research articles and reviews on all aspects of science and technology relating to the tropics. All manuscripts are reviewed by at least two referees, and the editorial decision is based on their evaluations.

Manuscripts are considered on the understanding that their contents have not been previously published, and they are not being considered for publication elsewhere. The authors are presumed to have obtained approval from the responsible authorities, and agreement from all parties involved, for the work to be published.

Submission of a manuscript to JOSTT carries with it the assignment of rights to publish the work. Upon publication, the Publishers (COSTAM and ASM) retain the copyright of the paper.

Manuscript preparation

Manuscript must be in English, normally not exceeding 3500 words. Type double spaced, using MS Word, on one side only of A4 size with at least 2.5 cm marigins all round. Number the pages consecutively and arrange the items in the following order: title page, abstract, key words, text, acknowledgements, references, tables, figure legends.

Title page

Include (i) title, (ii) names, affiliations and addresses of all authors, (iii) running title not exceeding five words, and (iv) email of corresponding author.

Abstract and key words

The abstract, not more than 250 words, should be concise and informative of the contents and conclusions of the work. A list of not more than five key words must immediately follow the abstract.

Text

Original research articles should be organized as follows: Introduction, Materials and Methods, Results, Discussion, Acknowledgement, References. The International System of Units (SI) should be used. Scientific names and mathematical parameters should be in italics.

References

References should be cited in the text as numbers enclosed with square [] brackets. The use of names in the text is discouraged. In the references section, the following examples should be followed:

1 Yong H.S., Dhaliwal S.S. and teh K.L (1989) A female Norway rat, *Rattus norvegicus*, with XO sex chromosome constitution. *Naturwissenschaften* **76:** 387-388.

2 Beveridge W.I.B. (1961) *The Art of Scientific Investigation*. Mercury Book, London.

3 Berryman A.A. (1987) The theory and classification of outbreaks. In Barbosa P. and Schultz J.C. (eds.) *Insect outbreaks* pp. 3-30. Academic Press, San Diego.

Tables

Tables should be typed on separate sheets with short, informative captions, double spacing, numbered consecutively with Arabic numerals, and do not contain any vertical lines. A table should be set up to fit into the text area of at most the entire page of the Journal.

Illustrations

Black-and-white figures (line drawings, graphs and photographs) must be suitable for high-quality reproduction. They must be no bigger than the printed page, kept to a minimum, and numbered consecutively with Arabic numerals. Legends to figures must be typed on a separate sheet. Colour illustrations can only be included at the author's expense.

Proofs and reprints

Authors will receive proofs of their papers before publication. Ten reprints of each paper will be provided free of charge.

Submission

Manuscripts should be submitted in triplicate (including all figures but not original artwork), together with a floppy diskette version of the text, to:

The Managing Editor
Journal of Science and Technology in the Tropics
C-3A-10, 4th Floor Block C, Lift No: 5
No. 1 Jalan SS20/27
47400 Petaling Jaya
Selangor Darul Ehsan
Malaysia

in the guppy, *Poecilia reticulata. Zool. Sci.* **16:** 431-437.

18. Phang V.P.E., Khoo G. and Ang S.P. (1999) Interaction between the autosomal recessive bar gene and the Y-linked snakeskin body (Ssb) pattern gene in the guppy, *Poecilia reticulata. Zool. Sci.* **16:** 905-908.

Journal of Science and Technology in the Tropics (2007) **3**: 81-95

Resveratrol miracle: Prevention against a wide spectrum of diseases

Arpad Tosaki[1], Samarjit Das[1,2] and Dipak K. Das[2]
[1]Department of Pharmacology, Faculty of Pharmacy, School of Medicine, Health Science Center, University of Debrecen, Debrecen, Hungary
[2]Cardiovascular Research Center, University of Connecticut School of Medicine, Farmington, Connecticut, USA
(Email: DDAS@NEURON.UCHC.EDU)

Received 27.03.2007; accepted 18.06.2007

Abstract The concept that wine consumption has beneficial effects on the function of various cells and organs is not a new idea. Wine consumption is a part of human culture for thousands of years. Observations regarding the beneficial effects of wine, especially red wine, intake were followed by formal and general scientific approaches and studies. One of the major components, as a biological active structure, of red wine is resveratrol. Beside red wine, resveratrol can be found in different fruits and plants over the world. Many mechanisms have been proposed for the beneficial effects of resveratrol in various disorders including ischemia/reperfusion, preconditioning, inflammation, diabetes, cancer, aging, and ulcer. The present review focuses on the role and beneficial effects of resveratrol in various disorders, and emphasizing its potential as an important and effective therapeutic tool in alternative medicine.

Keywords resveratrol – history – pharmacological effects in various disorders

INTRODUCTION

Oxidative stress caused by free radicals plays a crucial role in the pathophysiology associated with atherosclerosis, neoplasia and neurodegenerative diseases. Therefore, extensive attention is focusing on the naturally occurring antioxidative phytochemicals. One of the most recognized as well as hopeful of these compounds is resveratrol, a member of a family of polyphenols called viniferins. A mild-to-moderate wine drinking habit attenuates cardiovascular, cerebrovascular and peripheral vascular risk due to reduced platelet and monocyte adhesion, and attenuates the risk of prostate as well as a variety of cancers including pancreatic, gastric and thyroid cancer. Among approximately 500 different antioxidants, recent studies revealed that resveratrol and proanthocyanidins are the two most important polyphenolic antioxidants present in wine that attenuate various health problems. Resveratrol, a polyphenol phytoalexin, possesses diverse biochemical and physiological properties including estrogenic, antiplatelet and anti-inflammatory actions. Several recent studies revealed that resveratrol mediated protections from a wide variety of degenerative diseases. The most important point about resveratrol is that at a lower concentration, it inhibits apoptotic cell death, thereby providing protection from various diseases including myocardial ischemia/reperfusion-induced injury, atherosclerosis and ventricular arrhythmias. Both in acute and chronic models, resveratrol-mediated cardioprotection is achieved through the preconditioning effect (the state-of-the-art technique of cardioprotection), rather than direct effect as found in conventional medicine. Resveratrol used in higher doses, facilitates apoptotic cell death, behaving in contrast as a chemo-preventive agent. Resveratrol likely fulfills the definition of a pharmacological preconditioning compound and gives hope for its therapeutic application in alternative medicine. The purpose of this review is to provide evidence in favour of resveratrol to be used as a preventive medicine for the maintenance of health.

CHEMISTRY

Resveratrol, also known as 3,4',5-trihydroxystilbene and 3,4',5-stilbenetriol, has a molecular formula,

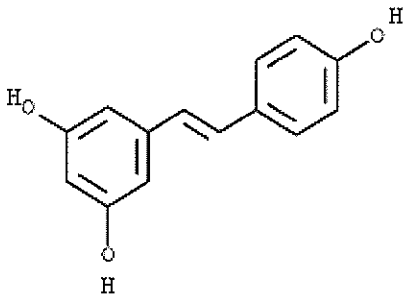

Figure 1. Structure of resveratrol.

$C_{14}H_{12}O_3$, and its molecular weight is 228.25 Daltons (Fig. 1). Resveratrol exists in *cis* and *trans* isomeric forms. Although, both *cis*- and *trans*-resveratrol (with their glucosides) occur naturally and seem to exert similar biological effects, the actions of the trans-isoform are more widely investigated and better known. Resveratrol-3-O-beta-D-glucoside is called piceid.

OCCURRENCE

Resveratrol is biosynthesized from one molecule of *p*-coumaroyl CoA and three molecules of malonyl CoA by the stilbene synthase (STS) in certain higher order plants, such as eucalyptus, spruce, lily, mulberries and peanuts [1]. External stimuli such as fungal attack and UV-radiation activate the stilbene synthase genes in grapes to produce resveratrol in order to adequately protect grapes from those stimuli [2]. This STS gene is also found in peanut root, strawberry, blueberry, mulberry, grapes, etc and other plants like eucalyptus, spruce, and lily. *Vitis vinifera*, labrusca, and muscadine types of grapes contain high concentrations of resveratrol. Skins and seeds of these types of grapes contain 50–100 μg/g of resveratrol [3]. These varieties of grapes are particularly suitable for making red wine. Thus, grapes and red wines are considered as the major sources of resveratrol. In addition to grapes, a large variety of fruits including mulberry, bilberry, lingo berry, sparkle-berry, deer berry, partridgeberry, cranberry, blueberry, jackfruit, peanut, and a wide variety of flowers and leaves including gnetum, white hellebore, corn lily, butterfly orchid tree, eucalyptus, spruce, poaceae, Scots pine, rheum and *Polygonum cuspidatum* (Japanese knotweed) [4] also contain resveratrol. In contrast to the constitutive isoform of stilbene synthase occurring in the *Rheum rhaponticum* (rhubarb), an inducible enzyme is expressed in the Vitaceae family [1, 5]. Resveratrol is a naturally occurring phytoalexin ("defender of the plant") that is produced in response to injury, such as mechanical trauma, ultraviolet light and infection by pathogenic microorganisms, especially fungi, providing means for defense [6-10]. Since fungal infections are more common in cooler climates, grapes grown in cooler climates have a higher concentration [11, 12]. However, grapes cultured in the zone of equator also contain resveratrol in high concentration, because of higher ultraviolet irradiation [12].

During the wine making process, resveratrol as well as other polyphenols, including quercetin, catechins, gallocatechins, procyanidins and prodelphidins (condensed tannins) are primarily extracted from grape skins. Red wines of different origin contain about 0–15 μg/mL *trans*-resveratrol, while the level of *cis*-resveratrol ranges between 0–5 μg/mL. Furthermore, red wines contain *trans*- or *cis*-piceid at 0–30 μg/mL or 0–15 μg/mL, respectively [12].

HISTORICAL BACKGROUND

Wine is a part of the human culture for thousands of years. Civilizations in the Middle East started to cultivate *Vitis vinifera* almost seven thousand years ago, around 5000 BC. *Vitis vinifera* occidentalis, said to be the forebear of most of our red varieties originates from the Nile Delta. The tomb of Tutankhamen contained murals that depict the art of winemaking in great detail. The wine was made in a way similar to our modern methods [13]. In another civilization, "Darakchasava" was used dating back to 4500 years. This Indian herbal preparation is mainly a grape-vine preparation, the major ingredient is *Vitis vinifera* L. (dried grape berries) [14]. Recently, HPLC analysis of this age old formulation has revealed the presence of polyphenols like resveratrol and pterostilbene. This "ayurvedic" medicine was prescribed as a cardiotonic agent and also given for other disorders as these phenolic compounds are now known as antioxidants, cancer chemopreventive agents, and also known to reduce mortality from coronary heart disease by increasing high density lipoprotein-cholesterol and inhibiting platelet aggregation [15].

Traditional Japanese and Chinese medicine also exploited the beneficial use of resveratrol as it is also found in significant amounts in the dried roots and stems of the plant *Polygonum cuspidatum*. The dried root and stem of this plant is used in traditional

Chinese and Japanese medicines as a circulatory tonic.

Wine production and consumption were significantly increased as civilizations became more refined. In the 8th century BC, Homer in The Iliad described what wine did to his heroes and villains. Coming along ages yet another ancient Greek, the father of medicine, Hippocrates mentioned wine in almost all his recorded memoirs dating back to 460 BC. He recommended it for cooling fevers, convalescence and even as a diuretic. Moreover, he made distinctions between the different varieties: soft dark wines were to benefit the bowel, and harsh white wine was used to expel excess fluids. Hippocrates, more than two thousand years ago, was correct in attributing wine with healing properties. He could not have had any idea which components of wine make it so beneficial to health, but nevertheless his observation and trial, left him with the idea that red wine is beneficial in several diseases. Grapes and wines are also mentioned many times in the Bible, and are still an important part of Christian and Jewish ritual. In the early days, wine was used not only as a beverage, but also as a healing liquid; it was used to disinfect wounds and, mixed with myrrh, acted as a painkiller. Another example for the early presence of wine is provided in the book of Genesis that mentions that Noah planted a vineyard after the animals disembarked from the Ark.

EPIDEMIOLOGIC OBSERVATIONS

There are several lines of epidemiologic data suggesting beneficial effects of resveratrol. There are some circumscribed areas around the globe where the average age of people is remarkably high and there is an unusual presence of centenarians. These areas are either wine-drinking areas (like the Burgundy and Toulouse regions of France, furthermore the Northern region of the isle of Sardinia) or other regions (such as the Southern Island of Okinawa), where people consume some foods that contain resveratrol in high concentrations [16].

It is well-known the French paradox, a phenomenon first noted by Irish physician Samuel Black in 1819. Back in the nineteenth century, he was the first to observe the fact that people in France suffer relatively low incidence of coronary heart disease, despite their diet being rich in saturated fats. It was proposed that France's profound red wine consumption is a primary factor contributing to the protective effect. The first scientific evidence, however, for the cardiovascular benefits of red wine was put forward by Renaud and associates in 1992 [17]. In this study, popularly known as 'French Paradox', the researchers found that there had been a low mortality rate from, and incidence of, coronary heart disease among the French men aged above 40 years compared to men in the UK and USA, despite their high consumption of saturated fats and the prevalence of other risk factors such as smoking. This was attributed to their so-called 'Mediterranean diet', which includes a moderate intake of wine. It has been proposed that one of the active ingredients potentially related to this effect in red wine is resveratrol [18, 19].

WINE OR ALCOHOL?

The original observations concerning beneficial effects of red wine intake were followed by formal and general scientific studies. The relationship between alcohol consumption and atherosclerosis was first published in the Journal of the American Medical Association in 1904 by Cabot [20]. On the basis of epidemiological data, Pearl reported in 1926 [21] that moderate drinkers exhibited greater longevity than abstainers or heavy drinkers. Then, a robust relationship between moderate ethanol consumption and lower risk of cardiovascular diseases was established, thought to be associated with increased level of high-density lipoprotein cholesterol (HDL-C) and a decrease in the level of inflammatory mediators [22]. The question was raised whether components other than ethanol or alcohol itself can be primarily responsible for the advantageous effects of red wine. Gronbaek *et al.* [23] corroborated the protective effect of alcohol, but observed that wine intake had a beneficial effect on all-cause mortality being additive to that of alcohol. This effect was attributable to a reduction in death from both coronary heart disease and cancer. On the other hand, some data may tinge the picture, e.g., significantly increased risk of rectal cancer was found in response to alcohol intake in a Danish population [24]. However, the risk appeared to be reduced when alcohol was consumed as wine [24]. Most recently, Baur and co-workers [25] have shown that resveratrol significantly improves health and survival of mice on high-calorie diet. Thus, several evidences indicate that improving general health of mammals using small molecules is an attainable goal,

and may contribute to powerful therapeutic strategies for age-related disorders [26, 27].

PRECONDITIONING EFFECTS

Preconditioning (PC) was initially reported by Murry *et al.* in 1986 with brief period of ischemia which caused cardioprotection against heart injury [28]. Since then, thousands of experiments have been sought the exact mechanisms of PC. Furthermore, investigators tried to mimic the protective effects of PC by exogenous agents, and thereby to produce pharmacological PC. Resveratrol also has a cardioprotective effect related to its antioxidant activity. Therefore, Bradamante *et al.* [29] have investigated how resveratrol affects high-energy phosphate metabolism (using ^{31}P-nuclear magnetic resonance) and contractility of isolated Langendorff perfused rat hearts subjected to 20 min no-flow ischemia and 30 min reperfusion. During 10 min resveratrol infusion (10 μM) before ischemia, basal phosphorylation potential dropped by 40% ($p < 0.05$ vs. pre-infusion value) without affecting contractility. The adenosine effluent level was increased by 68%, parallel to a 50% increase in coronary flow. Because adenosine (A) receptors also play a crucial role in PC, Das *et al.* [30-31] examined whether these receptors play any role in resveratrol-mediated PC. In these studies beside the resveratrol pretreatment, 1 μM 8-cyclopentyl-1,3-dimethylxanthine (CPT; adenosine A_1 receptor blocker) or 1 μM 8-(3-chlorostyryl)caffeine (CSC; adenosine A_{2a} receptor blocker) or 1 μM 3-ethyl-5-benzyl-2-methyl-4-phenylethynyl-6-phenyl-1, 4-(+/-)-dihydropyridine-3,5-dicarboxylate (MRS-1191; adenosine A_3 receptor blocker) or 3 μM 2-(4-morpholinyl)-8-phenyl-1(4H)-benzopyran-4-one hydrochloride [LY294002, phosphatidyl-inositol (PI) 3-kinase inhibitor] were applied. Hearts were then subjected to 30 minutes ischemia followed by 120 minutes reperfusion. In addition, Akt, p-Akt, Bcl-2, p-Bcl-2, Bad, p-Bad, CREB, p-CREB were also determined. The results of the present study are parallel with many other reports, which indicate the role of A_1 and A_3, but not A_{2a} receptors, in the resveratrol-mediated PC [30-33]. The main findings [30-33] are that resveratrol-mediated PC is related to the activation of A_1 and A_3 receptors, which triggers a survival pathway through the phosphatidylinositol (PI) 3-kinase-Akt-Bad/Bcl-2 and by activating adenosine A_3-CREB-Bcl-2 (anti-apoptotic) signaling. In a further study, mitogen-activated extracellular signal-regulated protein kinase inhibitor PD098059 [2-(2-amino-3-methoxyphenyl)-4H-1-benzopyran-4-one], or a combination of LY294002 and PD098059 were examined by Das *et al.* [30-32]. The results of this study demonstrated that resveratrol-mediated PC is linked to the A_3 receptors that trigger p-CREB via both PI3-kinase-Akt and MEK-CREB pathway, specify the previous finding.

Hattori *et al.* [34] also proved the preconditioning effects of resveratrol to be mediated by nitric oxide (NO) or nitric oxide synthase. To confirm the hypothesis, a NO inhibitor, N^G-nitro-L-arginine methyl ester (L-NAME), as well as an inducible NO synthase (iNOS) blocker, aminoguanine (AG), were used in their studies. The L-NAME, and AG pretreatment abolished the resveratrol-mediated cardioprotection, suggesting the role of nitric oxide in resveratrol-induced cardioprotection. To gather further evidence Imamura *et al.*, used isolated iNOS knockout mouse hearts [35]. Both resveratrol treated and non-treated iNOS knockout mice hearts displayed relatively poor recovery in cardiac function as compared to the wild type mice. Obviously, resveratrol induced an increased expression of iNOS in the wild type mice, but (could) not in the iNOS knockout hearts, indicating an essential role of iNOS in resveratrol-mediated PC. In an additional study, the expression of the molecular targets of NO (e.g., vascular endothelial growth factor (VEGF), KDR, iNOS, eNOS) were examined by western blot and immunohistochemistry by Das *et al.* [36-37]. Recent studies have also demonstrated that NO can induce the expression of heme-oxygenase (HO-1). Das *et al.* [31] showed that protoporphyrin (SnPP), an HO-1 inhibitor treatment was able to abolish the cardioprotective effects of resveratrol (i.e., increased cardiac function parameters, reduced myocardial infarct size, decreased cardiomyocytes apoptosis). The HO-1 mediated mechanisms were related to the p38MAP kinase and Akt survival signaling, but independent of NFkappaB activation using p38MAPK, and Akt inhibitor. The cardioprotective mechanisms of resveratrol using sour cherry seed kernel extract, against ischemia-reperfusion-induced damage through the reduced caspase-3 activity was confirmed by Bak *et al.* [38]. It is also well documented that NO plays a crucial role in VEGF-induced angiogenesis. VEGF has been characterized as a heparin binding angiogenic growth factor, displaying high specificity for endothelial

cells [39-40], and then the identification of the VEGFR-1 (flt-1) and VEGFR-2 (KDR/flk-1) genes that encode VEGF specific tyrosine-kinase receptors [41-42]. In addition, resveratrol enhanced myocardial angiogenesis by induction of VEGF, which was regulated by thioredoxin-1 (trx-1) and HO-1 pathway. Chen *et al.* [43] demonstrated similar HO-1 up-regulation via the antioxidant response element (ARE)-mediated transcriptional activation of NF-E2-related factor-2 (Nrf2). Up-regulation of VEGF is a double edge sword due to its controversial effects. Nevertheless, this could be beneficial in certain cardiovascular diseases. VEGF-induced angiogenesis plays a central role in several additional diseases associated with abnormal angiogenesis and in lesion repair [44-46].

ANTIINFLAMMATORY EFFECTS

Recently, numerous possible ways have been identified by which resveratrol may attenuate tumor propagation. The mechanisms of action include induction of apoptosis, inhibition of key steps in signal transduction, promotion of cellular differentiation, scavenging the reactive oxygen species (ROS) and anti-inflammatory activity. The anti-inflammatory response of resveratrol was realized from its ability to down-regulate pro-inflammatory cytokines [47].

In general, multi-step processes are involved when a tissue is injured and such processes last till the time the region is healed. The first step of inflammation includes the activation and migration of leukocytes, including neutrophils, monocytes and eosinophils, to the injured tissue site from the various parts of the body. Polymorphonuclear leukocytes (PMNs) play an important role in the initial stage of inflammation. Resveratrol reduces inflammatory responses induced by fMLP, component fragment C5a, or calcium ionophore A23187 [48]. After PMN, the macrophages take over the process of inflammation. NO production can have some beneficiary effects on the activation of macrophages. Inducible NO synthase (iNOS) plays an important role in this process. Resveratrol has been found to induce iNOS [49, 50]. Resveratrol also interferes with the pro-inflammatory signaling of thrombin resulting in the inhibition of adenosine nucleotide secretion from activated platelets and decreased neutrophil functions via inhibition of PAP and P2-receptor signaling through MAPK and cJun and JNK [51]. A recent study showed that in mouse epidermal cells, resveratrol activated extracellular signal-regulated kinases (ERK), c-Jun NH_2-terminal kinases (JNK), and p38 MAPK, leading to the serine 15 phosphorylation of p53 [52].

There are two different types of inflammation. The first type of inflammation known as acute inflammation brings about morphological changes causing intense vasodilation resulting in increased blood flow, which leads to increased vascular permeability at the damaged region. This kind of changes lasts for a few minutes to few days when the leukocytes and mast cells try to heal the region. When the reaction is uncontrolled, then the acute inflammation attains chronic stage of inflammation lasting for long time. Chronic inflammation involves lymphocytes, blood vessel proliferation and macrophages apart from mast cells and leukocytes activation. This makes the region to exudate with cellular migration by both endogenous as well as exogenous substances and edema production. Several chemotactic agents may be released from microorganisms including formyl methionyl leucyl phenylalanine (fMLP) or from macrophages, which finally causes the release of the vasoactive mediators, like platelet-activating factor (PAF), leukotriene (LT)-B_4, metabolite of arachidonic acid, NO, cytokines like tumor necrosis factor alpha (TNF-α), interleukin (IL)-1, IL-6, and ROS.

Studies revealed that resveratrol protects from inflammation by acting at different phases of inflammation. Protection at the pro-inflammatory phase appears to be very important for reducing inflammation effectively and promptly. A recent study [53] has shown that resveratrol inhibits macrophage expression of EMMPRIN by activating PPAR-γ. In another similar study, Ma *et al.* [54] showed a similar observation, but additionally found a role of nuclear transcription factor κB (NFκB) in macrophage inhibition. Numerous studies confirmed that resveratrol suppresses the TNF-α activation [55-57]. Some preclinical as well as clinical studies have shown significant suppression of IL-1 and IL-6 with resveratrol [58-59]. Similarly, IL-8 plays an important role in inflammation as it recruits leukocytes [60]. Donnelly *et al.* [61] showed that resveratrol (1-100 μM) can inhibit IL-8. In another study, resveratrol inhibited the TNF-α and histamine release by immunoglobulin E (IgE) in mouse mast cells [62]. There are three different soluble adhesive molecules present in the leukocytes and endothelium;

integrins (α- and β- integrins), selectins (L-, P- and E-selectin) and immunoglobulin subfamily of cell surface proteins (vascular cell adhesion molecule-1, VCAM-1 and intracellular adhesion molecule-1, ICAM-1). In an acute in vivo study, Das and Maulik [27] successfully showed that resveratrol significantly inhibited the generation of adhesion molecules.

There are two different enzyme systems that are involved in the synthesis of pro-inflammatory mediators, such as cyclooxygenase (COX) and lipoxygenase, which finally release inflammatory substances, prostanoids and LTs, respectively. Resveratrol inhibited the induction of LTB_4 and attenuated PAF in rats [63]. Similarly, it was found that resveratrol has significant effect on the production of the peptide leukotriene LTC_4 [64]. The anti-inflammatory response of resveratrol was showed by Jang *et al.* [65] who found inhibition of PG synthesis by the inhibitory effect of COX-1 with resveratrol. Subsequently, the same group found that resveratrol could selectively inhibit COX activity by inhibiting COX-1 pathway, but not through COX-2 pathway. Szewczuk *et al.* [66] confirmed this finding. In contrast, another study found that resveratrol suppressed the synthesis PGE_2 by the inhibition of COX-2, but not altering the COX-1 [67]. In a related study, resveratrol significantly reduced colonic injury, neutrophil infiltration and drastically reduced the PGD_2 concentration by inhibiting COX-2, but not affecting COX-1 [68]. It appears that the anti-inflammatory activity of resveratrol may be realized through the inhibition of both COX-1 and COX-2 mediated pro-inflammatory signaling, suppression of pro-inflammatory mediator production as well as from its potent antioxidative effects.

ANTIDIABETIC EFFECTS

Diabetes is a disease when islets of Langerhans cells in the pancreas do not or poorly produce insulin or the body is not properly using the insulin present in the system. What is the cause of diabetes is still a mystery to the research world. According to the latest report of American Diabetes Association in 2006, there are at least 20.8 million children and adults in the United States, or 7% of the population, who have diabetes. While an estimated 14.6 million have been diagnosed with diabetes, unfortunately, 6.2 million people (or nearly one-third) are unaware that they have the disease. That's why diabetes is also known as "Silent Killer".

A little over a year ago, a scientist from California, USA, hypothesized based on the evidences that IKK-β, a crucial catalyst of NFκB activation, is an obligate mediator of the disruption of insulin signaling induced by excessive exposure of tissues to free fatty acids, the inhibitors of IKK-β may have some important role against the type 2 diabetes. Indeed, resveratrol, a well known IKK-β inhibitor, reverses fat-induced insulin resistance [69]. This observation provides more enthusiasm to the researchers to use resveratrol as an anti-diabetic agent. As an outcome of this, the year 2006 brings quite a number of publications which suggest resveratrol possesses an insulin-like effect and can be used for the protection against diabetes. In a very recent study, Su *et al.* [70] showed that resveratrol significantly reduced the plasma glucose concentration as well as the dramatic reduction of triglyceride concentration in streptozotocin (STZ) induced diabetic mellitus rats in 14 days treatment. They concluded from this observation that resveratrol possesses hypoglycemic and hypolipidemic property. Baur *et al.* [25] added more value to this conclusion. As a part of an outstanding study, Baur and Sinclair [26] showed that resveratrol increases insulin sensitivity by lowering the blood glucose level in a group of high calorie diet mice and they have pointed out reduced insulin-like growth factor-1 (IGF-I) levels and increased AMP-activated protein kinase (AMPK) probably play a major role.

Some other related studies established that resveratrol can attenuate diabetic nephropathy in rats [71, 72] and reduce thermal hyperalgesia and cold allodynia in streptozotocin-induced diabetic rats [73]. In a very recent finding by the same group, who suggested that the resveratrol attenuates diabetic neuropathic pain by, at least, nitric oxide and TNF-α are actively involved in this process [74]. This is just the beginning and there is lot to go with this compound's potential to reduce the mortality by the Silent Killer.

ANTICANCER PROPERTIES

Resveratrol plays critical roles in signal mechanisms of different tumors. Currently it is well documented that many factors play a role in the pathomechanisms of cancers. However, the exact mechanisms are not precisely known. If resveratrol could provoke

an influence in only one pathological factor, then the effects of anticancer drugs (i.e., in combination therapy) might beneficially modulate the signal transduction pathways. This is the basic reason to investigate the precise mechanisms and effects of resveratrol and its derivatives on various cancers.

The inhibition of cyclooxygenase-2 (COX-2) (inducible form of COX) could be an important strategy for preventing the development of cancers. Subbaramaiah *et al.* [75] treated human mammary and oral epithelial cells with phorbol ester (PMA), which induced the COX-2 mRNA, COX-2 protein, protein-kinase C, c-Jun (promoter of COX-2), and prostaglandin synthesis. Phorbol ester-mediated inductions of these agents were inhibited by resveratrol. Nakagawa *et al.* [76] studied the effects of resveratrol on the growth of estrogen receptor (ER)-positive (KPL-1 and MCF-7) and negative (MKL-F) human breast cancer cell lines. Synthetic resveratrol at high concentration (>or = 44 μM) suppressed the cell growth in all cell lines. The chemical structure of resveratrol is similar to the 4,4'-dihydroxy-trans-diethylstilbene that belongs to the type I class of estrogens and acts as an ER agonist [77]. The effect of resveratrol was related to the apoptosis cascade (up-regulated Bax and Bak proteins, down-regulated Bcl-xL proteins, and activated caspase-3). Jazirehi and Bonavida [78] have also shown that resveratrol selectively down-regulated the expression of antiapoptotic proteins Bcl-xL and myeloid cell differentiation factor-1 (Mcl-1) and up-regulated the expression of proapoptotic proteins (Bax), and apoptosis protease activating factor-1 (Apaf-1). Scarlatti *et al.* [79] found that resveratrol could provoke growth inhibition and apoptosis in metastatic breast cancer cells (MDA-MB-231) by activating the ceramide synthesis pathway. Furthermore, Dorrie *et al.* [80] showed that resveratrol induced extensive apoptotic cell death by depolarizing mitochondrial membranes in CD95-sensitive leukemia cell lines as well as B-lineage leukemic cells which are resistant to CD95-signaling. In addition, resveratrol induced the activation of caspase-9 in all lines. However, the benzyloxycarbonyl-Val-Ala-Asp-fluoromethylketone (wide spectrum caspase-inhibitor) failed to inhibit the depolarization of mitochondrial membranes elicited by resveratrol, suggesting that resveratrol activation is independent of upstream caspase-8 activation via receptor ligation.

Resveratrol is a sensitizer of tumor necrosis factor-related apoptosis through p53-independent induction of p21 and p21-mediated cell cycle (G_1) arrest associated with down-regulation of surviving cells [81]. Kuwajerwala *et al.* [82] reported that resveratrol-induced increase in DNA synthesis was associated with enrichment of LNCaP cells in S phase, and a concurrent decrease in nuclear p21Cipl and p27Kip1 levels. In addition, Cao *et al.* [83] have shown that resveratrol inhibited hypoxia-inducible-factor 1α (HIF-1α) and VEGF expression in human ovarian cancer through multiple mechanisms: (i) inhibition of Akt, and mitogen-activated protein kinase activation, (ii) inhibition of protein translational regulators, (iii) proteosome pathway [84]. Resveratrol also reduced the antiapoptotic kinase Akt in various uterine cancer cell lines [85]. Similar effects occurred in human tongue squamous cell carcinoma and hepatoma cells [86]. It was reported that resveratrol down-regulated the expression of NF-kappaB, TNF-α, interleukin 1β, interleukin-6, Bcl-2, Bcl-xL, XIAP, c-IAP, VEGF, and matrix metalloproteinase-9 (MMP-9) in human multiple myeloma (MM) cells or ex vivo studies [87, 88]. In a further study, it was investigated whether resveratrol-Cu(II) system is capable of causing DNA degradation in lymphocytes isolated from human peripheral blood [89]. This study partially supports the hypothesis that anticancer properties of resveratrol may involve mobilization of endogenous copper and the consequent prooxidant action. Kotha *et al.* [90] was among the initial group to identify Src-Stat3 signaling as a target of resveratrol in tumors. Beside the effects of resveratrol and its derivates alone, it is important to emphasize the combination of resveratrol with other anticancer drugs. Therefore, resveratrol combined with cisplatin or doxorubicin produced an additive growth-inhibitory and anticancer effects and protection against doxorubicin-induced cardiac toxicity both in human gynecologic cancer cell lines, and *in vivo* [91].

ANTIAGING EFFECTS

In many eukaryotic cells such as rodents, flies and nematode worms, and even single-celled organisms such as baker's yeast, only SIR2 among many longevity regulatory genes have received significant attention from researchers [92]. In human cells, the analogous gene of SIR2 is SIRT1, which can extend lifespan [93]. In a recent study, Howitz *et al.* [93] showed red wine derived resveratrol could increase

the SIRT1 activity 13-fold by inhibiting apoptotic cell death through the deacetylation of p53. In the same study they also showed that resveratrol extended the lifespan by 70% by mimicking calorie restriction by stimulating SIR2 in the yeast cells and, thus, increased DNA stability. In another very recent study on calorie restriction experiments on monkey and other mammalian species, the concept of wine as 'fountain of youth' was re-confirmed [94].

ANTIULCER EFFECTS

In 1982, when the *Helicobacter pylori* was discovered by Marshall and Warren, rather than stress and lifestyle, to be the major cause of peptic ulcer disease by its rupturing of the mucus membrane of the stomach. In an *in vitro* study, Marimon *et al.* showed that wine could effectively reduce the growth of *H. pylori* propagation [95]. A few other studies showed that red wine is more effective over white wine to inhibit the growth of *H. pylori* [96-97]. Mahady *et al.* [97, 98] showed in their study, resveratrol is the active component which causes the inhibitory effect of 15 different strains of *H. pylori* propagation [97].

OTHER HEALTH BENEFITS

The resveratrol induced protection against ischemia/reperfusion has been documented in various organs (e.g., kidney, brain, heart, liver etc). In a study of spinal cord ischemia model (SCI), resveratrol-induced neuroprotection was found mediated by decreased oxidative stress, and increased NO release. Organotopic hippocampal cultures were exposed to oxygen-glucose deprivation (OGD) using LY294002 and PD98059 treatment to confirm the exact mechanism. Neuroprotection was arrested by LY294002 but not by PD98059. Thus, these findings suggest that PI3-k/Akt pathway but not mitogen-activated protein kinase (MAPK) are involved in the neuroprotection [99]. Ischemic PC was mimicked by resveratrol in the brain via the SIRT1 pathway confirmed by sirtinol [100]. Recent studies have suggested that resveratrol may act as not only an antioxidant agent, but as a signaling molecule [101] within tissues and cells to modulate the expression of genes and proteins (i.e., HO-1, COX-2, eNOS, iNOS, endotelin-1,TNF-α, insulin-like growth factor binding protein). HO-1 protein has been documented with different functions in the brain. Since HO-1 is a heat-shock protein, which is induced in several cells and following different stimuli (e.g., hypothermia, global ischemia, subarachnoid hemorrhage, Parkinson disease, Alzheimer disease, etc), the modulation of the different genes may explain the cytoprotective actions afforded by resveratrol, as well as the influence of resveratrol on blood flow, cell death, and inflammatory cascades [102].

Protection against ischemia/reperfusion-induced oxidative injury occurred in rat kidney as well. Resveratrol caused a significant increase in tissue glutathione (GSH), and decreased the renal luminal, lucigenin CL, MDA levels, MPO activity and collagen content [103]. Acute renal failure (ARF) can be induced by glycerol, and glycerol provokes a marked decrease in tissue and urine nitric oxide levels, causes renal oxidative stress, deterioration of renal morphology, and renal function. Resveratrol could reverse the aforementioned effects. However, the renoprotective effect was abolished using N^G-nitro-L-arginine methyl ester, a nonspecific NO-synthase-inhibitor (L-NAME) cotreatment, suggesting that resveratrol exerts the protective effects through the nitric-oxide release [104-105]. Leikert *et al.* [106] also reported that renoprotective effects of resveratrol were also attributed to the release of endothelial nitric oxide. It is well known that ROS are harmful for glomeruli and tubular epithelial cells. The up-regulation of NF-κB activates the cytokines, chemokines, and adhesion molecules. These are very harmful mediators of inflammation, leading to fibrosis, glomerular damage, and tubulointerstitial damage. Resveratrol reinforces endogenous antioxidant systems that depurates ROS and thereby contributes to cytoprotective effects [107]. The deterioration of lipid peroxidation caused by resveratrol is also related to lung, liver, and kidney protection [108]. Angiotensin II (Ang II) also plays a crucial role in the progression of renal diseases by activated membrane-bound nicotinamide adenine dinucleotide phosphate (NADPH) oxidase and superoxide anion leading to hypertrophy of renal tubular cells. Since Ang II regulates the overexpression of TGF-β and TNF-α, this "side"-mechanism also contributes to the obstructive nephropathy. This pathomechanism pathway (Ang II) is inhibited by resveratrol and could also play an important role in nephroprotection [109].

The oxidative stress also plays a key role in the pathogenesis of various liver diseases and their progression. The use of resveratrol has been proposed

as a therapeutic agent as well as coadjuvant, to prevent liver damage [110]. The antioxidant activity was evaluated by measuring the inhibition of citronellal thermo oxidation or the reduction of 2,2-diphenil-1-picrylhydrazy radical [110]. Furthermore, resveratrol can directly interact with DNA polymerases alpha and delta beyond the antioxidant activity [111]. In a further study, hepatotoxicity was induced by acetaminophen (AA). Alanine aminotransferase (ALT), aspartate aminotransferase (AST), MDA, TNF-alpha levels, and MPO activity were significantly increased, and GSH level was significantly decreased after the AA treatment. Co-treatment with resveratrol reversed these effects. In addition, the increased luminal and lucigenin CL levels in the AA treated group were significantly reduced by resveratrol pretreatment. The AA is not the only medicine, which can provoke liver damage. Therefore, these results suggest that resveratrol and natural antioxidant nutriments can be used as therapeutic agents in order to prevent hepatic oxidative injury due to hepatotoxic drugs.

It is also well documented that antioxidant-rich diet protects against age-related macular degeneration (AMD), the leading cause of vision loss among the elderly. Development of AMD in the retinal pigment epithelium (RPE) is associated with oxidative stress. King *et al.* [112] reported that resveratrol treatment (100 μmol/L) inhibited basal and H_2O_2-induced intracellular oxidation, and protected RPE cells from cell death via the MAPK/ERK and extracellular signal-regulated kinase (ERK 1/2) pathways. Moreover, Sparrow *et al.* [113] showed that resveratrol reduced A2E-epoxide formation in RPE. Doganay *et al.* [114] demonstrated that resveratrol suppressed selenite-induced oxidative stress and cataract formation in rat's eye. The protective effect was associated with higher GSH and lower MDA in lens and erythrocytes. The main point of this study is that resveratrol-rich diet could prevent human senile cataract. The protection of resveratrol against the ischemia/reperfusion injury can also occur in the eye (e.g., in retina). Retinal ischemia/reperfusion resulted in a significant reduction in HO-1 protein expression, and HO-1 related endogenous CO production that affected the ion levels in the retina. Cellular Na^+ and Ca^{2+} levels were increased, and K^+ content was decreased. In rats treated with resveratrol-rich extract, tissue Na^+ and Ca^{2+} accumulation and K^+ loss were prevented through the HO-1 related endogenous CO production [115].

Huang *et al.* [116] reported that resveratrol induced HO-1 protein up-regulation in rat aortic smooth muscle cells via the NF-kB pathway. Pendurthi *et al.* [117] showed that resveratrol inhibited the tissue factor (TF) expression, LPS-induced expression of TNF-α, and IL-1β in vascular cells. In contrast, Di Santo *et al.* [118] demonstrated that resveratrol significantly reduced the TF activity, which was originated from a reduction in nuclear binding activity of the transacting factor c-Rel/p65 in human endothelial and mononuclear cells. Antiplatelet activity of resveratrol is beneficial in many diseases. Olas *et al.* [119] showed that resveratrol inhibited chemiluminescence and generation of $O_2^{\cdot}$ in blood platelets caused by LPS or thrombin. This antiplatelet effect is in agreement with the results obtained by Bertelli *et al.* [120]. Moreover, resveratrol significantly inhibited ICAM-1 and VCAM-1 expression on TNF-α -stimulated human umbilical vein endothelial cells and LPS-stimulated human saphenous vein endothelial cells [121]. These investigators [121] showed that resveratrol induced a significant inhibition in the adhesion of U937 monocytoid cells, and neutrophils to TNF-α-stimulated NIH/3T3 ICAM-1-transfected cells. These results suggest an independent pathway of its antioxidant function.

Acknowledgments – The authors thank Rudolf Gesztelyi and Bela Juhasz for the preparation of the manuscript. This study was supported by grants from OTKA (T-46145), RET-006/2004, and NKFP 1A/008/2004, Hungary to AT and NIH HL 22559, HL33889, and HL69910 to DK Das.

REFERENCES

1. Rupprich, N., Hildebrand, H., and Kindl, H. (1980) Substrate specificity in vivo and in vitro in the formation of stilbenes. Biosynthesis of rhaponticin. *Arch. Biochem. Biophys.* **200:** 72-78.
2. Morelli, R., Das, S., Bertelli, A., Bollini, R., Scalzo, R.L., Das, D.K., and Falchi M. (2006) The introduction of the stilbene synthase gene enhances the natural antiradical activity of Lycopersicon esculentum mill. *Mol. Cell. Biochem.* **282:** 65-73.
3. Das, S., Bertelli, A.A., Bertelli, A., Maulik, N., and Das D.K. (2006) Antiinflammatory action of resveratrol: a novel mechanism of action. *Arzneimittel*

Editorial

Some personal rambling thoughts as a result of my participation at the Science and Technology in Society Forum, Kyoto – our earth is finite and the aspirations of the people are to enjoy as high a standard of living as possible, drawing on the limited resources of the earth.

It is important that development progresses in harmony with nature otherwise there will be an imbalance as in the case of fossil fuel, where its utilization results in build up of green house gases which effect our climate. Efforts have been considered in reducing the level of green house gases such as the Kyoto Protocol. Japan has recently proposed the cool earth 50, meaning that Japan will reduce 50% of these gases by the year 2030. Water has been considered as a depleting resource.

Many countries are looking forward to the application of Science and Technology in solving these challenges. It is important that innovation should also be nurtured. Research in science provides knowledge and when knowledge is translated into application in society, innovation results. It is thus apparent that research is of great importance in solving the problems of the future world.

In this context the universities are expected to play an increasingly important role in this millennium. Universities whose primary function is in educating students are envisaged to generate knowledge which should then play an important role in contributing to social and economic development by promoting innovation through business-academia-government collaboration.

Thus, research and development addressing the problems of the tropics should be intensified and the fruits of such research will hopefully be channelled to this journal.

Academician Professor Emeritus
Tan Sri Datuk Dr S. H. Ong
Co-Chairman, Editorial Board

Forschung Drug Res. **56:** 700 – 706.

4. Aggarwal, B.B., Bhardwaj, A., Aggarwal, R.S., Seeram, N.P., Shishodia, S., and Takada Y. (2004) Role of resveratrol in prevention and therapy of cancer: preclinical and clinical studies. *Anticancer Res.* **24:** 2783-2840.
5. Schubert, R., Fischer, R., Hain, R., Schreier, P.H., Bahnweg, G., Ernst, D., and Sandermann H. Jr. (1997) An ozone-responsive region of the grapevine resveratrol synthase promoter differs from the basal pathogen-responsive sequence. *Plant Mol. Biol.* **34:** 417-26.
6. Celotti, E., Ferrarini, R., Zironi, R., and Conte, L.S. (1996) Resveratrol content of some wines obtained from dried Valpolicella grapes: Recioto and Amarone. *J. Chromatogr. A* **730:** 47-52.
7. Hain, R., Bieseler, B., Kindl, H., Schroder, G., and Stocker R. (1990) Expression of a stilbene synthase gene in Nicotiana tabacum results in synthesis of the phytoalexin resveratrol. *Plant Mol. Biol.* **15:** 325.
8. Jang, M., Cai, L., Udean, G.O., Slowing, K.V., Thomas, C.F., Beecher, C.W., Fong, H.H., Farnsworth, N.R., Kinghorn, A.D., Mehta, R.G., Moon, R.C., and Pezzuto, J.M. (1997) Cancer chemopreventive activity of resveratrol, a natural product derived from grapes. *Science* **275:** 218-20.
9. Langcake, P., and Pryce R.J. (1977) A new class of phytoalexins from grapevines. *Experientia* **33:** 151.
10. Schoeppner, A., and Kindl, H. (1979) Stilbene synthase (pinosylvine synthase) and its induction by ultraviolet light. *FEBS Lett.* **108:**349-52.
11. Kopp, P. (1998) Resveratrol, a phytoestrogen found in red wine. A possible explanation for the conundrum of the 'French paradox'? *Eur. J. Endocrinol.* **138:** 619-620.
12. Stervbo, U., Vang, O., and Bonnesen, C. (2007) A review of the content of the putative chemopreventive phytoalexin resveratrol in red wine. *Food Chem.* **101:** 449-457.
13. Sipos, P., Gyory, H., Hagymasi, K., Ondrejka, P., and Blazovics A. (2004) Special wound healing methods used in ancient egypt and the mythological background. *World J. Surg.* **28:** 211-621.
14. Paul, B., Masih, I., Deopujari, J., and Charpentier, C. (1999) Occurrence of resveratrol and pterostilbene in age-old darakchasava, an ayurvedic medicine from India. *J. Ethnopharmacol.* **68:** 71-76.
15. Soleas, J.S., Diamandis E.P., and Goldberg D.M. (1997) Resveratrol: a molecule whose time has come? And gone? *Clin. Biochem.* **30:** 91-113.
16. Murakami, A., Ishida, H., Kobo, K., Furukawa, I., Ikeda, Y., Yonaha, M., Aniya, Y., and Ohigashi H. (2005) Related Suppressive effects of Okinawan food items on free radical generation from stimulated leukocytes and identification of some active constituents: implications for the prevention of inflammation-associated carcinogenesis. *Asian Pac. J. Cancer Prev.* **6:** 437-448.
17. Renaud, S., and de Lorgeril, M. (1992) Wine, alcohol, platelets, and the French paradox for coronary heart disease. *Lancet* **339:** 1523-1526.
18. Das, D.K., Sato, M., Ray, P.S., Maulik, G., Engelman, R.M., Bertelli, A.A., and Bertelli A. (1999) Cardioprotection of red wine: role of polyphenolic antioxidants. *Drugs Exp. Clin. Res.* **25:** 115-120.
19. Sun, A.Y., Simonyi, A., and Sun, G.Y. (2002) The "French Paradox" and beyond: neuroprotective effects of polyphenols. *Free Radic. Biol. Med.* **32:** 314-318.
20. Cabot, R.C. (1904) The relation of alcohol to atherosclerosis. *J. Am. Med. Assoc.* **43:** 774-775.
21. Pearl, R. (1926) *Alcohol and Longevity.* NY: Knopf.
22. Li, J.M., and Mukamal K.J. (2004) An update on alcohol and atherosclerosis. *Curr. Opin. Lipidol.* **15:** 673-680.
23. Gronbaek, M., Becker, U., Johansen, D., Gottschau, A., Schnohr, P., Hein, H.O., Jensen, G., and Sorensen, T.I. (2000) Type of alcohol consumed and mortality from all causes, coronary heart disease, and cancer. *Ann. Intern. Med.* **133:** 411-419.
24. Pedersen, A., Johansen, C., and Gronbaek, M. (2003) Relations between amount and type of alcohol and colon and rectal cancer in a Danish population based cohort study. *Gut* **52:** 861-867.
25. Baur, J.A., Pearson, K.J., Price, N.L., Jamieson, H.A., Lerin, C., Kalra, A., Prabhu, V.V., Allard, J.S., Lopez-Lluch, G., Lewis, K., Pistell, P.J., Poosala, S., Becker, K.G., Boss, O., Gwinn, D., Wang M., Ramaswamy, S., Fishbein, K.W., Spencer, R.G., Lakatta, E.G., Le Couteur, D., Shaw, R.J., Navas, P., Puigserver, P., Ingram, D.K., de Cabo R., and Sinclair D.A. (2006) Related Resveratrol improves health and survival of mice on a high-calorie diet. *Nature* **444:** 337-342.
26. Baur, J.A., and Sinclair, D.A. (2006) Therapeutic potential of resveratrol: the in vivo evidence. Nat Rev *Drug Discov.* **5:** 493-506.
27. Das, D.K., and Maulik, N. (2006) Resveratrol in cardioprotection: a therapeutic promise of alternative medicine. *Mol. Interv.* **6:** 36-47.
28. Murry, C.E., Jennings R.B., and Reimer, K.A. (1986) Preconditioning with ischemia: a delay of lethal cell injury in ischemic myocardium. *Circulation* **74:** 1124-1136.
29. Bradamante, S., Piccinini, F., Barenghi, L., Bertelli, A.A., De Jonge, R., Beemster, P., and De Jong J.W. (2000) Does resveratrol induce pharmacological preconditioning? *Int. J. Tissue React.* **22:** 1-4.
30. Das, S., Cordis, G.A., Maulik, N., and Das, D.K. (2005) Pharmacological preconditioning with

resveratrol: role of CREB-dependent Bcl-2 signaling via adenosine A3 receptor activation. *Am. J. Physiol. Heart Circ. Physiol.* **288:** H328-335.

31. Das, S., Fraga, C.G., and Das, D.K. (2006) Cardioprotective effect of resveratrol via HO-1 expression involves p38 map kinase and PI-3-kinase signaling, but does not involve NFkappaB. *Free Radic. Res.* **40:** 1066-75.
32. Das, S., and Das, D.K. (2006) Wine and the Heart: a Journey from Grapes to Resveratrol. *S. Afr. J. Enol. Vitic.* **27:** 127-132.
33. De Jonge, R., Out, M., Maas, W.J., and De Jong J.W. (2002) Preconditioning of rat hearts by adenosine A1 or A3 receptor activation. *Eur. J. Pharmacol.* **441:** 165-172.
34. Hattori R., Otani H., Maulik N., and Das D.K. (2002) Pharmacological preconditioning with resveratrol: role of nitric oxide. *Am. J. Physiol. Heart Circ. Physiol.* **282:** H1988-1995.
35. Imamura, G., Bertelli, A.A., Bertelli, A., Otani, H., Maulik, N., and Das, D.K. (2002) Pharmacological preconditioning with resveratrol: an insight with iNOS knockout mice. *Am. J. Physiol. Heart Circ. Physiol.* **282:** H1996-2003.
36. Das, S., Alagappan, V.K., Bagchi, D., Sharma, H.S., Maulik, N., and Das D.K. (2005) Coordinated induction of iNOS, VEGF, KDR, eNOS after resveratrol consumpion: a potential mechanism for resveratrol preconditioning of the heart. *Vasc. Pharmacol.* **42:** 281-289.
37. Das, S., Tosaki, A., Bagchi, D., Maulik, N., and Das, D.K. (2005) Resveratrol-mediated activation of cAMP response element-binding protein through adenosine A3 receptor by Akt-dependent and -independent pathways. *J. Pharmacol. Exp. Ther.* **314:** 762-769.
38. Bak, I., Lekli I., Juhasz B., Nagy N., Varga E., Varadi J., Gesztelyi R., Szabo G., Szendrei L., Bacskay I., Vecsernyes M., Antal M., Fesus L., Boucher F., de Leiris J., and Tosaki A. (2006) Cardioprotective mechanisms of *Prunus cerasus* (sour cherry) seed extract against ischemia-reperfusion-induced damage in isolated rat hearts. *Am. J. Physiol. Heart Circ. Physiol.* **291:** H1329-1336.
39. Ferrara, N., and Henzel, W.J. (1989) Pituitary follicular cells secrete a novel heparin-binding growth factor specific for vascular endothelial cells. *Biochem. Biophys. Res. Commun.* **161:** 851-858.
40. Gospodarowicz, D., Abraham, J.A., and Schilling, J. (1989) Isolation and characterization of a vascular endothelial cell mitogen produced by pituitary-derived folliculo stellate cells. *Proc. Natl. Acad. Sci. USA* **86:**7311-7315.
41. Devries, C., Escobedo, J.A., Ueno, H., Houck, K., Ferrara, N., and Williams L.T. (1992) The fms-like tyrosine kinase, a receptor for vascular endothelial growth factor. Science **255:** 989-991.
42. Terman, B.I., Dougher-Vermazen, M., Carrion, M.E., Dimitrov, D., Armellino, D.C., Gospodarowicz, D., and Bohlen, P. (1992) Identification of the KDR tyrosine kinase as a receptor for vascular endothelial cell growth factor. *Biochem. Biophys. Res. Commun.* **187:** 1579-1586.
43. Chen, C.Y., Jang, J.H., Li, M.H., and Surh, Y.J. (2005) Resveratrol upregulates heme oxygenase-1 expression via activation of NF-E2-related factor 2 in PC12 cells. *Biochem. Biophys. Res. Commun.* **33:** 993-1000.
44. Adamis, A.P., Miller, J.W., Bernal, M.T., Damico, D.J., Folkman, J., Yeo, T.K., and Yeo K.T. (1994) Increased vascular endothelial growth factor levels in the vitreous of eyes with proliferative diabetic retinopathy. *Am. J. Ophthalmol.* **118:** 445-450.
45. Aiello, L.P., Avery, R.L., Arrigg, P.G., Keyt, B.A., Jampel, H.D., Shah, S.T., Pasquale, L.R., Thieme, H., Iwamoto, M.A., Park, J.E., Nguyen, H.V., Aiello, L.M., Ferrara, N., and King, G.L. (1994) Vascular endothelial growth factor in ocular fluid of patients with diabetic retinopathy and other retinal disorders. *N. Engl. J. Med.* **331:** 1480-1487.
46. Brown, L.F., Yeo, K.T., Berse, B., Yeo, T.K., Senger, D.R., Dvorak, H.F., and Van de Water, L. (1992) Expression of vascular permeability factor (vascular endothelial growth factor) by epidermal keratinocytes during wound healing. *J. Exp. Med.* **176:** 1375-1379.
47. Pervaiz, S. (2003) Resveratrol: from grapevines to mammalian biology. *FASEB J.* **17:** 1975-1985.
48. Rotondo, S., Rajtar, G., Manarini, S., Celardo, A., Rotillo, D., de Gaetano, G., Evangelista, V., and Cerletti, C. (1998) Effect of trans-resveratrol, a natural polyphenolic compound, on human polymorphonuclear leukocyte function. *Br. J. Pharmacol.* **123:** 1691-1699.
49. Sharma, S., Chopra, K., and Kulkarni, S.K. (2007) Effect of insulin and its combination with resveratrol or curcumin in attenuation of diabetic neuropathic pain: participation of nitric oxide and TNF-alpha. *Phytother. Res.* **21:** 278-283.
50. Chander, V., and Chopra, K. (2005) Role of nitric oxide in resveratrol-induced renal protective effects of ischemic preconditioning. *J. Vasc. Surg.* **42:** 1198-1205.
51. Kaneider, N.C., Mosheimer, B., Reinisch, N., Patsch, J.R., and Wiedermann, C.J. (2004) Inhibition of thrombin-induced signaling by resveratrol and quercetin: effects on adenosine nucleotide metabolism in endothelial cells and platelet-neutrophil interactions. *Thromb. Res.* **114:** 185-194.
52. She, Q.B., Bode, A.M., Ma, W.Y., Chen, N.Y., and

Dong, Z. (2001) Resveratrol-induced activation of p53 and apoptosis is mediated by extracellular-signal-regulated protein kinases and p38 kinase. *Cancer Res.* **61:** 1604-1610.

53. Ge, H., Zhang, J.F., Guo, B.S., He, Q., Wang, C.Q. (2006) Resveratrol inhibits macrophage expression of EMMPRIN by activating PPARgamma. *Vascular Pharmacol.* **46:** 114-121.
54. Ma, Z.H., Ma, Q.Y., Wang, L.C., Sha, H.C., Wu, S.L., and Zhang, M. (2006) Effect of resveratrol on NF-kappaB activity in rat peritoneal macrophages. *Am. J. Chin. Med.* **34:** 623-630.
55. Lee, B., and Moon, S.K. (2005) Resveratrol inhibits TNF-alpha-induced proliferation and matrix metalloproteinase expression in human vascular smooth muscle cells. *J. Nutr.* **135:** 2767-2773.
56. Moon, S.O., Kim W., Sung M.J., Lee S., Kang K.P., Kim D.H., Lee S.Y., So J.N., and Park S.K. (2006) Resveratrol suppresses tumor necrosis factor-alpha-induced fractalkine expression in endothelial cells. *Mol. Pharmacol.* **70:** 112-119.
57. Takada, Y., Bhardwaj, A., Potdar, P., and Aggarwal, B.B. (2004) Nonsteroidal anti-inflammatory agents differ in their ability to suppress NF-kappaB activation, inhibition of expression of cyclooxygenase-2 and cyclin D1, and abrogation of tumor cell proliferation. *Oncogene* **23:** 9247-9258.
58. Baggiolini, M., Loetscher, P., and Moser, B. (1995) Interleukin-8 and the chemokine family. *Int. J. Immunopharmacol.* **17:** 103-108.
59. Marier, J.F., Chen, K., Prince, P., Scott, G., del Castillo, J.R., and Vachon, P. (2005) Production of ex vivo lipopolysaccharide-induced tumor necrosis factor-alpha, interleukin-1beta, and interleukin-6 is suppressed by trans-resveratrol in a concentration-dependent manner. *Can. J. Vet. Res.* **69:** 151-154.
60. Olas, B., Wachowicz, B., Saluk-Juszczak, J., Zielinski, T., Kaca, W., and Buczynski, A. (2001) Antioxidant activity of resveratrol in endotoxin-stimulated blood platelets. Cell Biol. *Toxicol.* **17:** 117-125.
61. Donnelly, L.E., Newton, R., Kennedy, G.E., Fenwick, P.S., Fenwick, P.S., Leung, R.H., Ito, K., Russell, R.E., and Barnes, P.J. (2004) Anti-inflammatory effects of resveratrol in lung epithelial cells: molecular mechanisms. *Am. J. Physiol. Lung Cell. Mol. Physiol.* **287:** L774-L783.
62. Baolin, L., Inami, Y., Tanaka, H., Inagaki, N., Inagaki, N., Iinuma, M., and Nagai, H. (2004) Resveratrol inhibits the release of mediators from bone marrow-derived mouse mast cells in vitro. *Planta Med.* **70:** 305-309.
63. Shigematsu, S., Ishida, S., Hara, M., Takahashi, N., Takahashi, N., Yoshimatsu, H., Sakata, T., and Korthuis, R.J. (2003) Resveratrol, a red wine constituent polyphenol, prevents superoxide-dependent inflammatory responses induced by ischemia/reperfusion, platelet-activating factor, or oxidants. *Free Radic. Biol. Med.* **34:** 810-817.
64. Kimura, Y., Okuda, H., and Kubo, M. (1995) Effects of stilbenes isolated from medicinal plants on arachidonate metabolism and degranulation in human polymorphonuclear leukocytes. *J. Ethnopharmacol.* **45:** 131-139.
65. Jang, M., Cai, L., Udeani, G.O., Slowing, K.V., Thomas, C.F., Beecher, C.W., Fong, H.H., Farnsworth, N.R., Kinghorn, A.D., Mehta, R.G., Moon, R.C., and Pezzuto, J.M (1997) Cancer chemopreventive activity of resveratrol, a natural product derived from grapes. *Science* **275:** 218-220.
66. Szewczuk, L.M., Forti L., Stivala L.A., and Penning T.M. (2004) Resveratrol is a peroxidasemediated inactivator of COX-1 but not COX-2. *J. Biol. Chem.* **279:** 22727-22737.
67. Subbaramaiah, K., Chung, W.J., Michaluart, P., Telang, N., Tanabe, T., Inoue, H., Jang, M., Pezzuto, J.M., and Dannenberg, A.J. (1998) Resveratrol inhibits cyclooxygenase-2 transcription and activity in phorbol ester-treated human mammary epithelial cells. *J. Biol. Chem.* **273:** 21875-21882.
68. Martín, A.R., Villegas, I., La Casa C., and de la Lastra, C. (2004) Resveratrol, a polyphenol found in grapes, suppresses oxidative damage and stimulates apoptosis during early colonic inflammation in rats. *Biochem. Pharmacol.* **67:** 1399-1410.
69. McCarty, M.F. (2005) Potential utility of natural polyphenols for reversing fat-induced insulin resistance. *Med. Hypotheses* **64:** 628-635.
70. Su, H.C., Hung, L.M., and Chen, J.K. (2006) Resveratrol, a red wine antioxidant, possesses an insulin-like effect in streptozotocin-induced diabetic rats. *Am. J. Physiol. Endocrinol. Metab.* **290:** E1339-E1346.
71. Ates, O., Cayli, S.R., Yucel, N., Altinoz, E., Kocak, A., Durak, M.A., Turkoz, Y., and Yologlu, S. (2007) Central nervous system protection by resveratrol in streptozotocin-induced diabetic rats. *J. Clin. Neurosci.* **14:** 256-260.
72. Sharma, S., Anjaneyulu, M., Kulkarni, S.K., and Chopra, K. (2006) Resveratrol, a polyphenolic phytoalexin, attenuates diabetic nephropathy in rats. *Pharmacology* **76:** 69-75.
73. Sharma, S., Kulkarni, S.K., and Chopra, K. (2006) Resveratrol, a polyphenolic phytoalexin attenuates thermal hyperalgesia and cold allodynia in STZ-induced diabetic rats. *Indian J. Exp. Biol.* 44: 566-569.
74. Sharma, S., Chopra, K. and Kulkarni, S.K. (2007) Effects of insulin and its combination with resveratrol or curcumin in attenuation of diabetic neuropathic

pain: participation of nitric oxide and TNF-alpha. *Phytoter. Res.* **21:** 278-283.

75. Subbaramaiah, K., Michaluart, P., Chung, W.J., Tanabe, T., and Telang, N. (1999) Dannenberg A.J. Resveratrol inhibits cyclooxygenase-2 transcription in human mammary epithelial cells. *Ann. N.Y. Acad. Sci.* **889:** 214-223.
76. Nakagawa, H., Kiyozuka, Y., Uemura, Y., Senzaki, H., Shikata, N., Hioki, K., and Tsubura, A. (2001) Resveratrol inhibits human breast cancer cell growth and may mitigate the effect of linoleic acid, a potent breast cancer cell stimulator. *J. Cancer Res. Clin. Oncol.* **127:** 258-264.
77. Levenson, A.S., Gehm, B.D., Pearce, S.T., Horiguchi, J., Simons, L.A., Ward, J.E. 3rd, Jameson, J.L., and Jordan, V.C. (2003) Resveratrol acts as an estrogen receptor (ER) agonist in breast cancer cells stably transfected with ER alpha. *Int. J. Cancer* **104:** 587-596.
78. Jazirehi, A.R., and Bonavida, B. (2004) Resveratrol modifies the expression of apoptotic regulatory proteins and sensitizes non-Hodgkin's lymphoma and multiple myeloma cell lines to paclitaxel-induced apoptosis. *Mol. Cancer Ther.* **3:** 71-84.
79. Scarlatti, F., Sala, G., Somenzi, G., Signorelli, P., Sacchi, N., and Ghidoni, R. (2003) Resveratrol induces growth inhibition and apoptosis in metastatic breast cancer cells via de novo ceramide signaling. *FASEB J.* **17:** 2339-2341.
80. Dorrie, J., Gerauer, H., Wachter, Y., and Zunino, S.J. (2001) Resveratrol induces extensive apoptosis by depolarizing mitochondrial membranes and activating caspase-9 in acute lymphoblastic leukemia cells. *Cancer Res.* **61:** 4731-4739.
81. Fulda S., and Debatin, K.M. (2004) Sensitization for tumor necrosis factor-related apoptosis-inducing ligand-induced apoptosis by the chemopreventive agent resveratrol. *Cancer Res.* **64:** 337-346.
82. Kuwajerwala, N., Cifuentes, E., Gautam, S., Menon, M., Barrack, E.R., and Reddy, G.P. (2002) Resveratrol induces prostate cancer cell entry into s phase and inhibits DNA synthesis. *Cancer Res.* **62:** 2488-2492.
83. Cao, Z., Fang, J., Xia, C., Shi, X., and Jiang, B.H. (2004) Trans-3,4,5'-Trihydroxystilbene inhibits hypoxia-inducible factor 1alpha and vascular endothelial growth factor expression in human ovarian cancer cells. *Clin. Cancer Res.* **10:** 5253-5263.
84. Kim, K.J., Li, B., Winer, J., Armanini, M., Gillett, N., Phillips, H.S., and Ferrara, N. (1993) Inhibition of vascular endothelial growth factor induced angiogenesis suppresses tumor growth in vivo. *Nature* (London) **362:** 841-844.
85. Sexton, E., Van Themsche, C., LeBlanc, K., Parent, S., Lemoine, P., and Asselin, E. (2006) Resveratrol interferes with AKT activity and triggers apoptosis in human uterine cancer cells. *Mol. Cancer* **5:** 45.
86. Zhang, Q., Tang, X., Lu, Q.Y., Zhang, Z.F., Brown, J., and Le, A.D. (2005) Resveratrol inhibits hypoxia-induced accumulation of hypoxia-inducible factor-1alpha and VEGF expression in human tongue squamous cell carcinoma and hepatoma cells. *Mol. Cancer Ther.* **4:** 1465-1474.
87. Millauer, B., Shawver, L.K., Plate, K.H., Risau, W., and Ullrich, A. (1994) Glioblastoma growth inhibited in vivo by a dominant-negative Flk-1 mutant. *Nature* (London) **367:** 576-579.
88. Sun, C., Hu, Y., Liu, X., Wu, T., Wang, Y., He, W., and Wei, W. (2006) Resveratrol downregulates the constitutional activation of nuclear factor-kappaB in multiple myeloma cells, leading to suppression of proliferation and invasion, arrest of cell cycle, and induction of apoptosis. *Cancer Genet. Cytogenet.* **165:** 9-19.
89. Azmi, A.S., Bhat, S.H., and Hadi, S.M. (2005) Resveratrol-Cu(II) induced DNA breakage in human peripheral lymphocytes: implications for anticancer properties. *FEBS Lett.* **579:** 3131-3135.
90. Kotha, A., Sekharam, M., Cilenti, L., Siddiquee, K., Khaled, A., Zervos, A.S., Carter, B., Turkson, J., and Jove, R. (2006) Resveratrol inhibits Src and Stat3 signaling and induces the apoptosis of malignant cells containing activated Stat3 protein. *Mol. Cancer Ther.* **5:** 621-629.
91. Rezk, Y.A., Balulad, S.S., Keller, R.S., and Bennett, J.A. (2006) Use of resveratrol to improve the effectiveness of cisplatin and doxorubicin: study in human gynecologic cancer cell lines and in rodent heart. *Am. J. Obstet. Gynecol.* **194:** e23-e26.
92. Hall, S.S. (2003) Longevity research. In vino vitalis? Compounds activate life-extending genes. *Science* **30:** 1165.
93. Howitz, K.T., Bitterman,,K.J., Cohen, H.Y., Lamming, D.W., Lavu, S., Wood, J.G., Zipkin, R.E., Chung, P., Kisielewski, A., Zhang, L.L., Scherer, B., and Sinclair, D.A. (2003) Small molecule activators of sirtuins extend Saccharomyces cerevisiae lifespan. *Nature* **425:** 191-196.
94. Kujoth, G.C., Hiona, A., Pugh, T.D., Someya, S., Panzer, K., Wohlgemuth, S.E., Hofer, T., Seo, A.Y., Sullivan, R., Jobling, W.A., Morrow, J.D., Van Remmen, H., Sedivy, J.M., Yamasoba, T., Tanokura, M., Weindruch, R., Leeuwenburgh, C., and Prolla, T.A. (2005) Mitochondrial DNA mutations, oxidative stress, and apoptosis in mammalian aging. *Science* **309:** 481-484.
95. Marimon, J.M., Bujanda, L., Gutierrez-Stampa, M.A., Cosme, A., and Arenas, J.I. (1998) In vitro bactericidal effect of wine against Helicobacter

pylori. *Am. J. Gastroenterol.* **93:** 1392.

96. Daroch, F., Hoeneisen, M., Gonzalez, C.L., Kawaguchi, F., Salgado, F., Solar, H., and Garcia, A. (2001) In vitro antibacterial activity of Chilean red wines against Helicobacter pylori. *Microbios* **104:** 79-85.
97. Mahady, G.B., Pendland, S.L., and Chadwick, L.R. (2003) Resveratrol and red wine extracts inhibit the growth of CagA+ strains of Helicobacter pylori in vitro. *Am. J. Gastroenterol.* **98:** 1440-1441.
98. Mahady, G.B., and Pendland, S.L. (2000) Resveratrol inhibits the growth of Helicobacter pylori in vitro. *Am. J. Gastroenterol.* **95:** 1849.
99. Zamin, L.L., Dillenburg-Pilla, P., Argenta-Comiran, R., Horn, A.P., Simao, F., Nassif, M., Gerhardt, D., Frozza, R.L., and Salbego, C. (2006) Protective effect of resveratrol against oxygen-glucose deprivation in organotypic hippocampal slice cultures: Involvement of PI3-K pathway. *Neurobiol. Dis.* **24:** 170-182.
100. Raval, A.P., Dave, K.R., and Perez-Pinzon, M.A. (2006) Resveratrol mimics ischemic preconditioning in the brain. *J. Cereb. Blood Flow Metab.* **26:** 1141-1147.
101. Dore, S. (2005) Unique properties of polyphenol stilbenes in the brain: more than direct antioxidant actions; gene/protein regulatory activity. *Neurosignals* **14:** 61-70.
102. Sener, G., Toklu, H.Z., Sehirli, A.O., Velioglu-Ogunc, A., Cetinel S., and Gedik, N. (2006) Protective effects of resveratrol against acetaminophen-induced toxicity in mice. *Hepatol. Res.* **35:** 62-68.
103. Sener, G., Tugtepe, H., Yuksel, M., Cetinel, S., Gedik, N., and Yegen, B.C. (2006) Resveratrol improves ischemia/reperfusion-induced oxidative renal injury in rats. *Arch. Med. Res.* **37:** 822-829.
104. Chander, V., and Chopra, K. (2005) Role of nitric oxide in resveratrol-induced renal protective effects of ischemic preconditioning. *J. Vasc. Surg.* **42:** 1198-205.
105. Chander, V., and Chopra, K. (2006) Protective effect of resveratrol, a polyphenolic phytoalexin on glycerol-induced acute renal failure in rat kidney. *Ren. Fail.* **28:** 161-169.
106. Leikert, J.F., Rathel, T.R., Wohlfart, P., Cheynier, V., Vollmar, A.M., and Dirsch, V.M. (2002) Red wine polyphenols enhance endothelial nitric oxide synthase expression and subsequent nitric oxide release from endothelial cells. *Circulation* **106:** 1614-1617.
107. Rodrigo, R., and Bosco, C. (2006) Oxidative stress and protective effects of polyphenols: comparative studies in human and rodent kidney. A review. *Comp. Biochem. Physiol. C Toxicol. Pharmacol.* **142:** 317-327.
108. Bertelli, A.A., Migliori, M., Panichi, V., Origlia, N., Filippi, C., Das, D.K., and Giovannini, L. (2002) Resveratrol, a component of wine and grapes, in the prevention of kidney disease. *Ann. N.Y. Acad. Sci.* **957:** 230-238.
109. Klahr, S. (1998) Obstructive nephropathy. *Kidney Int.* **54:** 286-300.
110. Vitaglione, P., Morisco, F., Caporaso, N., and Fogliano, V. (2004) Dietary antioxidant compounds and liver health. *Crit. Rev. Food Sci. Nutr.* **44:** 575-586.
111. Stivala, L.A., Savio, M., Carafoli, F., Perucca, P., Bianchi, L., Maga, G., Forti, L., Pagnoni, U.M., Albini, A., Prosperi, E., and Vannini, V. (2001) Specific structural determinants are responsible for the antioxidant activity and the cell cycle effects of resveratrol. *J. Biol. Chem.* **276:** 22586-22594.
112. King, R.E., Kent, K.D., and Bomser, J.A. (2005) Resveratrol reduces oxidation and proliferation of human retinal pigment epithelial cells via extracellular signal-regulated kinase inhibition. *Chem. Biol. Interact.* **151:** 143-149.
113. Sparrow, J.R., Vollmer-Snarr, H.R., Zhou, J., Jang, Y.P., Jockusch, S., Itagaki, Y., and Nakanishi, K. (2003) A2E-epoxides damage DNA in retinal pigment epithelial cells. Vitamin E and other antioxidants inhibit A2E-epoxide formation. *J. Biol. Chem.* **278:** 18207-18213.
114. Doganay, S., Borazan, M., Iraz, M., and Cigremis, Y. (2006) The effect of resveratrol in experimental cataract model formed by sodium selenite. *Curr. Eye Res.* **31:** 147-153.
115. Szabo, M.E., Gallyas, E., Bak, I., Rakotovao, A., Boucher, F., de Leiris J., Nagy, N., Varga, E., and Tosaki, A. (2004) Heme oxygenase-1-related carbon monoxide and flavonoids in ischemic/reperfused rat retina. *Invest. Ophthalmol. Vis. Sci.* **45:** 3727-3732.
116. Huang, H.M., Liang, Y.C., Cheng, T.H., Chen, C.H., and Juan, S.H. (2005) Potential mechanism of blood vessel protection by resveratrol, a component of red wine. *Ann. N.Y. Acad. Sci.* **1042:** 349-356.
117. Pendurthi, U.R., Williams, J.T., and Rao, L.V. (1999) Resveratrol, a polyphenolic compound found in wine, inhibits tissue factor expression in vascular cells: A possible mechanism for the cardiovascular benefits associated with moderate consumption of wine. Arterioscler. *Thromb. Vasc. Biol.* **19:** 419-426.
118. Di Santo, A., Mezzetti, A., Napoleone, E., Di Tommaso, R., Donati, M.B., De Gaetano, G., and Lorenzet, R. (2003) Resveratrol and quercetin down-regulate tissue factor expression by human stimulated vascular cells. *J. Thromb. Haemost.* **1:** 1089-1095.
119. Olas, B., Wachowicz, B., Saluk-Juszczak, J., Zielinski, T., Kaca, W., and Buczynski, A. (2001) Antioxidant activity of resveratrol in endotoxin-stimulated blood platelets. *Cell Biol. Toxicol.* **17:**

117-125.
120. Bertelli, A.A., Giovannini, L., Giannessi, D., Migliori, M., Bernini, W., Fregoni, M., and Bertelli, A. (1995) Antiplatelet activity of synthetic and natural resveratrol in red wine. *Int. J. Tissue React.* **17:** 1-3.
121. Ferrero, M.E., Bertelli, A.E., Fulgenzi, A., Pellegatta, F., Corsi, M.M., Bonfrate, M., Ferrara, F., De Caterina, R., Giovannini, L., and Bertelli, A. (1998) Activity in vitro of resveratrol on granulocyte and monocyte adhesion to endothelium. *Am. J. Clin. Nutr.* **68:** 1208-1214.

Journal of Science and Technology in the Tropics (2007) **3**: 97-100

Removal of colour, UVA, TOC and THMFP by ozonation

K. H. Chua[1] and N. Saifuddin[2]
[1]Water and Environmental Engineering Unit, Civil Engineering Department
[2]Chemistry unit, Department of Science
College of Engineering, University of Tenaga Nasional,
Km 7, Jalan Puchong-Kajang, 43900 Kajang, Selangor, Malaysia
(Email: ckh@uniten.edu.my)

Received 01.11.2006; accepted 19.06.2007

Abstract A study was carried out to examine the effectiveness of ozonation process in removing colour, total organic carbon content TOC, ultraviolet light adsorbance UVA at 254 nm, and trihalomethanes formation potential THMFP from raw waters. A small scale ozone generator was used for ozonating raw waters using high grade oxygen. The ozonated stream was directed into a contactor filled with raw waters. After ozonation, the raw waters were tested for TOC concentration, colour, UVA and THMFP. Four raw water samples were used. Results showed that at 1 mg O_3/mg TOC, the THMFP removal ranged from 24-36 %, colour removal ranged from 77-93 %, UVA removal ranged from 44.4-65.2 % and TOC removal ranged from 1.6-11.2 %. The removal of colour as a function of ozone dosage shows that the relationship is a hyperbolic function curve. The colour reduction per unit dose of ozone diminishes with increasing dosage.

Keywords ozonation – colour – THMFP – TOC – UVA

INTRODUCTION

Most water treatment plant (WTP) uses chemical physical method to remove raw water colour and turbidity and other parameters. The average percentage removal for colour, UVA, THMFP and TOC using aluminum sulfate as coagulant are 82%, 68%, 57% and 41%, respectively [1]. A comparison study was carried out using ozone as an agent to remove colour and turbidity. Ozone is a very strong oxidant. It is frequently used in water treatment for taste and odour control, colour removal and disinfection [2-4]. It is very unstable in solution. Its disinfection and oxidation potentials are caused by splitting off the third atom on the breakdown of molecules. The reaction is promoted by pH values above 7.

Ozone is produced in an ozone generator when an oxygen-containing gas is subjected to a high voltage alternating current across a discharge gap. A concentration of 1 to 3 percent ozone is generated with air as feed gas. On the other hand, 2 to 6 percent could be expected with oxygen as the feed gas. At room temperature the solubility of ozone in water exceeds the solubility of that of oxygen. Ozone boils at –122°C at atmospheric pressure. The rate of decomposition of ozone in aqueous solution depends on solution pH, temperature, and number of parameters which are difficult to control. The efficiency of ozonation, i.e. the amount of ozone transferred to the water divided by the amount of ozone in the gas fed to the contactor, is dependent on ozone concentration at the output, temperature and the contact area between gas and liquid phase.

In practice ozone transfer usually involves chemical reaction as well as physical absorption. Iron, manganese and other heavy metals ions that occur in raw water either as discrete ions or complexes with large organic molecules such as humic acids can be precipitated by the oxidative action of ozone. The effects of ozonation on humic substances include the formation of hydroxyl and carboxyl group, loss of double bonds and aromaticity and conversion of high molecular weight into lower range [5]. The reactions then form aldehydes, ketones and carboxylic acids. Then the rate of oxidation reaction with organic molecules in water is very low, hence

direct elimination by mineralisation is negligible. The extent of trihalomethane formation potential or THMFP reduction by ozonation depends on the ozone contact time and applied dosages. Most treatment plants employ filtration after ozonation. This reflects the theory that ozonation converts high molecular weight organic matter into smaller species which are more degradable.

The removal of THMFP by ozonation alone is between 5 to 20 percent at ozone doses typically used in practice (0.4-1.2 mg O_3/mg TOC) [4]. With an ozone dose of 2 mg O_3/mg TOC the removal of DBP precursors with preozonation and biodegradation removes up to 50 percent THM precursors [6]. Using high ozone dosage coupled with substantial bromide concentration favours the conversion of bromide into bromate. Besides bromate, ozonation can produce bromoform too. This is one drawback of ozonation of water containing bromide. Possible solutions are ozonating at lower pH, addition of ammonia before ozonation and reducing the bromine concentration. Changing ozonation pH from 8 to 6 results in a significant bromate reduction (about 79 %) [7]. Lowering the pH during ozonation could result in lower bromate formation but increase bromoform formation [8]. The production of bromoform and bromate increased with increasing TOC from 5 to 9 mg/L. This could be due to insufficient ozone for the formation of HOBr and thus lower bromoform production. The addition of hydrogen peroxide during ozonation reduces the formation of bromoform significantly while it increases bromate formation. Once bromate is formed, the possible ways of removing it are chemical reduction and physical or chemical retention. Bromate can be reduced by sulphite with a ratio of 1:6 bromate:sulphite [9]. There are three main options to retain bromate: resins adsorption, GAC adsorption and membrane filtration using nanofiltration or reverse osmosis.

MATERIALS AND METHODS

A small scale ozone generator was used for ozonating raw water. Four samples of raw water were used in this bench scale study. The ozone generator (Microzone Ozone Generator series GSG, manufactured by Sorbius of Germany) employed Otto-plate technique to produce ozone. The feed gas was oxygen with flow rate set to 25 L/hour and the pressure at 0.5 bar. The ozonated stream was directed into a head space of 210 mm high x 100 mm diameter PVC ozone contactor of 2-litre capacity. Both ends of the contactor were sealed with PVC end caps having attached connectors. The top connector acted as gas inlet and the bottom connector as the sample outlet. A side tube was connected to the bottom connector and acted as an overflow chamber. A three ways valve was attached at a short distance from the top connector. It directed the ozone either to the contactor or ozone reduction system. The ozone reduction system consisted of three Drechsel bottles connected in series and containing potassium iodide solutions. Prior to the ozonation tests, the generator was checked for ozone production efficiency using indigo solution.

Before the generator was switched on, the system was purged with oxygen. The same flow pattern was maintained when the generator was switched on. After 5 minutes in operation, the ozone was directed to the contactor. Once the amount of ozone required was delivered to the vessel head space, the valve was turned to divert the ozone flow to the ozone reduction system and the generator was turned off. The contactor was then disconnected from the ozonation system and mixed vigorously by a rotational movement over a contact time of 5 minutes. The sample was then tested for TOC, colour, UVA and residual ozone. THMFP tests were carried out on both the pre and post ozone treated samples.

Total organic carbon concentration (TOC) measurement was conducted using persulfate-ultraviolet oxidation method using ASTRO 2001 system carbon analyzer. Ultraviolet light absorbance (UVA) was measured at 254 nm using 1 cm quartz cell and UV-visible spectrophotometer. Colour measurement was conducted using spectrophotometer method at 460 nm. In this study, THMFP test (a test to measure the potential of water to produce trihalomethane upon chlorination) involved 7 days incubation at 25°C, pH adjusted to 7 and applied chlorine dose three times the TOC. A liquid-liquid extraction method was used to measure the concentration of THM in the water. The extraction solvent was n-pentane at a ratio of sample to extraction solvent of 10:2. The THM concentration was measured by injecting 1 microlitre of the supernatant pentane extract into a gas chromatograph (Shimazu GC – 17A) equipped with nickel electron capture detector.

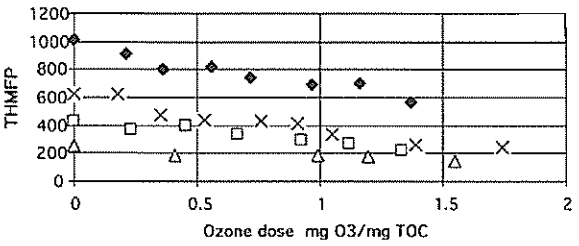

Figure 1. Influence of ozone on THMFP. Δ SSF 1, × LG, ♦ LT, □ BU.

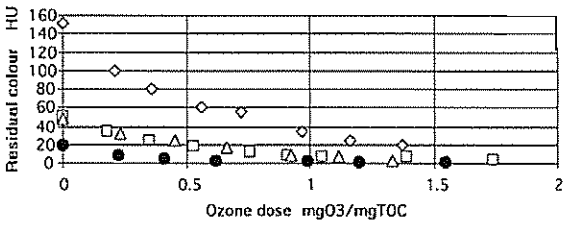

Figure 2. Influence of ozone dose on colour of water. • SSF 1, □ LG, ◊ LT, Δ BU.

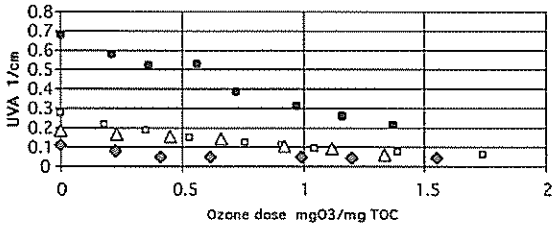

Figure 3. Influence of ozone dose onUVA. ♦ SSF 1, □ LG, ■ LT, Δ BU.

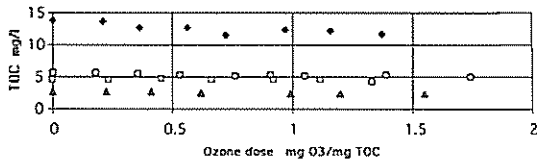

Figure 4. Influence of ozone dose on TOC. ▲ SSF 1, ○ LG, ♦ LT, □ BU.

RESULTS AND DISCUSSION

Figure 1 shows the influence of ozone dosage on THMFP. The results show that there was significant reduction in THMFP by ozonation. The percentage removal ranges from 24 to 36.4 %. This is much higher than reported [4, 6]. One possible reason is that the ozone dosage used in this study was high, 4.2 to 13.5 mg O_3 /L.

Figure 2 illustrates the effects of ozonation on colour of water. The percentage reduction ranged from 77 to 93 %. When a solution is ozonated, its colour and UVA are reduced. Colours in raw water are normally caused by the presence of high atomic molecular weight conjugated natural organic matter (NOM). When ozone reacts with NOM, the conjugation is disrupted by the oxidation process and the colour disappears. These compounds also absorb UV light. Hence modification of this compound also causes reduction in UV absorbance (Fig. 3). The UVA reduction ranged from 44 to 65 percent.

In the case of TOC removal, the percentage ranged from 0 to 11.2 % (Fig. 4). The experimental results show that very little TOC reduction was achieved with ozonation ranging from zero to 17 percent. Sample LT showed the best TOC removal. This sample contained a high proportion of vegetation-derived organic matter which is more susceptible to oxidation. The higher TOC reduction demonstrates that some mineralisation did occur. This is due to ozone reaction with organic carbons and their oxidation to carboxylic acids and eventually to CO2.

CONCLUSION

Reduction of colour, UVA, TOC and THMFP by ozone at a dosage of 1 mg O_3/mg TOC is listed in Table 1. Ozonation preferentially removed colour first, folllowed by UVA then THMFP and finally TOC. It can destroy some THMFP precursors directly without removing TOC. Overall, ozone is effective in reducing colour and UVA, but has a relatively minor effect on TOC reduction.

Table 1. Influence of ozonation on colour, UVA, TOC, THMFP removal at 1 mgO_3/mg TOC.

Parameter	Percentage removal range (%)	Mean (%)
Colour	77 – 93	84
UVA	44.4 – 65.2	55.6
TOC	1.6 – 11.2	8.1
THMFP	24 – 36.4	29.4

REFERENCES

1. Chua K.H. (2001) Removal of colour, UVA, TOC, and THMFP by alum coagulation. *Proceedings, Malaysian Science and Technology congress, 2001.*

2. Cameron D. (1982) *Preozonation and slow sand filtration for the removal of humic colourisation from water*. Thesis submitted to QUB for the degree of MSc (October 1982).
3. O'Donovan (1965) Treatment with ozone. *Journal of AWWA* **57**(9): 1195.
4. Ferguson et al. (1991) Applying ozone for organic control and disinfection: a utility perpectives. *Journal of AWWA* **83**(5):32.
5. Goel *et al.* (1995) Biodegradation of NOM: Effect of NOM source and ozone dose. *Journal of AWWA* **87**(1): 90.
6. Speitel *at al.* (1993) Effects of ozone dosage and subsequent biodegradation on removal of DBP precursors. *Journal of AWWA* **85**(5): 86.
7. Symons J.M. at al. (1994) Precursor control in waters containing bromide. *Journal of AWWA* **86**(6): 48.
8. Siddiqui M.S. and Amy G.L. (1993) Factors affecting DBP formation during ozone-bromide reactions. *Journal of AWWA* **85**(1): 63.
9. Ciba *et al.* (1993) Available techniques for reducing bromate in drinking water. *JWSA Proceedings from JWSA-international Workshop on Bromate and Water treatment, Paris, 1993.*

Journal of Science and Technology in the Tropics (2007) 3: 101-105

An instrumentation technique in site selection of gravitational wave observatory: The study of geological structure to influence seismic noise level

K. K. Chong [1], B. H. Lim[2], C. S. Lim[2] and Y. T. Chen[2]
[1]Faculty of Engineering and Science, Universiti Tunku Abdul Rahman, Off Jalan Genting Klang, Setapak, 53300 Kuala Lumpur, Malaysia
[2]Department of Astronomy and Applied Physics, University of Science and Technology of China, China
(Email: chongkk@mail.utar.edu.my)

Received 23.07.2007; accepted 06.11.2007

Abstract While most of the gravitational wave observatories are constructed either under the ground or outer space in order to reduce seismic noise, Tianyin-100 is located on top of a stable and thick clay hill, which has long been spotted to be a good damper for the ground activities. An instrumentation technique of measuring seismic noise level and the results of the measurement are reported in this paper.

Keywords seismic noise – gravitational wave detector – mechanical damper – geological structure – accelerometer

INTRODUCTION

There are many sources of ground noise, i.e., elastic surface waves in the ground; man-made sources (such as factories, trains, airplane and human activities); meteorological sources (such as atmosphere turbulence and winds on building and trees) which are in a high frequency range of 1-100Hz; etc [1]. Obviously, with such a wide variety of potential noise sources, the level of seismic noise can vary greatly from place to place. Measurement of the seismic spectrum at the frequency greater than 0.5 Hz has been carried out by many researchers. It seems that the levels of seismic noise in the vertical and horizontal direction are essentially of the same order of magnitude. One fairly consistent finding at reasonably quiet sites is that the linear spectral density of displacement in each dimension appears to vary to a good approximation as $1/f^2$. Thus, the root mean square (r.m.s.) spectral displacement can be sufficiently well approximated by the formula

$$\delta x = \frac{a}{f^2} \ \mathrm{m(Hz)}^{-\frac{1}{2}} \qquad (1)$$

where $a \cong 10^{-6}$ to 10^{-8} at the earth surface in a relatively quiet place. Ground noise measurement at 1 Hz – 1 kHz range for some gravitational wave detection groups are listed in Table 1 [2-9].

Table 1. Seismic noise level at various locations of gravitational observatories around the world measured in spectral displacement density.

R.M.S. spectral displacement density	Location
$(3\times10^{-7}/f^2)$ m(Hz)$^{-½}$	Garching
$(1\times10^{-6}/f^2)$ m(Hz)$^{-½}$	Pisa
$(3\times10^{-6}/f^2)$ m(Hz)$^{-½}$	Glasgow
$(1\times10^{-7}/f^2)$ m(Hz)$^{-½}$	Mitaka (TAMA300 site), Japan
$(1\times10^{-7}/f^2)$ m(Hz)$^{-½}$	MIT laboratory, USA.

Following its predecessor Tenko-100 from the Institute of Space and Astronautical Science (ISAS) of Japan, a prototype gravitational wave observatory Tianyin ("sound from heaven")-100 is built in the campus of Universiti Technologi Malaysia. Tianyin-100 is a delay-line type of laser interferometer with two arms of 100 meters long. Similar to the projects of LIGO-4km, GEO-600, TAMA-300 and other gravitational wave detectors, the site location is one of the most important factors to lower the seismic

noise level and hence to improve the sensitivity of the laser interferometer [2-9]. Although an extra mechanical isolation system is normally designed to suppress the seismic noise level, there is no doubt that the advantage of the site with lower seismic noise can result a lower overall noise level of the detector compared to the site with higher seismic noise. Many places have been considered to ensure the minimal seismic ground noise. Tianyin-100 is located at an isolated forest area, 5 km away from the highway, 2 km away from the main road and 30 km away from the nearest sea. In addition of that, we have also carefully studied the influence of geological structure to the level of seismic noise.

We installed the interferometer on top of a stable hill. Civil engineering work has been carried out to flatten the hill to make a plateau to install the 100m × 100m arms. The hill where Tianyin-100 is located is purely composed of beds of clay. The height of the hill is about 50m from the nearest ground. The idea is based on Alan Cook's comment that a large scale of soil structure could act as a damping medium to filter out vibration. The structure of the site will therefore help to reduce the possible seismic disturbance whether it is from man made activities or geologically associated, e.g., orogeny, oscillation of the earth, ocean wave, etc [10]. First seismic measurement was done in the year 1998 to study the effect of a specially designed isolated block for its effectiveness in the seismic noise isolation and the data was presented in the International Meeting on Frontier of Physics [11]. In this paper, we will discuss more detail about seismic noise measurement technique. The significant of this paper is to study the effect of the clay hill in the seismic noise isolation and therefore seismic measurement was made at the top of the hill and that of the foot of the hill for comparison.

INSTRUMENTATION TECHNIQUE FOR SEISMIC NOISE MEASUREMENT

TEAC 710Z, a wide-band (0.02-200 Hz), high sensitivity (3000 mV/g) tri-axial piezoelectric type accelerometer has been used to detect the ground surface displacement. The electrical signal generated by the accelerometer is gained up 200 times by a DC amplifier (TEAC SA-16P) before sending to a Fast Fourier Transform (FFT) Network Analyzer (HP35665A) for spectral analysis. In order to achieve optimal performance of an accelerometer, it is necessary for us to ensure that

a. An accelerometer has been mounted rigidly on the surface under test (the contact plane shall be as clean and flat as possible);
b. The mounting introduces minimum distorting motions of its own (for example, a simple symmetrical mounting is the best);
c. The mass of the accelerometer and mounting are small in comparison with that of the structure under test.

There are two significant considerations in making a good seismic noise measurement. Firstly, the output of an accelerometer is an acceleration, which has to be integrated twice in order to get a displacement signal. The second consideration is that the seismic noise spectrum obtained from FFT network analyzer, consists of points that are linear in frequency. When the points are plotted in logarithmic frequency axis, each point tends to depart from its neighboring points at the low frequency region, causing a loss of precision. It is because, for an identical span widths and display resolution points, frequency resolution for both linear and logarithm scale is identical. Thus, the precision of the spectrum at lower frequency of logarithmic scale is worse.

Since the raw output of an accelerometer is an acceleration signal, double integration over the acceleration signal has to be made to generate displacement signal. The Fourier Transform of integration is essentially a division of the angular frequency, jw. Hence, for the first problem, the spectral density of seismic displacement can be computed by dividing each acceleration point by a factor proportional to the square of the corresponding frequency, f [12]. There are indeed many acceleration-displacement conversion methods being designed in the commercial accelerometer package. Some commercial spectrum analyzers come with a couple of built-in functions through which the input spectrum can be integrated or differentiated once or twice, by a simple division or multiplication in the frequency domain. On the other hand, a modern charge-preamplifier (duel with the charge-coupled type accelerometer) equipped with three operations mode: linear (acceleration), single integration (velocity) and double integration (displacement). Nevertheless, we have employed a different approach to do the task. We made use of the spectrum analyzer to acquire the spectrum of the ground acceleration. Then, we save every point of the spectrum into a Standard Data

Format (SDF) file, from which the raw data is then retrieved, rearranged and doubly integrated by using computer software. The SDF Utilities programs are installed to translate data files from the HP35665A analyzer to formats compatible with ASCII, PC-MATHLAB or MATRIXx. Then, Microsoft Excel is used to import the data and to manipulate it by performing some simple arithmetic where every point is divided by $(2\times\pi\times f)^2$ to obtain a displacement spectral density.

As to solve the second problem, different frequency spans of FFT network analyzer are used when the seismic displacement spectral density measurements are taken. For example, we choose frequency bands of 0.094-1.656 Hz, 1.0-13.5 Hz, 10.0-60.0 Hz, 50.0-100.0 Hz and 100-200 Hz with 800 resolution points for each frequency span. The total data collection time for the selected frequency spans is approximately three hours. In that case, we have ensured the surrounding condition, so that it is free from any unnecessary disturbance nearby during the measurement time. Later, the extracted raw data for different frequency spans are combined together accordingly to reproduce a new spectral density in the range of 1 Hz to 100 Hz and 200 Hz. By doing this, we can significantly increase the spectral resolution, especially at the low frequency portion. Finally, the combined data can thus be easily manipulated as well as plotted using Microsoft Excel. By employing such a digital data processing method to the seismic displacement spectrum, the resolution at lower frequencies will be on par of the higher frequencies.

RESULTS AND DISCUSSION

Seismic noise measurement instrument has been set-up for data collection since 12 October 1999 and the seismic data was continuously taken for a year at the hilltop (the site of Tianyin-100) and at the foot of the hill for comparison. The spectral density curves of seismic noise are almost the same for different day over the year. Figure 1 shows the spectral density curve at Tianyin-100 site. The relationship between the amplitude and the frequency very well follow the formula as

$$\delta x = \frac{10^{-8}}{f^2} \ \mathrm{m(Hz)}^{-\frac{1}{2}} \qquad (2)$$

From Figure 1, the curve at the site (hilltop) is smooth and has fewer peaks than the curve at the foot of the hill. The improper electrical grounding causes the harmonics of power line frequency, such as the 25 Hz peak and the 50 Hz peak on the displacement spectral density curve at the site.

By comparing the seismic noise curve at the site and the foot of the hill, we found that the seismic noise level on the hilltop is 10 dB (5 times) lower than that at the foot of the hill for frequency range below 50 Hz (see Fig. 1). Whereas, for the frequency range of 50-

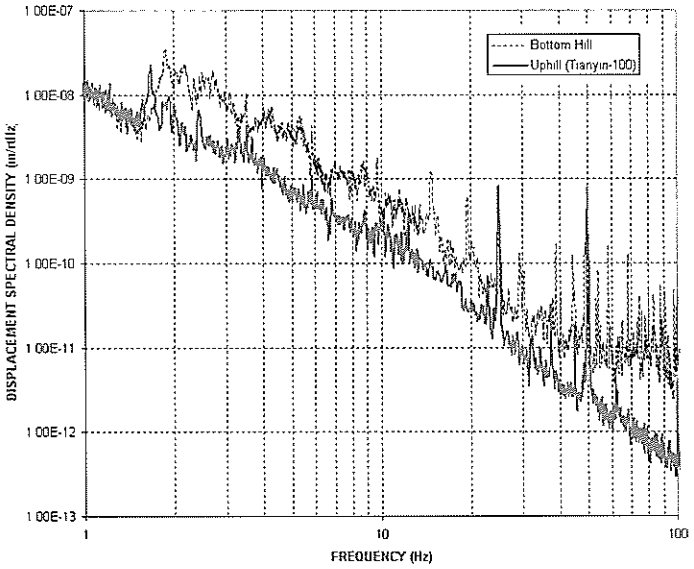

Figure 1. Horizontal seismic noise at uphill (Tianyin-100) and bottom hill (frequency axis in logarithm scale with range of 1 to 100Hz).

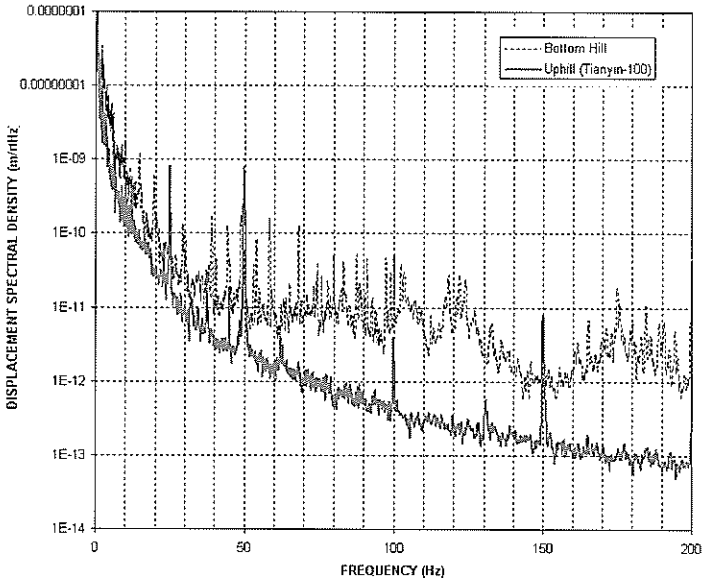

Figure 2. Horizontal seismic noise at uphill (Tianyin-100) and bottom hill (frequency axis in linear scale with range of 0 to 200Hz).

200 Hz, it is 20 dB to 40 dB (10 to 100 times) lower (see Fig. 2). The difference of the noise level between these two locations is due to two types of amplitude losses. One is the effect of geometrical spreading that produces a diminution of amplitude without loss of seismic energy. In the homogeneous medium, wave fronts are spheres whose surfaces vary as the square of the radius. Thus, the diminution of amplitude is due to the spreading of the same energy over the wider surface, resulting in a reduction of energy per unit surface but the total energy remain unchanged. The other type of loss is frequency selective absorption. As the seismic wave propagates through the earth, it loses its higher frequencies and the earth acts as low pass filter. Over a fixed distance, a high frequency disturbance goes more cycles than a low frequency so that if the loss can be expressed in dB per cycle or wavelength, the attenuation is greater for higher frequency. Besides of the amplitude losses, the refraction and reflection effect at interface between two types of soil medium (hilltop and the foot of the hill) also reduces the transmission of seismic vibration to our site [13].

CONCLUSION

The location of Tianyin-100 on the clay hill about 50 m above the ground enjoys a good isolation from seismic noise. It is found that there is about 10 dB attenuation for noise below 50 Hz, and 20-40 dB attenuation for noise between 50-200 Hz. The r.m.s. spectral displacement density of our site is approximately $(1\times10\text{-}8/f\ 2)$ m(Hz)–½.

Acknowledgements – The authors would like to thank K. Kawamura (TEAC Corporation) and Y.H. Cheng (Bruel & Kjaer) for providing the technical information of instruments.

REFERENCES

1. Chen Y.T. and Cook A. (1993) *Gravitational Experiments in the Laboratory*. Cambridge Univ. Press.
2. Stochino A., DeSalvo R., Huang Y. and Sannibale V. (2007) Improvement of the seismic noise attenuation performance of the Monolithic Geometric Anti-Spring filters for gravitational wave interferometric detectors. *Nuclear Instruments and Methods in Physics Research Section A: Accelerators, Spectrometers, Detectors and Associated Equipment* **580**(3): 1559-1564.
3. Takamori A., Raffai P., Márka S., DeSalvo R., Sannibale V., Tariq H., Bertolini A., Cella G., Viboud N., Numata K., Takahashi R. and Fukushima M.

(2007) Inverted pendulum as low-frequency pre-isolation for advanced gravitational wave detectors. *Nuclear Instruments and Methods in Physics Research Section A: Accelerators, Spectrometers, Detectors and Associated Equipment* **582**(2) 683-692.

4. Braccini S., Barsotti L., Bradaschia C., Cella G., Di Virgilio A., Ferrante I., Fidecaro F., Fiori I., Frasconi F., Gennai A., Giazotto A., Paoletti F., Passaquieti R., Passuello D., Poggiani R., Campagna E., Guidi G., Losurdo G., Martelli F., M. Mazzoni M. et al. (2005) Measurement of the seismic attenuation performance of the VIRGO Superattenuator. *Astroparticle Physics* **23**(6): 557-565.
5. Bertolini A., Cella G., Chenyang W., de Salvo R., Kovalik J., Márka S., Sannibale V., Takamori A., Tariq H. and Viboud N. (2001) Recent progress on the R&D program of the seismic attenuation system (SAS) proposed for the advanced gravitational wave detector, LIGO II. *Nuclear Instruments and Methods in Physics Research Section A: Accelerators, Spectrometers, Detectors and Associated Equipment* **461**(1-3): 300-303.
6. Blair D.G. (1991) *The Detection of Gravitational Waves*. Cambridge Univ. Press.
7. VIRGO (1989) Proposal for the Construction of a Large Interferometric Detector of Gravitational Waves.
8. Giazotto A. (1997). *Proceedings of the TAMA Workshop on the Gravitational Wave Detection* p.193-202. Universal Academy Press Inc., Tokyo.
9. Fritschel P. and Whitcomb S. (1997) *Proceedings of the TAMA Workshop on the Gravitational Wave Detection* p.137-146. Universal Academy Press Inc., Tokyo.
10. Chen Y.T., Kawashima N., Othman M., Chia S.P., Karim M., Sanugi B., Lim B.H. and Chong K.K. (1999) Gravitational Wave Detection in the Laboratory. *Proceeding of the International Meeting on Frontiers of Physics 1998* p. 632-645. World Scientific Publishing Co. Pte. Ltd.
11. Chong K.K., Lim B.H., Kawashima N. and Chen Y.T. (1999) Measurement of Seismic Noise at the Site of Tianyin-100 in UTM. *Proceeding of the International Meeting on Frontiers of Physics 1998* p. 657-662. World Scientific Publishing Co. Pte. Ltd.
12. Broch J.T.(1980) *Mechanical Vibration and Shock Measurements*. Bruel & Kjaer Publication.
13. Pieuchot M. (1984) *Handbook of Geophysical Exploration* Vol. 2, Section 1. Geophysical Press.

Journal of Science and Technology in the Tropics (2007) **3:** 107-113

The optimization of digital circuit design using evolutionary algorithm

K. H. Chong[1], I. B. Aris[2], M. A. Sinan[2] and B. M. Hamiruce[2]
[1] Department of Physic & Science, Faculty of Engineering & Science, Setapak Campus,
Universiti Tunku Abdul Rahman, Jalan Genting Klang, Setapak, 53300 Kuala Lumpur, Malaysia
[2] Department of Electrical & Electronics Engineering, Faculty of Engineering,
Universiti Putra Malaysia, 43400 UPM Serdang, Selangor, Malaysia
(Email: chongkh@mail.utar.edu.my)

Received 17.07.2006; accepted 05.07.2007

Abstract Evolutionary Electronic (EAs) covers all the applications involving the use of Evolutionary Computation in electronic system's design. It is largely applied to complex optimization problems. EAs is able to sample many possible solutions in order to find the most optimal solution to satisfy the specifications, even the numbers of solutions sampled is insignificant compared to the search space which contains huge size of solutions. EAs introduces a new idea for automatic design of electronic systems; instead of imagine model, abstractions, and conventional techniques, it uses search algorithm to design a good circuit.

In this paper, a new method for automatic optimization of digital circuit design method has been introduced. This method is based on randomized search techniques mimicking natural genetic evolution. The proposed method is an iterative procedure that consists of a constant-size population of individuals, each one encoding a possible solution in a given problem space.

The structure of the circuit is encoded into one-dimensional genotype as represented by a finite string of bits. A number of bit string is used to represent the possible logic gates. The structure of gates is arranged in a *m* * *n* matrix form.

The numerical results have shown that this method can produce the circuit design based on user specified performance requirement. The representation approach also has been implemented with a computer program which can give a better achievement in terms of quality solution and speed of convergence.

Keywords digital structure design – evolutionary algorithm – optimization – genetic algorithm

INTRODUCTION

Evolutionary Algorithm (EA) has been widely applied to complex optimization problems [1]. One of the applications can be presented as the nation of structure design for the digital circuit. EA was used to conceive arrangements of digital gates that could solve a specific problem, such as the parity function. This idea was highly original, since the evolutionary algorithm is performed through automatic circuit design from scratch; no human knowledge was needed.

Genetic Algorithm (GA) is one of the search techniques of EA. GA search technique was founded by Holland [2] and extensively applied into optimization tasks by Goldberg [3]. GA is a stochastic search method that mimics the metaphor of natural biological evolution. It operates on a population of potential solutions applying the principle of survival of the fittest to produce better approximations to a solution. At each generation, a new set of approximations is created by the process of selecting individuals according to their level of fitness in the problem domain and breeding them together using operators borrowed from natural genetics. This process leads to the evolution of populations of individuals that are better suited to their environment than the individuals that they were created from, just as in natural adaptation.

The conventional digital circuit design is a very complex task which requires much knowledge in domain-specific rules [4]. The design procedures

involve the process of choosing the suitable gate types to match the logical specification, and minimizing and optimizing the Boolean representation with respect to the user defined constraints.

The application of GA in combination logic design was proposed by Louis [5]. In his work, he combined GA with knowledge-based systems and used masked crossover operator to solve the combination logic circuit. Masked crossover operator removes the bias towards short schemas representation of the solution. The probability of disruption of schema is dependent on the masks. The bit positions in both parent masks corresponding to the schema can be combined to disrupt the schema in the following generation. His method can solve the functional output for the combination logic but does not emphasize on the optimization of the gate usage.

A combination technique of case-based reasoning (CBR) and GA was proposed to design the parity checker [6]. This approach borrows ideas from CBR, a problem solving paradigm in many respects; it is able to utilize the specific knowledge of previously experienced and concrete problem situations. A new problem is solved by finding a similar past case, and reusing it in the new problem situation. CBR also is an approach to incremental, sustained learning, since a new experience is retained each time a problem has been solved, making it immediately available for future problems [7]. When combining GA and CBR, appropriate cases are injected into an initial population and run the genetic algorithm. The injected cases guide a GA's search, by providing domain information learned from a previous search and consequently improve the current search.

Fuzzified Simulation Evolution (SimE) Algorithm for combination digital logic design uses two fitness operators for functional fitness and objective fitness [8]. The functional fitness called Multilevel Logic Based Goodness Measure is based on the assumption that the higher the level of a gate in a multilevel logic circuit, the more minterms are covered at the output of that gate. Therefore, the goodness of a gate is affected by the number of minterms covered at its output and the level where the gate is located. Besides targeting the correctness of the output, some other parameters are being considered. The first parameter is the area used by the number of gates per system. The second parameter is the propagation delay of signals in the circuit which consists of two elements, switching delay of gates and interconnection delay. The overall circuit delay is determined by the delay along the longest path. The third parameter is the power consumption dissipated by the number of gates per system. This research emphasises on the objective fitness which includes the measure of the quality of solution in terms of optimization of area, delay and power consumption.

METHODS

In this work a selected optimisation method is based on a GA. GA is an adaptive heuristic search algorithm premised on the ideal of natural evolution. The basic concept of GA is designed to simulate processes in natural system necessary for evolution, specifically those that follow the principles first laid down by Darwin of the survival of the fittest.

GA works by creating many random solutions to the problem at hand. These solutions will be subjected to an imitation of the evolution of species. All these solutions are encoded as genetic chromosomes and they go through the process of mating. The offspring generated will include some solutions that are better than the original.

The proposed approach is used to design the digital circuit; which is the solution inside the block in Figure 1. The digital circuit can generate the output binary bits based on the minterm defined by the user. The input signals are represented by I and the output signals are represented by O. For the m input bit circuit, there are 2^m of possible input combination signals. Therefore, there are 2^m sets of output signals that will be produced at the output bit as well. The

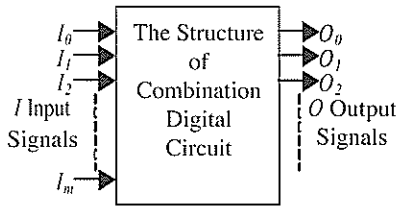

Figure 1. Block representation of combination digital circuit structure.

Table 1. Logic gates epresentation.

Bit representation	Gate representation
0	Wire 1
1	Wire 2
2	XOR
3	XNOR
4	NAND
5	NOR
6	AND
7	OR

proposed approach is able to design the combination of logic gates to produce the desired output bits with the optimum number of gates used.

The combination of gates inside the block are encoded into a string of chromosome bits and subjected to the process of GA. A two-dimension phenotype is encoded into one-dimension genotype as represented by a finite string of decimal bits. Each decimal bit represents a type of logic gate. The numbers from 0 to 7 are used to represent 6 types of possible logic gates and two wire connections between the gates (Table 1). Every logic gate has two inputs and one output terminal.

The structures of gates are arranged in $G_{x,y}$ matrix form in which x represents the gate in row and y represents the gate in the column. The m inputs are connected to y column of the logic gates. The possible input combination is based on 2^m. The output constraint signal is obtained at $y+n$ column of the logic gates; n is the number of columns.

$$\begin{bmatrix} G_{x,y} & G_{x,y+1} & G_{x,y+2} & \cdots & G_{x,y+n} \\ G_{x+1,y} & G_{x+1,y+1} & \cdots & & G_{x+1,y+n} \\ G_{x+2,y} & \cdots & & & \\ \vdots & & & & \\ G_{x+m,y} & G_{x+m,y+1} & \cdots & & G_{x+m,y+n} \end{bmatrix} \quad (1)$$

We define that $G_{x,y+1}$ gate always obtains one signal from the output of $G_{x,y}$ gate and another signal from $G_{x+1,y}$ gate, while $G_{x+m,y+1}$ obtain the signals from the output of $G_{x+m,y}$ and $G_{x,y}$. The system process is started with the random generation of initial population. The length of the chromosomes depends on the size of the entire structure. The number of bits in the chromosomes represents the type of gate. The collection of all individuals of the cell represents a solution.

The algorithm for the proposed system is as follows:

```
begin
    create a random initial population N;
    evaluate the fitness of each chromosome in the
    population;
    while (there is no design with error = 0) do
        conduct selection, crossover and
        mutation
        replace the old generation by the new
        generation of designs
        re-evaluate fitness of the designs in the
        population
    end while;
    decode the chromosome with error = 0
end
```

The design with zero error indicates that all output bits satisfy the defined minterm. Otherwise the design of the circuit structure deviates from the performance specification. To eliminate the error, the circuit structure design needs to be modified through crossover and mutation operators. Crossover is a randomized approach to exchange information between two chromosomes. Crossover operation creates a variation in the population by producing offspring that have some parts of both parent's genetic material. The new population replaces the existing population. Therefore, a new set of circuit structure is generated and the fitness evaluation is executed again. Mutation is an approach to prevent the solutions in the population falling into a local optimum. Mutation randomly changes the offspring that resulted from crossover.

The fitness of the process is the correctness of the obtained logic circuit output bits in matching the user defined output bits; in other word, the error is zero. In this work, we proposed a fitness function called Constraint Fitness. The Constraint Fitness is based on the comparison of circuit output with the constraint output. The formula for Constraint Fitness (CF) is:

$$F_C = \frac{1}{1 + error} \quad (2)$$

$$error = \sum_{o=1,2,3,\ldots,2^m}^{m} |c_o - f_o| \quad (3)$$

Table 2. Error and constraint fitness evaluation for a 3-bit digital circuit.

Output bit	c_o	f_o	$\lvert c_o - f_o \rvert$
O_0	1	1	0
O_1	0	1	1
O_2	0	0	0
O_3	0	0	0
O_4	1	1	0
O_5	1	0	1
O_6	0	1	1
O_7	0	0	0
Error			3
F_c			0.25

Journal of Science and Technology in the Tropics (2007) **3**: 65-68

Reproduction by queens and gamergates in the Oriental ponerine ant *Pachycondyla* (= *Ectomomyrmex*) *leeuwenhoeki* var. *sumatrensis* Forel

Fuminori Ito[1], **Yohei Ikeshita**[1,2], **Ayako Gotoh**[1] **and Rosli Hashim**[3]
[1]Laboratory of Entomology, Faculty of Agriculture, Kagawa University, Ikenobe, Miki 761-0795, Japan
[2]Higashisakamoto 3573-15, Hanzan, Marugame 762-0081, Japan
[3] Institute of Biological Sciences, University of Malaya, 50603 Kuala Lumpur, Malaysia
(Email: ito@ag.kagawa-u.ac.jp)

Received 08.10.2007; accepted 22.10.2007

Abstract Colony composition and behavioural characteristics of the Oriental ponerine ant *Pachycondyla* (= *Ectomomyrmex*) *leeuwenhoeki* var. *sumatrensis* Forel were investigated in Ulu Gombak, Peninsular Malaysia. The species is AQ+G type: sexual reproduction was performed by dealated queen (seven colonies) or mated worker (eight colonies). All colonies were monogynous with one mated egg-laying female. Colony size was very small with a handful of workers. In both the gamergate and queen colonies, dominance interactions were very rare but frequent aggressions were observed in orphan colonies. The most dominant worker in an orphan subcolony mated with a male. Alpha worker of the other orphan subcolony was intensively attacked by workers of the mother colony when the subcolony was merged to the mother colony.

Keywords *Pachycondyla leeuwenhoeki* – ponerine ant – reproduction – gamergates

INTRODUCTION

Ants in the subfamilies Amblyoponinae, Ectatomminae, and Ponerinae show remarkable diversity in reproductive structure of colonies [1-3]. Most species show sexual reproduction only by morphologically distinctive queens. However, some species reproduce by mated and egg-laying workers (gamergates) without queens. Furthermore, sexual reproduction by both queens and gamergates is also known in other species [1, 3]. In the species with gamergates, the mechanism regulating reproduction among workers varies greatly. However, the significance of the diversity of reproductive regulation is still unknown. We still need information on the biology and behaviour of several gamergate species.

The ponerine genus *Pachycondyla* has many gamergate species [1, 3]. In the Oriental tropics, the colony composition and regulation of reproduction has been demonstrated for only *Pachycondyla* (= *Bothroponera*) sp. [4, 5]. In this paper, we report colony composition and behavioral characteristics of *P.* (= *Ectomomyrmex*) *leeuwenhoeki* var. *sumatrensis* collected in Malaysia.

MATERIALS AND METHODS

All colonies were collected from decayed woods on the forest floor or under the soil in Ulu Gombak, Peninsular Malaysia (Table 1). Adult females of all but three colonies were dissected just after collection to determine the reproductive condition. Three colonies (FI92-MG515, FI99-282, AG07-25) were kept in a laboratory. All adult individuals were marked by enamel paints (Fig. 1). Their behaviour was observed for 20 to 100 hours.

Two subcolonies consisted of six virgin workers each, were created from one gamergate colony (FI99-282) when the colony consisted of 20 workers. The behaviour of workers was observed for one hour per day until the establishment of a dominance relationship. After that, such observation was carried out once or twice a week. Three weeks after orphaning, a male that emerged in the other orphan

F_C achieves 1 when the error is zero. c_o is the constraint output set by the user and f_o is the functional output generated from the circuit. When the functional output is exactly equal to the constraint output, this will cause (3) equals to 0. Consequently, F_C will be equalled to 1 due to zero error. It is possible to get more then one string of chromosome with CF equals to 1 in a population. In order to determine the global optimum of the design, we accumulate the entire chromosomes with CF equal to 1 for further evaluation. The evaluation of error and CF is explained in Table 2.

Table 2 shows the output value of a 3-bit digital circuit that can produce 2^3 of output bits. O_1, O_5 and O_6 generate difference c_o then f_o. By substituting all values of c_o and f_o into equations (2) and (3), this produces the error value of 3, subsequently F_c equals to 0.25. The summation of error is shown as follows:

$$error = (|c_0 - f_0| + |c_1 - f_1| + |c_2 - f_2| + |c_3 - f_3| + |c_4 - f| + |c_5 - f_5| + |c_6 - f| + |c_7 - f_7|)$$

$$error = (|1 - 1| + |0 - 1| + |0 - 0| + |0 - 0| + |1 - 1| + |1 - 0| + |0 - 1| + |0 - 0|)$$

$$error = (0 + 1 + 0 + 0 + 0 + 1 + 1 + 0)$$

$$error = 3$$

Obviously, the error value shows that there are three wrongly generated bits at the output of the circuit. Error value will increase if more incorrect output bits are generated. Then, CF is obtained by substituting error value into equation (2) as:

$$F_C = \frac{1}{1 + error}$$

$$F_C = \frac{1}{1 + 3}$$

$$F_C = 0.25$$

In this work, we aim to optimise the number of gates used in the structure design. The second objective is to get the fitness of gate optimization used in the circuit design. The population for Gate Optimization Fitness (GOF) evaluation is formed by the chromosome string with CF equals to 1. Each string of chromosome is evaluated for the gate optimization fitness. The algorithm for this fitness is:

$$F_{GO} = \frac{\sum G_{F_C=1}}{\sum G_{x+m,y+n}} \qquad (4)$$

$$0 < F_{GO} < 1 \qquad (5)$$

The numerator part of (4) is the summation of the gates that produce the constraint fitness equal to 1. The denominator part is the total allowable gate per structure. The fitness of GOF should be between 0 and 1. The global optimal is achieved when the smaller value of GOF is met.

The authors used the proposed method to design a 3-bit circuit with the minterm F(a, b, c) = Σ(1, 4, 5, 7). Part of the results is illustrated in Table 3. The system evaluates the error as well as CF for each of the chromosome string. The error is equal to 6 at the early stage; this results in CF equals to 0.142857. The chromosome string is evolved through GA process to reduce the error value. Table 3 shows that error value

Table 3. The generated error and CF for each chromosome.

Chromosome						Error	CF
8	0	8	4	4	2	6	0.142857
4	6	3	1	3	4	5	0.166667
5	1	8	5	6	7	5	0.166667
2	5	1	0	4	8	4	0.200000
3	3	7	2	8	0	4	0.200000
0	8	1	1	7	2	4	0.200000
1	1	0	0	4	5	2	0.333333
7	5	1	0	9	2	2	0.333333
1	0	2	0	1	4	2	0.333333
6	4	7	8	2	2	0	1.000000

Table 4. The required number of gate and GOF for the digital circuit with F(a, b, c) = Σ(1, 4, 5, 7).

Chromosome						Output function	No. gate	GOF
5	5	4	2	5	7	$((a+b)'\oplus(b+c)')+((b+c)'+(ac)')'$	6	1
2	2	8	5	2	2	$((a\oplus b)+(b\oplus c))'\oplus((b\oplus c)\oplus c')$	6	1
6	4	5	0	3	3	$((ab)\oplus((bc)'\oplus(a+b)')')'$	5	0.8333
4	4	7	0	3	3	$((ab)'\oplus((bc)'\oplus(a+c))')'$	5	0.8333
8	3	3	8	5	2	$a\oplus((b\oplus c)+(a\oplus c))'$	4	0.6666

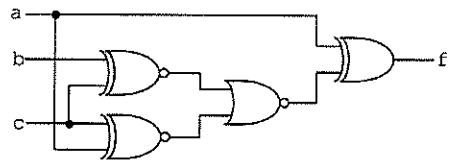

Figure 2. The schematic diagram of the digital circuit with F(a, b, c) = Σ(1, 4, 5, 7).

is getting reduced and eventually achieved zero; this makes CF equals to 1. Moreover, there are more than one combination of gates that can produce the desired output bit. The successful chromosome bits are shown in Table 4 together with the corresponding output function and GOF value. These five strings of chromosome can be decoded to the digital circuit that can produce the desired minterm. GOF is calculated using equation (4); where the value of the denominator part is 6. The last chromosome string produces lower GOF compared with others. The chromosome bits are 0 3 3 0 5 2. After the chromosome is decoded, the resulted circuit which can generate the corresponding minterm is shown in Figure 2. The output function of the circuit (Fig. 2) is $f = a \oplus (b \oplus c) + (a \oplus c))'$. The circuit needs 1 NOR, 1 XOR and 2 XNOR gates to generate the desired output bits. The design duration for this example takes 3.202825 s.

RESULTS AND DISCUSSION

The proposed system was written in MATLAB language. Experiments have been conducted using the system to investigate its effectiveness in constraint-directed logic synthesis. The results produced by the proposed approach were compared with those generated by Karnaugh Minimizer [14].

The experiments use population size N = 1000, percentage of crossover reproduction C = 70, percentage of mutation reproduction M = 10.

Seven digital circuits were designed. The following is the list of the circuit minterms:

D1: F(a,b,c) = Σ(3, 5, 6, 7)
D2: F(a,b,c,d) = Σ(0, 3, 5, 6, 9, 10, 12, 15)
D3: F(a,b,c,d) = Σ(2, 3, 5, 6, 8, 9, 12, 15)
D4: F(a,b,c,d) = Σ(1, 3, 4, 6, 9, 11, 12, 14)
D5: F(a,b,c,d) = Σ(15)
D6: F(a,b,c,d) = Σ(7, 10, 11, 13, 14, 15)
D7: F(a,b,c,d) = Σ(0, 1, 6, 7)

D1 is the 3 inputs circuit design and D2 through D7 are the 4 inputs circuit design. The results produced by the proposed method and Karnaugh Minimizer are shown in Table 5 and Table 6 respectively. The

Table 5. Result for proposed method.

D	Output function	Gates count
1	$ab + (a + b)c$	4
2	$((b \oplus c)' \oplus (a \oplus d)')'$	3
3	$(((bd) \oplus a) \oplus c)$	3
4	$b \oplus d$	1
5	$(((ab) \cdot c) \cdot d)$	3
6	$(c + (bd))(a + (c \cdot (bd)))$	5
7	$(a + (b \oplus c))'$	2

Table 6. Result for Karnaugh Minimizer.

D	Output function	Gates count
1	$ab + ac + bc$	5
2	$a'b'c'd + abc'd' + a'bc'd + ab'c'd + a'b'cd + abcd + a'bcd' + ab'cd'$	31
3	$a'cd' + a'b'c + ab'c' + ac'd' + a'bc'd + abcd$	19
4	$b'd + bd'$	5
5	$(((ab) \cdot c) \cdot d)$	3
6	$ac + bcd + abd$	7
7	$a'bc + a'b'c'$	5

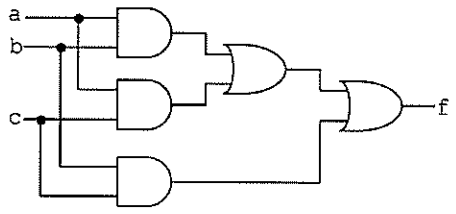

Figure 3. The schematic diagram for D1 designed by Karnaugh Minimizer.

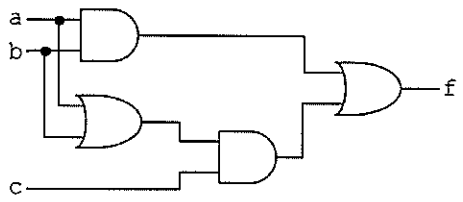

Figure 4. The schematic diagram for D1 designed by the proposed method.

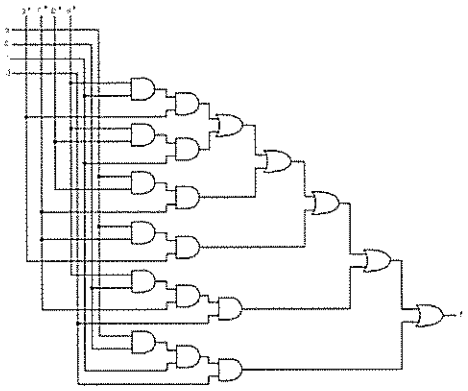

Figure 5. The schematic diagram for D3 designed by Karnaugh Minimizer.

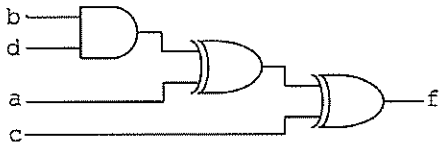

Figure 6. The schematic diagram for D3 designed by the proposed method

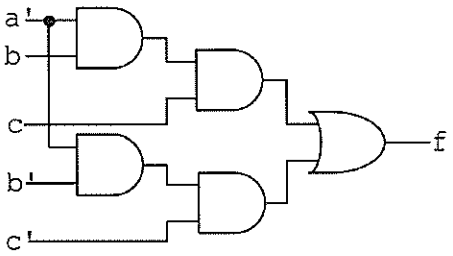

Figure 7. The schematic diagram for D7 designed by Karnaugh Minimizer.

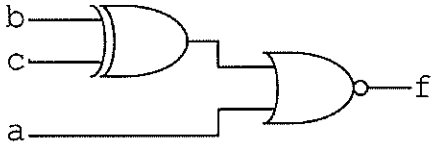

Figure 8. The schematic diagram for D7 designed by the proposed method.

gates count for both designs are based on 2 inputs gate listed in Table 1. These results show that the proposed system is able to produce effective solution of constraint-directed logic optimization.

For D1, the proposed method needs only 4 gates to generate the desired output; 2 AND and 2 OR gates. It is able to design the circuit with the nonstandard output functions in 3.374873 s. The same output specification was designed by Karnaugh Minimizer as well. The total number of gates required is 5; 3 AND and 2 OR gates. This method needs more gates because it can only give the circuit output function in sum of product (SOP) form. The schematic diagrams for both designs are illustrated in Figure 3 and Figure 4 respectively.

D2 and D3 need more gates count if they are designed by Karnaugh Minimizer. D2 needs 31 gates; 24 AND and 7 OR gates. D3 needs 19 gates; 14 AND and 5 OR gates (Fig. 5). The operation concept of Karnaugh Minimizer is based on Boolean algebra; it is unable to optimize the logic function using XOR and XNOR operation. The same output specification can be designed by the proposed method in order to reduce the total number of gates count. The result shows that only 3 gates are needed for each design; 3 XNOR gates for D2 and 3 XOR gates for D3 (Fig. 6). The time required to generate the design is 2.667775 s and 148.287202 s respectively.

D4 shows the optimization circuit for the XOR function. Karnaugh Minimizer produced the circuit design with 5 gates count. The same output can be represented by a single XOR gate if it is designed by the proposed method. The proposed method takes 1.303848 s to generate the design. In fact, the output function produced by Karnaugh Minimizer can be further optimized by applying Boolean algebra theorem. However, for complicated circuit design such as D2 and D3, Boolean algebra theorem may not be a practical option to be implemented.

D5 requires 3 gates count; 3 AND gates for both methods. This is the most optimal gates count for this design because it only covers 1 minterm. The duration required to generate the design is 3.550856 s.

D6 shows that the proposed method can reduce the total gates count to 5 compared with Karnaugh Minimizer which requires 7 gates. The proposed method generated the output function in nonstandard form which is the same as D1. Nonstandard output function requires less gate count compared to the SOP form. The process takes 173.804895 s for this design.

D7 can be optimized by the proposed method using 1 XOR gate and 1 NOR gate (Fig. 8). The proposed method successfully produced the design in

3.550856 s. Karnaugh Minimizer can only generate the same output specification in SOP form which requires 5 gates; 4 AND and 1 OR gates (Fig. 7).

These solutions show that the proposed method is able to optimize the gate count in the digital circuit design. The advantages of the proposed method over the conventional K-Map method or Boolean algebra function are: (i) it can generate the circuit output function in nonstandard form; (ii) it can optimize the circuit output function with XOR and XNOR function; and (iii) it excludes the use of NOT gate in the design.

The obtained results show that Evolutionary Algorithm (EA) can be applied into synthesis of logic circuits design.

REFERENCES

1. Zebulum R.S., Pacheco M.A.C. and Vellasco M.M.B.R. (2002) *Evolutionary Electronics: Automatic Design of Electronic Circuit and Systems by Genetic Algorithms.* CRC Press.
2. Holland J.H. (1992) *Adaptation in Natural and Artificial Systems. An Introductory Analysis with Applications to Biology, Control and Artificial Intelligence.* MIT Press, Cambridge, Massachusetts.
3. Goldberg D.E. (1989). *Genetic Algorithm in Search, Optimization and Machine Learning.* Addison-Wesley.
4. Mano M.M. (2002) *Digital Design.* Prentice Hall.
5. Louis S.J. (1993). *Genetic Algorithms as a ComputationalTool for Design,* Ph.D. thesis, Department of Computer Science, Indiana University.
6. Liu X. and Louis S.J. (1996). Combining genetic algorithms and case-based reasoning for structure design. In Cohen M.E. and Hudson D.L. (eds) *Proceedings of the ISCA Eleventh International Conference on Computers and their Applications* pp 103-106. ISCA.
7. Aamodt A. and Plaza E. (1994) Case-Based Reasoning: Foundational Issues, Methodological Variations, and System Approaches. *AI Communications IOS Press* 7(1): 39-59.
8. Sadiq M.S., Mostafa Abd-El-Barr, Uthman Al-Saiari and Bambang A.B. Sarif (2002) Fuzzified Simulation Evolution Algorithm for combination digital logic design targeting Multi-Objective Optimization. *IEEE Congress on Evolutionary Computation.*
9. Coello C.A., Christiansen A.D. and Aguirre A.H. (2001) Towards Automated Evolutionary Design of Combinational Circuits. *Computers and Electrical Engineering* **27**(1): 1-28.
10. Coello C.A. and Aguirre A.H. (2000) Evolutionary Multiobjective Design of Combinational Logic Circuits. *Proceedings of the Second NASA/DoD Workshop on Evolvable Hardware* pp. 161-170.
11. Coello C.A., Alan D. Christiansen A.D. and Aguirre A.H. (2000) Use of Evolutionary Techniques to Automate the Design of Combinational Circuits. *International Journal of Smart Engineering System Design* **2**(4): 299-314.
12. Miller J.F., Job D. and Vassilev V.K. (2000) Principles in the Evolutionary Design of Digital Circuits – Part I. *Journal of Genetic Programming and Evolvable Machines* **1**(1): 8-35.
13. Miller J.F., Fogarty T. and Thomson P. (1998) Designing Electronic Circuits Using Evolutionary Algorithms. Arithmetic Circuits: A Case Study. *Genetic Algorithms and Evolution Strategy in Engineering and Computer Science* pp. 105-131. John Wiley and Sons, Chichester.
14. Shuriksoft Software, "Karnaugh Minimizer", commercial software, http://karnaugh.shuriksoft.com/

Journal of Science and Technology in the Tropics (2007) **3:** 115-121

A friction material formulation for LRT brake pads

G. S. Darius, M. N. Berhan, N. V. David, M. Z. Akramin and H. Adam
Faculty of Mechanical Engineering, Universiti Teknologi MARA (UiTM),
Shah Alam, Malaysia
(Email: darius598@salam.uitm.edu.my)

Received 23.07.2007; accepted 09.10.2007

ABSTRACT Brake pads are being imported by most of the LRT operators in Malaysia. An attempt is being made to produce brake pads locally to reduce the cost of maintenance. So far 30 formulations have been made to find a suitable substitute to replace the commercial brake pads. The physical, mechanical and chemical properties of the specimens of these formulations have been tested and compared with the properties of the commercial specimen. The friction and wear tests have been carried out and the results of the formulations are compared with that of the commercial specimen. The following tests on the formulation S1 and commercial specimen are carried out and the comparisons of the results are presented: shore hardness, specific gravity, ESEM (environmental scanning electron microscopy), EDX (energy-dispersive x-ray spectroscopy), x-ray surface mapping, XRD (x-ray diffraction), TG-DTG (thermo gravimetry-differential thermo gravimetry) and TG-MS (thermo gravimetry-mass spectrometry). Discussions are made on the suitability of the formulation S1 as a substitute for the commercial specimen in the light of the friction and wear tests. It is shown that formulation S1 can be further improved to substitute the commercial LRT brake pad friction material.

Keywords brake pads – friction materials – LRT – friction and wear

INTRODUCTION

Semi-metallic friction material was introduced in the late 1960s and has gained widespread usage in the mid-1970s. The formulation of semi-metallic friction material takes advantage of using binder resins reinforced with metal, fillers, lubricants and abrasive particles. Generally speaking, when designing a friction material to obtain desirable friction/wear properties, a binder resin should enclose great usefulness such as durability, stability, ease of processing, and good heat resistance. From a practical viewpoint, synthetic resins, such as phenolic resin, are most commonly used as a binder material. However, thermal decomposition or liquescence of phenolic resin due to frictional heating can cause this type of material to fade away. It is known that fade might be avoided to some extent by adding various kinds of metallic powders into a semi-metallic friction material. To further improve the mechanical and tribological performance of polymer-based friction material, one of the most efficient methods is to add various kinds of fibers into the matrix as reinforcement. The addition of fibrous reinforcement plays a major role in maintaining strength, stiffness, thermal stability and frictional properties of the composite material. Asbestos due to its low price and wide variety has been used for years as a fibrous material. However, it is known that asbestos can degrade to airborne fibers and result in a long-term health problem which can contribute to lung diseases. Different kinds of fibers, e.g., metallic, glass, ceramic and carbon fibers, have been used to replace asbestos. Among the fibers mentioned above, the most frequently used metallic fiber material is low carbon steel. The practice of adding brass chips and copper powder in heavy duty organic lining is vital to breaking up surface film, thus improving fade performance. The friction material containing 5–40 vol. % cross-linkable organic fibers (such as acrylic fiber) used for brakes/clutches demonstrates improved friction and wear performance. Due to their good thermal stability and extreme hardness, ceramic materials were also used. The presence of ceramic fibers composed of alumina and silica improves the wear resistance, insulating properties and high temperature performance of plastic as well

as metal matrix composites. It seems obvious that the addition of different fibers could impose different effects on the tribological behaviour of semi metallic friction materials [1].

Friction materials for brake systems typically contain metallic ingredients to improve their wear resistance, thermal diffusivity, and strength. Various metals such as copper, steel, iron, brass, bronze, and aluminum have been used in the form of fibers or particles in the friction material, and it is known that the type, morphology, and hardness of the metallic ingredients can affect the friction and wear of friction materials [2].

This paper reports the results of the following tests carried out on the formulation S1 and commercial specimen: shore hardness, specific gravity, ESEM, EDX, x-ray surface mapping, XRD, TGA and TG-MS. Discussions are made on the suitability of the formulation S1 as a substitute for the commercial specimen in the light of the friction and wear tests. It is shown that formulation S1 can be further improved to substitute the commercial LRT brake pad friction material.

Commercial brake pad

Figure 1 shows a brake pad used in the PUTRA-LRT trains running in Kuala Lumpur, Malaysia. Two such brake pads are used in every hydraulic brake unit. There are 16 brake pads in every train. 35 trains operated by PUTRA-LRT in and around KL are fitted with this type of brake pads. These brake pads are non-asbestos, non-lead and semi-metallic.

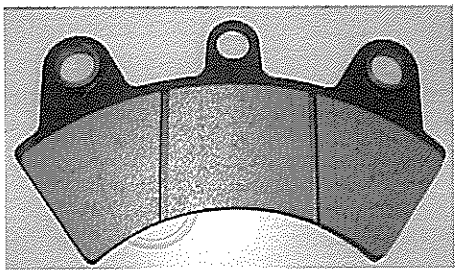

Figure 1. A railway brake pad (non-asbestos, non-lead and semi-metallic).

New formulations of brake friction materials

New formulations of brake friction materials are made using the following ingredients: resin, iron oxide, steel fiber, ceramic fiber, organic fiber, magnesium oxide, aluminium oxide, barium, sulphur, graphite, rubber, novacite, nipol and friction dust. Values of hardness, specific gravity and transverse rupture strengths of these formulations are compared with that of a commercial brake pad and the formulations which have their properties comparable with the commercial pad are identified. This paper reports the properties of specimen S1 and compares them with that of the commercial specimen.

TG-MS ANALYSIS

Mettler Toledo TGA/SDTA851e was used for the TG-MS coupled analysis. The mass spectrum of the gaseous products which evolved during heating is obtained by coupling the TG thermobalance on-line to the MS via a heated quartz glass capillary tube. Samples were heated from 30°C to 1000°C at a scan rate of 10°C/min under flow of 50 mL/min of nitrogen. The TG/DTG-MS spectra were generated by plotting the continuous change of sample weight and ion intensities (mass-to-charge ratio) of the gaseous products as a function of temperature.

Evolved gas analysis (EGA) is a technique to determine the nature and amount of a volatile product or products formed during the thermal degradation of materials. EGA technique involves the analysis of gaseous species evolved during combustion and/or pyrolysis in which a series of chemical reactions occur as a function of temperature and are analyzed using thermal analytical methods and/or multiple techniques. EGA is normally used to evaluate the chemical pathway of degradation reactions by determining the composition of the decomposition products from various materials. Two approaches are generally used for EGA, simultaneous analysis and combined analysis. In the simultaneous TG/MS on-line analysis, the decomposition products that evolve from pyrolyzed materials can be monitored simultaneously [3].

RESULTS AND DISCUSSION

Figure 2 shows the ESEM and mapping of commercial specimen. It is seen that Steel fibers, iron powders, iron oxide are distributed uniformly in the resin. Graphite, coke particles are evenly spread in the matrix. Clusters of magnesium sulfate can be seen at random locations by observing the distribution of magnesium (Mg), sulphur (S) and oxygen (O). Aluminium (Al) particles, barium (Ba), silica (Si) and

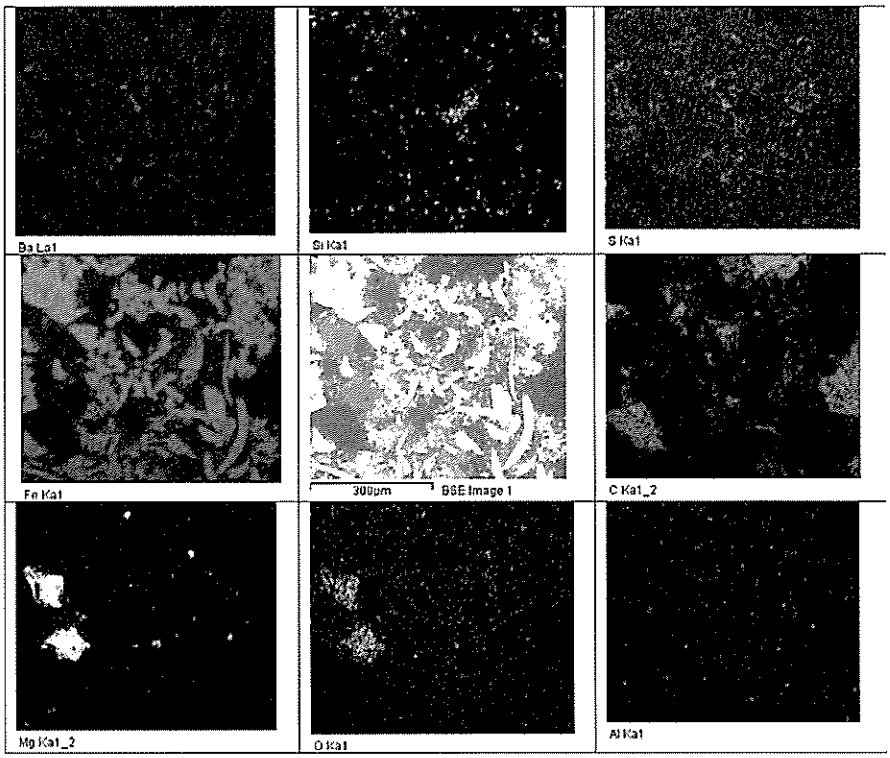

Figure 2. ESEM and mapping of commercial specimen.

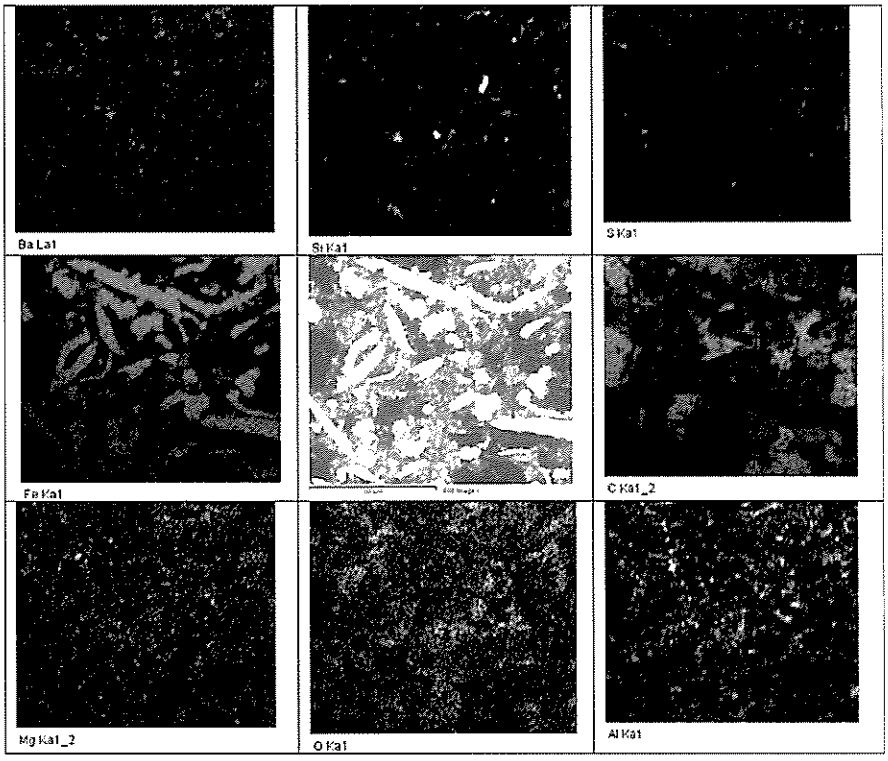

Figure 3. ESEM and mapping of Formulation S1.

sulphur (S) are uniformly spread.

Figure 3 shows the ESEM and mapping of formulation S1. Steel fibers, iron powders, iron oxide are distributed uniformly in the resin. Graphite, coke particles are evenly spread in the matrix. Aluminium oxide appears to be present all over. Silicon oxide and

Table 1. Shore hardness values of commercial and formulations.

	Shore hardness			Specific gravity	Friction coefficient	Wear rate (g/MJ)
	Minimum	Mean	Maximum			
Commercial	72.0	76.2	82.0	3.30	0.332	0.038
Formulation S1	73.0	76.8	82.6	2.72	0.374	0.043

barium oxide are seen at random. Fine particles of sulphur and magnesium are present.

Properties of formulations

Shore hardness. Hardness values of a commercial sample and the formulation S1 are tested using a shore hardness tester. Table 1 shows the minimum, mean and maximum shore hardness values of the commercial sample and the formulation. It can be seen that formulation S1 has a higher hardness value as compared to the commercial sample.

Specific gravity. The specific gravity of the formulation is less than that of the commercial specimen (Table 1). The density values of the ingredients used in the commercial specimen are not known and the density values of the ingredients used in the formulation could be different and hence the specific gravity of the formulation S1 seems to be smaller.

Friction and wear. Wan *et al.* [4] have studied the friction and wear properties of these formulations and reported the following results: Table 1 shows the co-efficient of friction and wear values for the commercial as well as the formulation. It can be seen that the friction coefficient as well as the wear rate of the formulation are higher compared to the corresponding values offered by the commercial specimen. Even though higher wear rate would reduce the life of the brake pad, higher friction coefficient would offer a better performance compared to the commercial specimen. Friction, wear and physical properties are compared with brake lining requirements [5].

Table 2 shows the elemental distribution of commercial and S1. The carbon content is more or less the same in both commercial and formulation. The iron content is less in the formulation which explains the reason for the lower specific gravity. Also the wear rate is high due to the lower content of iron fibers in the formulation. Higher barium oxide and aluminium oxide in the formulation would increase the friction coefficient, while lower silicon oxide and magnesium oxide in the formulation would increase the wear rate.

Table 2. EDX results showing elemental composition of commercial and S1.

Element	Weight %	
	Commercial	Formulation S1
C K	48.82	49.84
O K	11.45	14.17
Mg K	2.16	1.14
Al K	0.39	1.76
Si K	1.29	0.74
S K	0.54	2.19
Ca K	-	0.12
Fe K	33.15	27.18
Ba L	2.19	2.85
Total	100	100

Evolved gas analysis (EGA)

In thermogravimetric analysis (TGA), the weight of a sample is recorded as a function of temperature or time, under defined atmospheric conditions. Quantitative compositional analysis can be performed and the reaction kinetics investigated. Qualitative information of the gaseous products evolved is obtained by coupling the thermo balance on-line with a mass spectrometer. The TGA/SDTA851e is coupled to the MS via a heated quartz glass capillary tube. One end of the glass capillary is positioned close to the sample in the thermo balance. Part of the evolved gases is sucked into the capillary by the vacuum in the MS. The MS repeatedly measures the intensity of characteristic fragment ions (*m/z*, the mass-to-charge ratio).

TG-DTG curves for commercial brake pad

Figure 4 shows that the total mass loss which measured up to 950°C was around 5 %. This total mass loss corresponds to several mass losses by decomposition between 200°C and 750°C. There has been a slight decrease in mass of around 0.1 % below 120°C due to the evaporation of moisture and volatile from adhesive in the brake pad. A large rate of weight

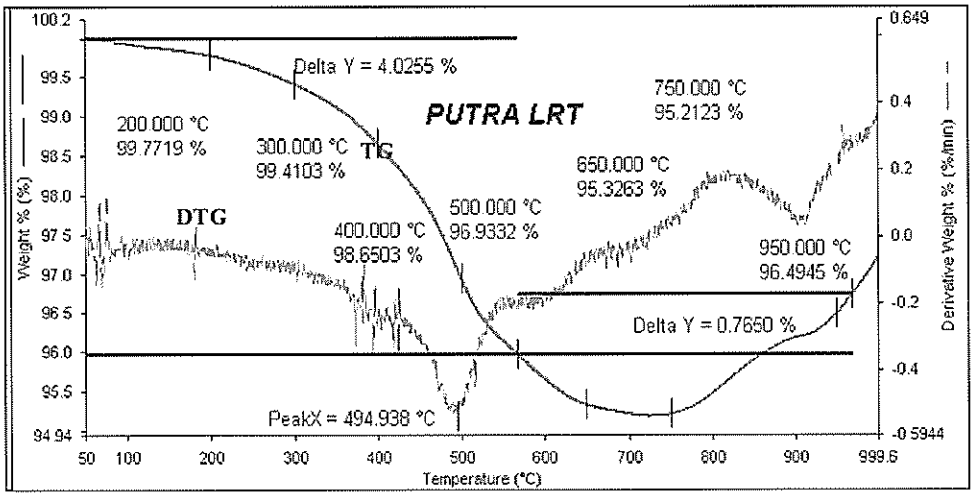

Figure 4. TGA curve of sample commercial brake pad PUTRA LRT, A semi-metallic friction material.

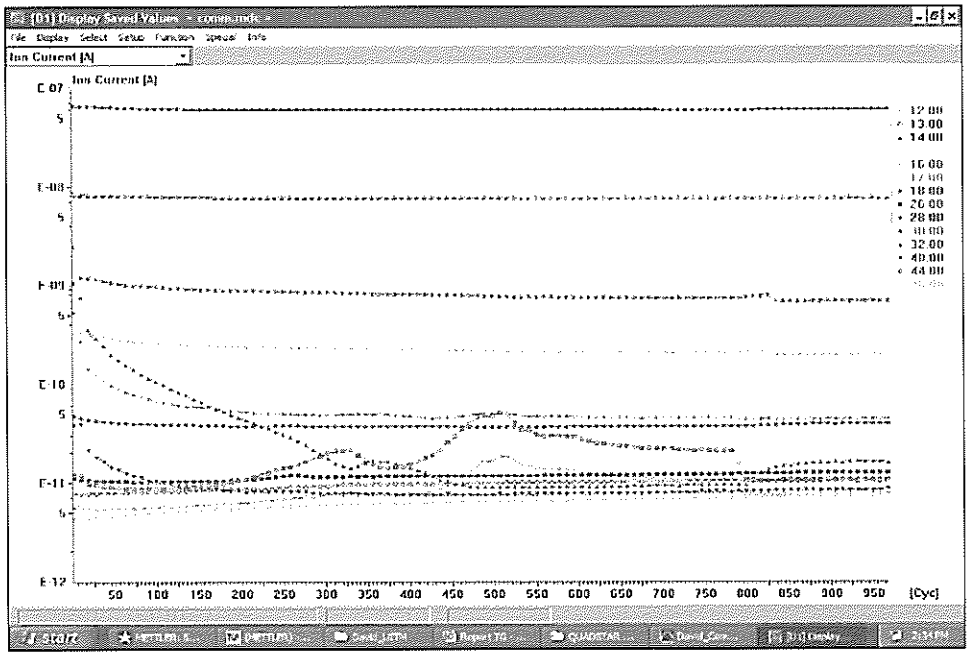

Figure 5. Mass spectrometry of commercial specimen.

change observed with maximum decompose rate for DTG was found to be at 494.4°C. Between 495°C to 750°C another decrease in mass around 1.7 % took place accompanied by a small, second derivative peak. Between 750°C and 950°C, there was a mass increase of around 1.2%. The temperature for 5 % decompose was very high at 680°C. This material was found to be very stable. Only a small percentage of material composition was decomposed partly due to the polymeric binder. The polymeric binder decomposed up to 550°C. The TG curve showed an increase in weight at a temperature of up to 680°C due to oxidation of the graphite and metals present in the sample of the brake pad.

Figure 5 shows the mass spectrum for the EGA. It can be seen that the gases evolve from 225°C to 780°C due to probable release of organic and inorganic substances. Table 3 shows the probable gases having *m/z* (the mass-to-charge ratio) 2 and 44. Mass-to-charge ratio 2 suggests the release of hydrogen. Mass-to-charge ratio 44 suggests the possible release of propane and carbon-di-oxide (CO_2) which may be

Table 1. Colony composition of *P. leeuwenhoeki*. Incipient colonies were excluded. DQ: dealated queen; AQ: alate queen; mW: mated worker; vW: virgin worker; C: cocoon; L: larva; E: eggs; -: not counted; +: present but not counted. FI,YI, and AG mean colonies collected by F. Ito, Y. Ikeshita and A. Gotoh, respectively.

	Number of individuals						
Colony code	DQ	AQ	mW	vW	C	L	E
FI92-MG515	1(1)	0	0	2	-	-	-
YI04-97	1(1)	0	0	3	-	-	-
FI92-MG610	1(1)	0	0	10	-	-	-
AG07-25	1(1)	1	0	11	0	8	+
YI04-69	0	0	1(1)	1	0	0	0
FI92-MG567	0	0	1(1)	3	0	4	7
FI03-54	0	0	1(1)	3	-	-	-
YI04-86	0	0	1(1)	3	0	0	0
FI92-MG53	0	0	1(1)	5	3	0	1
FI96-547	0	0	1(1)	6	-	-	-
YI04-43	0	0	1(1)	8	-	-	-
FI99-282	0	0	1(1)	12	-	-	-

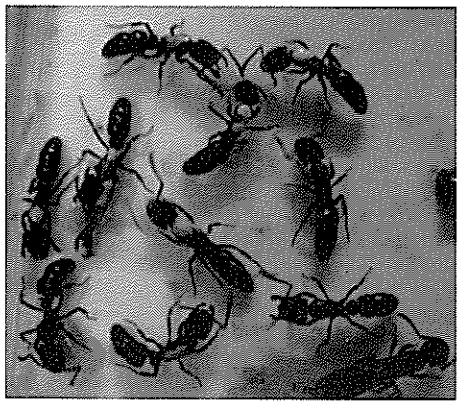

Figure 1. A colony of *Pachycondyla leeuwenhoeki* collected in Ulu Gombak. Individual was marked with enamel paints.

colony collected in the field was introduced into the subcolony A and subsequent behaviour of the workers was observed. Three weeks after the male was introduced, all workers in the subcolony were dissected. The other subcolony was merged with the mother colony after the establishment of a dominance hierarchy among the virgin workers, and behavioural interactions between workers of the mother colony and those of the subcolony was observed. After that all the workers of the subcolonies were dissected. Spermatheca width was measured under a light microscope for three randomly selected queens and 17 workers. Head width and width of the 2nd gaster segment of these individuals and other three queens and 15 workers were measured under binocular microscope.

RESULTS

Colony composition

In all fifteen complete colonies were collected over a nine-year period in the Southeast Asian tropics, indicating that *P. leeuwenhoeki* is not a common species. Seven of the 15 colonies were reproduced by only one dealated queen. Of these three were incipient colonies with a dealate queen and a few immatures, indicating that *P. leeuwenhoeki* queens start their colonies independently. Two incipient colonies produced three worker pupae each. The remaining eight colonies were reproduced by gamergates. All colonies were monogyny with one mated worker as gamergates. Virgin workers had neither yolky oocytes nor yellow bodies. Colony size of both queen colonies and gamergate colonies was small (mean number of virgin workers in queen colonies 6.5 $\pm$ 4.7, gamergate colonies 5.1 $\pm$ 3.5, Mann Whitney U test, $Z = -0.26$, $p = 0.79$).

Queen body size was significantly larger than workers (Head width, queens, 1.67 $\pm$ 0.08 mm, workers, 1.53 $\pm$ 0.06 mm, Mann Whitney U test, $Z = -2.87$, $p = 0.004$; 2nd gaster segment, queens, 1.60 $\pm$ 0.11 mm, workers, 1.41 $\pm$ 0.06 mm, $Z = -3.58$, $P = 0.0003$). However, as in other AQ+G species, the difference was not conspicuous. Both queens and workers had three ovarioles per ovary. Spermatheca size of queens (131.7 $\pm$ 20.8 µm) was slightly larger than workers (119.7 $\pm$ 13.2µm), but not statistically significant (Mann Whitney U test, $Z = 0.59321$, $p = 0.553$).

Reproduction

Aggression was never observed in the gamergate colony (FI99-282), and the queen colonies (FI92-MG 515, AG07-25). In FI99-282, egg-laying was observed 10 times, all of which were performed by the gamergate. As indicated by dissection data, the virgin workers never laid eggs during the 100 hours observation.

In the orphan subcolonies, aggressive antennations and biting were frequently observed among the workers. Just after creating these subcolonies, mutual antennations were very frequent but it was difficult to know who was the most dominant. Mutual antennation often continued for a few minutes. The frequency of

Table 3. MS results showing the possible molecule release.

m/z, the mass-to-charge ratio	Key Fragment	Probable molecule
2	H2+	H_2
44	C3H8+	C_3H_8
	CO2+	CO_2

caused by volatilization of organic compounds due to the release of steam at a higher temperature. Oxidation of the carbon content might also be possible. This result substantiates the corresponding weight loss seen in the corresponding portion in the TG curve.

TG-DTG curve for laboratory formulation S1

Three decomposition stages were detected from the TG/DTG curves as shown in Figure 6. This sample decomposed steadily from the onset of heating until 550°C. During this period, the total loss of weight is 11.8%. Decomposition of two possible raw materials i.e. barium or rubber may have caused the increment of rate of weight loss between 200°C and 300°C. These possibilities are based on the results of raw materials. This is not conclusive but subject to verification by other thermal analysis technique(s). A rapid rate of weight loss occurred between 468.2°C and 486°C.

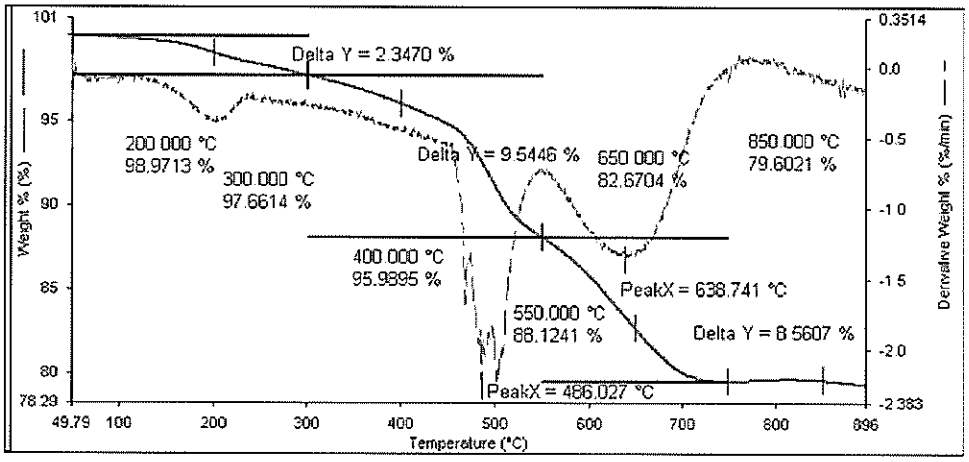

Figure 6. TG-DTG curve for sample S1.

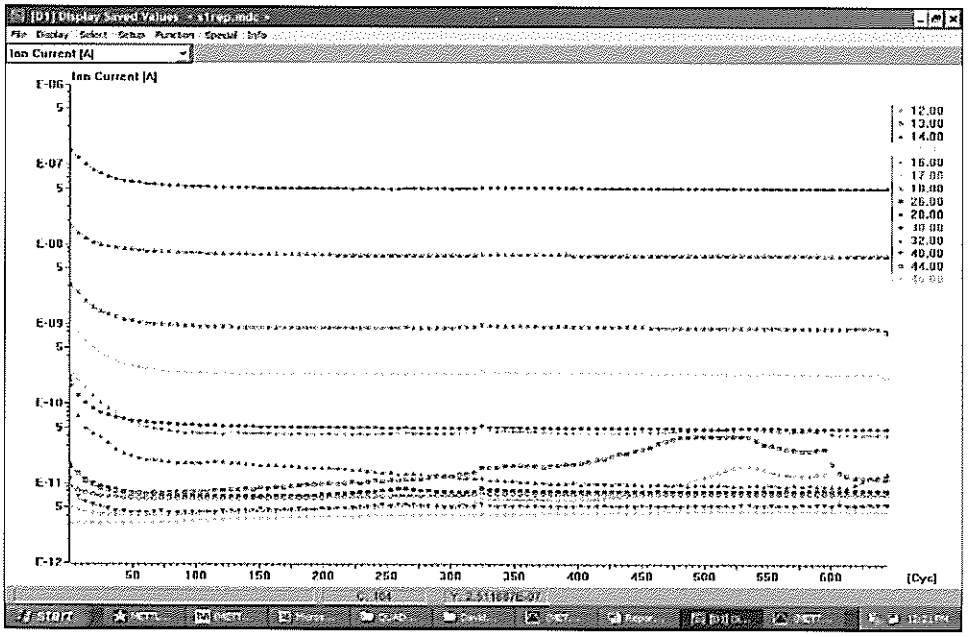

Figure 7. Mass spectrometry of Specimen S1

As indicated in the DTG curve, the peak at 486°C corresponds to the derivative weight of –2.3% per minute which is the highest rate registered for this sample across the temperature domain. The rate of decomposition then improved to –1.25% at 550°C. The final stage of weight reduction commenced at 550°C resulting in an 8.5% weight loss compared to the preceding stage. Decomposition stopped at 750°C. The significant weight loss occurred while heating the sample between 300°C and 700°C, contributing to an 18.1% reduction.

Figure 7 shows the mass spectrum for the EGA of Specimen S1. We can see the gases start evolving from 225°C to 640°C due to the probable release of organic and inorganic substances. A second peak is recorded at 638.7°C in the DTG curve which matches with the rate of release of gases having *m/z* (the mass-to-charge ratio) 2 and 44 around this temperature.

CONCLUSION

The following conclusions are drawn as a result of this study: Sample S1 shows a higher hardness value and a lower specific gravity compared to the commercial specimen. The friction coefficient and also the wear rate of specimen S1 are higher compared to the commercial specimen. An equal amount of carbon is present in specimen S1 and in the commercial specimen. The amounts of Aluminium, Oxygen, Sulphur and Barium are more in specimen S1 and the amounts of iron, Magnesium and Silica are less in specimen S1. Specimen S1 retains 88.12% and the commercial specimen retains 96.93% of the total material when heated to 550°C. Mass spectrometry results show that similar gases are released by both specimens S1 and the commercial specimen at a temperature range from 225°C to 640°C. Based on the hardness value, friction and wear properties, carbon content and the morphology studies, specimen S1 can be further improved to substitute the commercial specimen.

Acknowledgements–The Ministry of Science, Technology and Innovation, Malaysia is thanked for supporting this work through the IRPA grant [03-02-01-0055-PR0066/04-03]. We thank Prof. Dr. Azni Zain Ahmad, Assistant Vice-Chancellor, IRDC, UiTM Shah Alam, Prof. Madya Dr. Mohd Hanafiah Abidin, Research Head (Science & Technology), IRDC, UiTM, Shah Alam for their encouragement and support. We thank Prof. Madya Ir. Dr. Hj. Abdul Rahman Omar, Dean of the Faculty of Mechanical Engineering, UiTM Shah Alam for his support. The authors are also thankful to Dr. Mohmad Soib Selamat (AMREC, Kulim, Kedah), Dr. Talib Ria Jaafar (AMREC, Kulim, Kedah) and Dr. Mustafar Sudin, (Universiti Teknologi Petronas) for providing us specimens, facilities and whatever was necessary for the carrying out of this work. Mr. Andrew, Miss Mardiana of COMBICAT, University of Malaya, KL are thanked for their assistance in making ESEM and SEM images. All those who helped in this work in one way or other are thanked.

REFERENCES

1. Ho S.C., Chern Lin J.H and Ju C.P. (2005) Effect of fiber addition on mechanical and tribological properties of a copper/phenolic-based friction material. *Wear* **258:** 861–869.
2. Jang H., Koa K., Kima S.J., Basch R.H. and Fash J.W. (2004) The effect of metal fibers on the friction performance of automotive brake friction materials. *Wear* **256:** 406–414.
3. Xie W. and W.-P. (2001) Thermal Characterization of Materials Using Evolved Gas Analysis. *Journal of Thermal Analysis and Calorimetry* **65:** 669-685.
4. Wan M.A., Mohd, S. and Talib R.J. (2004) Friction Analysis of Light Rail Transit (LRT) Brake Pad Through CHASE Dynamometer Test. *2nd Malaysian Brake Friction Materials Colloquium 2004,* Universiti Teknologi MARA, Shah Alam, Malaysia, 3-4 December 2004.
5. G.S. Darius, M.N.Berhan, N.V. David, A.A.Sharul and M.B.Zaki. (2005) Characterization of brake pad friction materials. *WIT Transactions on Engineering Sciences* **51:**43-50.

Journal of Science and Technology in the Tropics (2007) **3:** 123-127

Development of a 3.3 kJ plasma focus as pulsed neutron source

S. L. Yap and C. S. Wong
Plasma Research Laboratory, Physics Department, University of Malaya
50603 Kuala Lumpur, Malaysia
(E-mail: yapsl@um.edu.my)

Abstract Recently there has been much interest in the development of compact pulsed neutron sources for applications such as interrogation of materials based on the technique of neutron activation. The dense plasma focus has been identified as a possible candidate for this purpose. This paper reviews the research efforts at the Physics Department, University of Malaya in the development of a 15 kV, 3.3 kJ plasma focus device which has been optimized for D-D fusion neutron production. Neutron yield of the order of 10^8 neutrons per 100 ns has been achieved. We have identified two possible mechanisms responsible for the neutron generation in this device, namely thermonuclear and beam target. At present we are looking into possibility of generating neutrons of energy spectra other than the D-D reaction by using the beam-target mechanism. For this purpose, the plasma focus device is modified to operate in the non focusing mode. Deuteron beam of energy up to 250 keV has been detected.

Keywords plasma focus – pulsed neutron - neutron source – deuteron beam

INTRODUCTION

The plasma focus is one of the most efficient plasma devices capable of producing nuclear fusion of deuterium with a modest input electrical energy of below 10 kJ. With its relatively low discharge current and voltage, research work on this device can be carried out in most small laboratory cost effectively. It is for this reason that the United Nations University (UNU) had conducted a training programme on this device for small laboratory [1].

The plasma focus is powered by a simple capacitive discharge circuit which is considered to be a simple, entry level pulse power technology. For the system described here, a 15 kV, 30 μF capacitor is discharged through the coaxial plasma load and delivers a peak current of about 150 kA. The discharge can be divided into three phases: the lift off phase, the axial acceleration phase and the radial compression phase. The hot dense plasma achieving fusion condition is formed during the radial compression phase. This plasma has electron temperature of several keV and electron density of 10^{18} particles per cm^3. Beside neutrons, the focused plasma also emits intense X-ray, high energy electron and ion beams.

In this paper, we review the research efforts by the Plasma Group at the Physics Department, University of Malaya to develop a compact pulsed neutron source based on the plasma focus device. Fusion neutrons were detected in 1975 [2]. Since then, much effort had been put in to investigate the neutron emission characteristics such as the angular distribution [3], to optimize the neutron production [4] and to understand the actual neutron production mechanism [5]. Work on the modification of the plasma focus for operation at low pressure has also been carried out [6]. In this low pressure mode of operation, the plasma focus is capable of generating ion beam of several hundreds keV to MeV energy. The utilization of these ion beams to produce beam-target neutrons will be tested.

THE PLASMA FOCUS DEVICE AND ASSOCIATED DIAGNOSTICS

The present setup of the plasma focus device in this laboratory is the product of a series of design and modification activities since the 1970s. Initially the plasma focus studied was UMDPF1 [4] which had parameters as shown in Table 1.

This plasma focus had been optimized for neutron production with a maximum yield of 10^9 neutrons per discharge. In the following, we report on results

Table 1. Parameters of UMDPF1 [4] and UNU-ICTP PFF [7].

Parameter	UMDPF1	UNU-ICTP PFF
Capacitance, C	60 μF	30 μF
Discharge voltage, V	20 kV	15 kV
Electrical energy, E	12.4 kJ	3.3 kJ
Periodic time, T	11.2 μs	12 μs
Current at first maximum, I	590 kA	150 kA
Deuterium filling pressure, P	2.5 mbar	6 mbar
Neutron yield, Y	10^9 neutrons per discharge	10^8 neutrons per discharge

on neutron emission characteristics of the UNU-ICTP PFF plasma focus device. This is the plasma focus device presently being investigated in this laboratory.

The parameters of UNU-ICTP PFF [7] are given in Table 1. It is a Mather-type plasma focus with hollow copper central electrode (160 mm length and 19 mm diameter) and an outer electrode made of six copper bars (160 mm length and 64 mm diameter). The device is powered by a single 30 μF capacitor charged to 15 kV, generating a peak current of 150 kA with a rise-time of 3 μs. The schematics of the system, together with some of the diagnostics are shown in Figure 1.

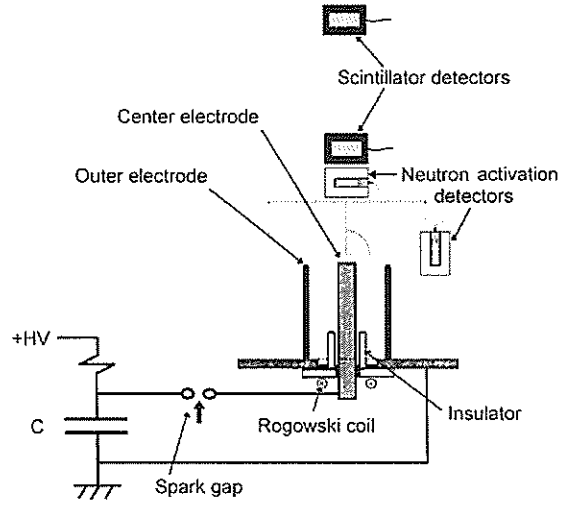

Figure 1. Experimental setup of plasma focus system.

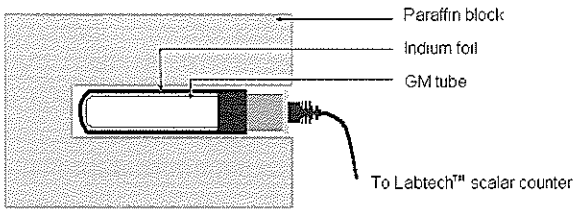

Figure 2. Neutron activation detector.

Both time-integrated and time-resolved neutron detection systems are employed to study the neutron emission characteristics of the plasma focus. The time-integrated neutron detector is based on neutron activation of indium foil. When exposed to slow neutrons, ^{115}In produces ^{116}In and ^{116m}In which subsequently undergo β-decay to ^{116}Sn. ^{116}In has a half-life of 14 seconds while ^{116m}In has a half-life of 54 minutes. If we choose a counting interval which is short compared to 54 minutes, the contribution of the decay of ^{116m}In towards the measured activity can be taken to be contributing to the background count. The β-particles are counted by using GM tube. The detector setup is shown in Figure 2.

For time-resolved measurements of the neutron emission, two channels of scintillator-photomultiplier systems are employed. To avoid pickup of electrical noise by the photomultiplier tubes, they are housed inside a screened room together with the oscilloscopes while the cylindrical scintillators are placed end-on at distances of 50 cm and 106 cm from the end of the central electrode respectively. This setup will allow us to measure the average energy of the neutrons by the time-of-flight technique. The light output of these scintillators is collected by fluorescent fibers wrapped

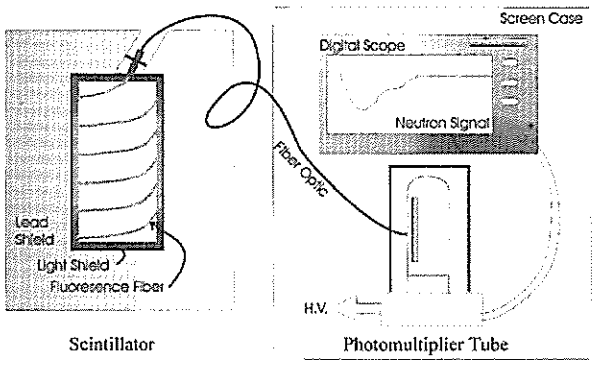

Figure 3. The scintillator-photomultiplier detection system for time-resolved measurement of plasma focus neutrons.

around them and transmitted to the photomultiplier tubes by single core optical glass fibers. The setup of one channel of this detection system is shown schematically in Figure 3.

MEASUREMENTS OF NEUTRON EMISSION OF DEUTERIUM PLASMA FOCUS DISCHARGE

For the production of D-D fusion reactions, the plasma focus chamber is first pumped to a base pressure of lower than 10^{-2} mbar and then filled in deuterium to a pressure of around 6 mbar. This has been found to be a suitable deuterium pressure for good focusing discharge and with high neutron yield. However, it is observed experimentally that discharges in deuterium doped with a small percentage of argon seem to enhance the neutron yield. From a series of discharges at 15 kV and with varying percentage of argon doping, the plasma focus device is capable of producing optimum neutron yields of the order of 10^7 to 10^8 neutrons per discharge consistently at filling gas of deuterium doped with 30% mass of argon at a pressure of 4 mbar.

The average energy of the neutrons is determined by the time-of-flight technique. From the signals of the two channels of scintillator-photomultiplier detectors (Fig. 4), the average energy of the neutrons can be deduced to be 2.7 ± 0.5 MeV. This differs from the value of 2.45 MeV expected as a consequence of the neutron production mechanism being not 100% thermonuclear. By using the Gaussian curve fitting technique, we are able to resolve the neutron pulse into two components (Fig. 5). Taking the areas under the two pulses to represent the relative neutron yield

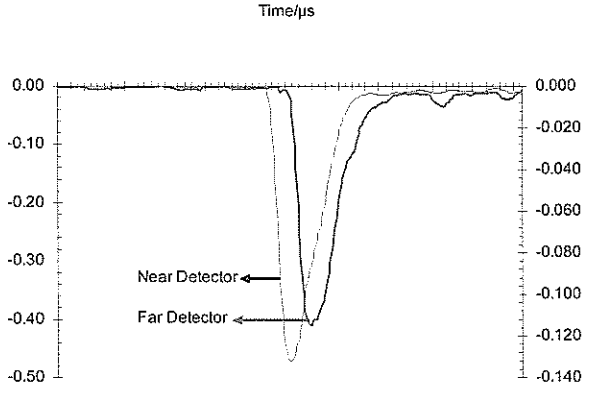

Figure 4. Neutron signals detected by near and far detectors (end-on) for pure deuterium discharge.

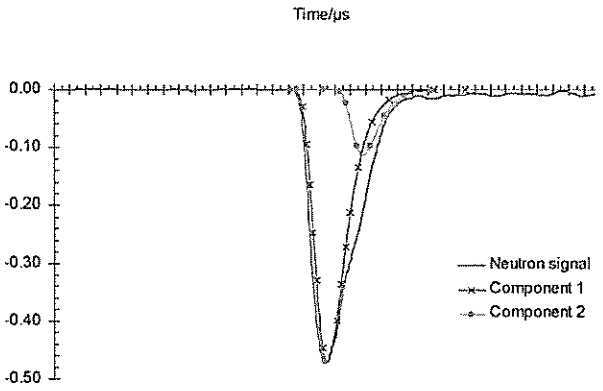

Figure 5. Resolving the neutron pulse into two components by Gaussian Curve Fitting Technique.

for the two components, the first component has an anisotropy close to one, indicating that it can be of thermonuclear origin. On the other hand, the second component has an anisotropy of 1.5, indicating that it can be produced by the beam target mechanism. While the thermonuclear neutrons are produced by the fusion reactions occurring inside the hot dense focused plasma, the beam target neutrons are believed to be produced by the bombardment of the ambient deuterium gas by energetic deuteron beams in the forward direction. The observation of highly energetic ion beams of up to MeV energy had been widely reported in the literature [8-11]. For small devices such as the one described in this paper, the two components occur within a time separation of about 20 ns (Fig. 5). For a large system such as the Poseidon (60 kV, 280 kJ), the two components are found to be clearly separated by more than 200 ns [12].

OPERATION OF PLASMA FOCUS AS A BEAM-TARGET NEUTRON SOURCE

We have shown earlier that the high energy ion beam produced by the plasma focus leads to the beam-target neutron generation. This ion beam can also be used for generation of neutrons of other energy spectrum besides fusion that can be more useful for applications. Some of the possible schemes that can be used include ^{7}Li(d,n)2^{4}He, ^{9}Be(d,n)^{10}B, and ^{12}C(d,n)^{13}N. Some of the possible applications of the fast neutron source include neutron therapy and the interrogative inspection of baggage for airport security based on the neutron activation technique. For these applications, it is necessary to modify the

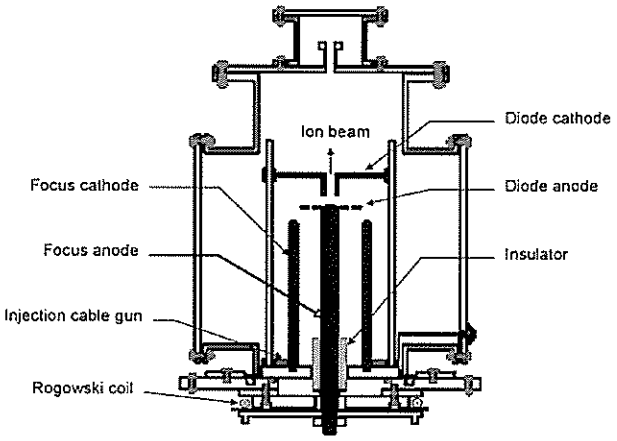

Figure 6. Schematics of the modified plasma focus.

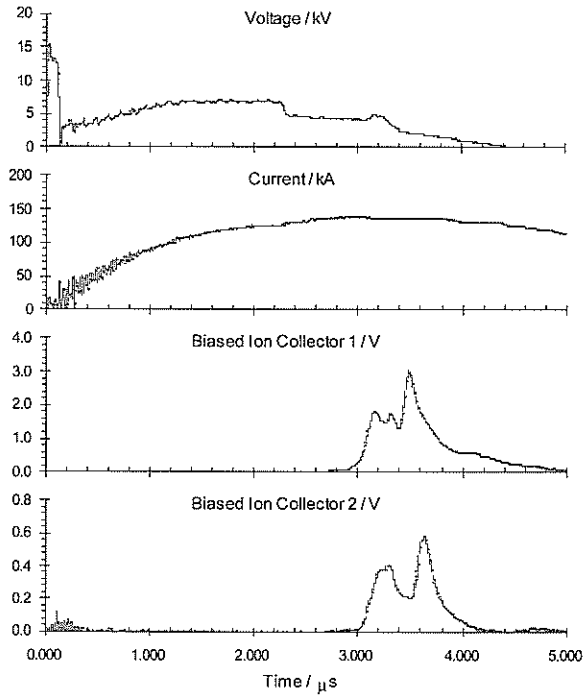

Figure 7. Typical results obtained for the modified plasma focus at 15 kV, 4×10^{-2} mbar deuterium.

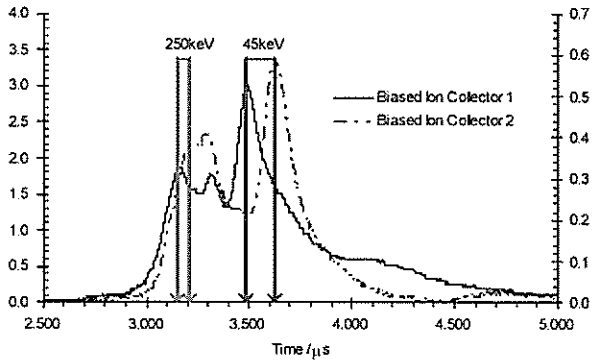

Figure 8. Time of flight measurement of the ion beam signals reveals the co-existence of several groups of deuteron beam with different energies.

plasma focus for operation in the ion beam enhanced mode.

The UNU-ICTP PFF plasma focus is modified (Fig. 6) to include the following features: (a) the anode is extended to 190 mm with a solid end to accommodate the mounting of a stopper; (b) a stopper is mounted at the tip of the anode – this stopper is made of a layer of insulation material facing the anode, while the opposite layer made of conducting material; it is made with a series of apertures eccentrically arranged around the anode. The conducting side of the stopper is layered with thin copper sheet and it forms the anode of an ion extraction diode mounted above the anode; (c) a set of 12 injection cable guns is mounted near the back-wall of the focus tube surrounding the cathodes; they are used to initiate breakdown for low pressure discharge; and (d) the operating pressure is shifted to 10^{-2} mbar instead of several mbar.

At optimum condition, the modified plasma focus is capable of generating intense high energy ion beams consistently. The ion beams are measured by using two biased ion collectors. These detectors are biased at negative 10V to give a positive polarity signals on picking up ions. A set of signals for a typical discharge are shown in Figure 7.

The time of flight of the ion beam signals obtained by the two biased ion collectors are analyzed to give the possible ion beam energy (Fig. 8). In this particular discharge, two deuteron beams are detected, one with beam energy of 45 keV and another with beam energy of 250 keV. Deuteron beams with energies up to 2 MeV have been observed from this device, though they are mostly of low intensities.

CONCLUSION

The plasma focus has been shown to be a cost effective device capable of generating fusion neutrons with relatively low electrical input energy by using pulsed power technology that is within the capability of most small laboratories in developing countries. Besides fusion neutrons, the plasma focus can also be operated in an ion beam enhanced mode to generate high intensity, high energy ion beams for beam-target neutron generation. This opens up new possibilities of producing a large variety of neutron spectrum

which will make the device a versatile pulsed neutron source. In the experiments reported here, we have obtained deuteron beams with energy above 250 keV. We are also in the process of fine tuning the modified plasma focus to enhance the ion beam intensity and energy. These ion beams will be used for beam target neutron generation using reaction such as $^{7}Li(d,n)2^{4}He$, $^{9}Be(d,n)^{10}B$ and $^{12}C(d,n)^{13}N$ in the near future.

Acknowledgement - This project on development of plasma focus as pulsed neutron source is supported by a grant 09-02-03-0027 awarded by the Ministry of Science, Technology and the Environment to University of Malaya under its IRPA programme. The authors are grateful to Mr Jasbir Singh for technical support.

REFERENCES

1 Lee S. and Wong C.S. (2006) Initialing and strengthening plasma research in developing country. *Physics Today* **59:** 31-36.

2 Lee S. and Chen Y.H. (1975) Measurement of neutrons from a plasma focus. *Mal. J. Sci.* **3(B):** 159-163.

3 Wong C.S., Lee S. and Moo S.P. (1980)Neutron measurements of a 12 kJ plasma focus. *Mal. J. Sci.* **6(B):** 167-174.

4 Chen Y.H. (1978) *Parametric Study of Focus Optimization.* PhD thesis, University of Malaya.

5 Yap S.L., Wong C.S., Choi P., Dumitrescu C. and Moo S.P., Observation of two phases of neutron emission in a low energy plasma focus. *Jpn. J. Appl. Phys.* **44:** 8125-8132.

6 Wong C.S., Choi P., Leong W.S. and Singh J. (2002) Generation of high energy ion beams from a plasma focus modified for low pressure operation. *Jpn. J. Appl. Phys.* **41:** 3943-3946.

7 Lee, S., Tou T.Y., Moo S.P., Eissa M.A., Gholap A.V., Kwek K.H., Mulyodrono S., Smith A.J., Suryadi S., Usada W. and Zakaullah M. (1988) A simple facility for the teaching of plasma dynamics and plasma nuclear fusion. *American J Phys.* **56:** 62-68.

8 Mozer A., Sadowski M., Herold H. and Schmidt H. (1982), Experimental studies of fast deuterons, impurity and admixture-ions emitted from a plasma focus. *J. Appl. Phys.* **53:** 2959-2964.

9 Yamamoto T., Shimoda K. and Hirano K. (1985) Neutrons, x-rays and charged particle beams emission in a 65 kV plasma focus. *Jpn. J. Appl. Phys.* **24:** 324-327.

10 Stygar W., Gerdin G., Venneri F. and Mandreakas H. (1982) Particle beams generated by a 6-12.5 kJ dense plasma focus. *Nucl. Fusion* **22:** 1161-1172

11 Takao K., Doi Y., Hirata S., Shiotani M., Kitamura I., Takahashi T. and Masugata K. (2001) Characteristics of Ion Beams Produced in a Plasma Focus Device. *Jpn. J. Appl. Phys.* **40:** 1013-1015.

12 Herold H. (1988) Physics and Technology of Large Plasma Focus Devices. *Proc. 3rd Tropical College on Appl. Phys., Kuala Lumpur, 1988.* pp 21-45.

Journal of Science and Technology in the Tropics (2007) **3:** 129-133

Ab initio calculation of the vibrational frequencies of $Ag_xGe_{x-1}Se_{2x+1}$ glass

Ahmad Nazrul Rosli, Hasan Abu Kassim and Keshav N. Shrivastava
Department of Physics, University of Malaya, Kuala Lumpur 50603, Malaysia
(Email: keshav_shri@yahoo.com)

Received 01.10.2007; accepted 01.11.2007

Abstract The vibrational frequencies of Ag_2, Ag_3, Ag_4, Ag_5, Ag_6, AgGe, Ag_2Ge, Ag_3Ge, Ag_4Ge, $AgGe_2$, Ag_2Ge_2, Ag_3Ge_2, Ag_4Ge_2, $AgGe_3$, Ag_2Ge_3, Ag_3Ge_3, Ag_4Ge_3, $AgGe_4$, Ag_2Ge_4, Ag_3Ge_4, Ag_4Ge_4, AgSe, Ag_2Se, Ag_3Se, Ag_4Se, $AgSe_2$, Ag_2Se_2, Ag_3Se_2, Ag_4Se_2, $AgSe_3$, Ag_3Se_3, $AgSe_4$, Ag_2Se_4 and Ag_4Se_4 are theoretically computed from the first principles by using density functional theory. The clusters are built in plane, pyramidal or ring shape configurations. We calculate the vibrational frequencies for all of the 47 clusters. The bond lengths and bond angles of all of the molecules are calculated. The vibrational frequencies of all of the clusters are calculated by using a variety of wave functions. We use the single zeta wave functions as well as the double zeta wave functions with and without the polarization. The experimental Raman spectra show almost a continuum of small frequencies. In particular below 100 cm^{-1}, the Raman response is due to particle size in the sample, where light scattering is a result of scattering from the edges of the particles. The spectra of glassy $GeSe_2$ are considerably modified by addition of silver. Most of the Raman spectra are weak and occur near 200 cm^{-1}. We made clusters of pure silver and calculated the vibrational frequencies in all cases. Ag_2 oscillates weakly at 185 cm^{-1}. Due to the metallic character, the intensity of Ag_2 is very small. The Ag_3 oscillates at 117 cm^{-1}. The pyramidal Ag_4 has a vibrational frequency of 107 cm^{-1} whereas the square shaped molecule Ag_4 oscillates at 140 cm^{-1}. The ring of Ag_5 oscillates at 141 cm^{-1}. The pyramidal Ag_5 has oscillations near 178 cm^{-1} and Ag_6 ring oscillates near 132 cm^{-1}. The calculated frequencies of the clusters $AgSe_2$, planar-Ag_3Se, Ag_2Ge_2, Ag_2Ge and planar Ag_3Ge are in the neighborhood of those found experimentally. We have determined the bond lengths and angles for the minimum energy configuration in all cases. Our calculated frequencies are usually very near the measured values.

Keywords AgGeSe glass – Raman – ab initio – vibrations

INTRODUCTION

The effect of Ag doping on the properties of glasses is of considerable interest [1-4]. In particular, in some cases, there are two sublattices in such a way that one sublattice remains a solid whereas the other starts melting. In AgI at some high temperature, the I atoms remain stationary whereas Ag atoms start moving. This property is known as "superionic conductivity" because the thermal conductivity becomes very large. It will be of interest to find the effect of doping by superionic atoms such as silver. The glasses are also characterized by their long relaxation times [5] due to self-organization and soft modes in which case the frequency of a phonon goes to zero [6]. There is a phase transition in the rigidity [7] as a function of concentration of one of the atoms. Recently, we have found a method [8-11] to optimize the bond distances and angles for the minimum energy of the Schrödinger equation. We are able to calculate the frequencies of vibrations of clusters of atoms to a very high accuracy. Since these calculated values can be compared with those measured by the Raman spectra for a real glass, we find that our predicted values are very good. In this way, we can identify the clusters actually present in the glass.

In this paper, we report the results of our first principles calculations of the formation of clusters of atoms in a glass, $Ag_xGe_{x-1}Se_{2x+1}$. We have calculated the vibrational frequencies of about 40 clusters of atoms and report here those which are closest to the experimental values obtained from the Raman

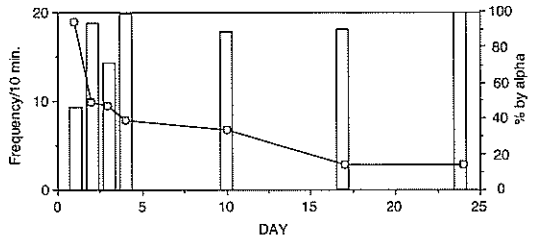

Figure 2. Successive change of frequnecy of aggressive behaviour/10 min (circle, left axis), and proportion of the behaviour performed by alpha workers (bar, right axis) in orphan subcolony A.

aggressions, however, drastically decreased on the 2nd to 4th day, then most aggressions were performed by one worker (Fig. 2). Once the dominance hierarchy was established, mutual aggression between alpha workers and the other workers became rare. The aggressed workers showed a typical subordinate behaviour against the alpha: they crouched and froze in response to the antennation.

In subcolony A, the first egg appeared 18 days after orphaning. Three weeks after orphaning, the alpha worker sometimes showed sexual calling behaviour inside the nest chamber: she bent her abdomen and extruded the sting. When the alpha worker showed such behaviour, we introduced a male produced in a different orphan colony that was collected in the field. The male quickly went to the nest chamber, rushed to the alpha worker and copulated with her (ca. 5 seconds). It repeated such copulation with her three times. He was never interested in the other workers. Insemination of the alpha worker was confirmed by dissection after the observation. Developing ovaries were found in the alpha worker only.

In subcolony B, egg laying by the alpha worker was confirmed on the 21st day after orphaning. The subcolony was merged with the parental colony on 30th day when five eggs were found in the subcolony. The alpha worker of subcolony B was intensively attacked by the resident workers in the parental colony. Subordinate workers of the subcolony were rarely attacked. Dissection after observation indicated that only the alpha worker had developed ovaries.

DISCUSSION

The present result of colony composition indicates that *Pachycondyla leeuwenhoeki* belongs to the AQ+G species [1, 3]. However, the data of colony composition is not enough for illustrating the life history of this species, because it is not common. Speculation of the life history, however, may be possible: single dealate queens start new colony independently, then, gamergate reproduction occurs after the death of the queen or after fission from queenright colonies. In seven of the eight AQ+G species so far reported, there is a rule that queen colonies are monogynous while gamergate colonies are polygynous (reproduction involving multiple gamergates) [6]. The remaining species, *Gnamptogenys striatula*, shows polygyny in both the queen and gamergate colonies [7]. In *P. leeuwenhoeki,* however, both the queen colonies and gamergate colonies are monogynous. One of the reasons why the species shows monogyny with gamergate may be their remarkably small colony size. The AQ+G species *Pachycondyla* (*Mesoponera*) sp. and *P.* (*Bothroponera*) sp., which also show monogyny in gamergate colonies also have small colony size with a handful of workers [4, unpub.]. In such small colony sized species, the presence of excess number of gamergates may result in high cost for colony productivity.

The significance of co-occurrence of queens and gamergates in the same species is still not well understood. In the Indian ponerine ant *Harpegnathos saltator,* it has been proposed that colonial fission by workers is absent because workers retain the very complex underground nests which are valuable for them [8]. Thus, alate queens are necessary for dispersal in this species. In *Gnamptogenys menadensis*, dispersal by alate queens is crucial, because they are arboreal ants [9]. Nests of *P. leeuwenhoeki* are just rotten wood on the forest floor, and it is unlikely that they inherit such fragile nest substrates. In other AQ+G species in the Oriental tropics, most of them nest in dead wood fallen on the ground [unpublished]. Thus, social structure of AQ+G species is not always associated with the existence of very valuable nests. In general, the retention of the dispersal form like alate queens of ants is adaptive even under stable environment [10]. Thus, if colony foundation by single alate queens is possible, alate queens may be produced even in species with gamergates.

In some other *Pachycondyla* species with gamergates – e.g. *P.* (*Bothroponera*) *sublaevis*, *P.* (*Bothroponera*) sp. – a dominance hierarchy based on aggressive dominant-subordinated behaviour is frequently observed among the workers, and

spectra of AgGeSe glass. We also find the vibrational frequencies in the pure Ag metal. The Ag_2 molecule oscillates but the number of these molecules is very small. The Ag_3 is also weak but pyramidal Ag_4 is reasonably strong. We thus report the formation of molecular clusters in a metal. We report a detailed study of vibrations in $AgSe_2$, Ag_3Se, Ag_2Ge_2, Ag_2Ge, Ag_3Ge and Ag_3Ge_3. We find that the vibrational frequencies of these clusters are in the proximity of the experimental values.

SILVER CLUSTERS

The solutions of the Schröedinger equation require the use of trial wave functions. Several different options are available in the computer programme. In the Amsterdam Density Functional (ADF) theory programme, the single zeta (SZ), the double zeta (DZ), the triple zeta (TZ), with and without polarization are available. We make the clusters of atoms by using the density functional theory and optimize the geometry for the minimum energy of the Schrödinger equation. Since Ag is a metal, the molecule formation is very weak. The Ag_2 molecule is found to stabilize at the bond distance of 262.4 pm (picometer) and its oscillation frequency is 185 cm^{-1} in single zeta wave function (SZ) but the intensity is almost zero, so that it will not be observable as a peak in the vibrational spectrum. The same values are obtained when double zeta wave function (DZ) is used. In the case of double zeta wave function with polarization (DZP), the bond length is reduced to 260.5 pm and the oscillation frequency is reduced to 176.8 cm^{-1} but the intensity continued to be zero. The results obtained with triple zeta wave function with polarization (TZP) are similar to those of DZP. The triple zeta with double polarization (TZ2P) gave 256.4 pm for the bond distance and 181.8 cm^{-1} for the oscillation frequency but the intensity is still zero. Similarly, 4 zeta with four polarizations (QZ4P), results are about the same as that of TZP. This type of wave functions has been applied to methane molecule [12] and also to water dimer [13].

In Ag_3 the bond distance of the optimized triangle is 277.1 pm and the vibrational frequency is 117.2 cm^{-1} in the single zeta wave function. These values remain unchanged when double zeta wave function is used. When the double zeta wave function with polarizations is used, the bond length of the triangle is slightly reduced to 276 pm and the frequency also reduces to 111.1 cm^{-1}. When triple zeta wave function is used the bond length is still 276 pm but the frequency is reduced to 110.8 cm^{-1}. Compared with Ag_2, which has almost zero intensity, the Ag_3 is having a strong peak. Hence, Ag_2 is not formed and Ag_3 is the smallest cluster, which vibrates in silver metal.

The clusters of atoms, Ag_4 stabilizes in more than one structure. We make several different models and then select the stable ones for which there exists a minimum in the energy. The minimization is carried out separately for each structure. One of the structures is pyramidal three dimensional object while another is a planar arrangement. Amongst the stable structures, one of them is of pyramidal structure and the other is square shape planar ring. In the case of pyramidal structure bond length is 287.8 pm and the angle is strictly 60 degrees as expected. The vibrational frequency is 107 cm^{-1} when single zeta wave function is used. The double zeta wave function (DZ) gave the same values as those obtained from single zeta (SZ). However, when double zeta wave function with polarization (DZP) is used, the frequency reduced to 100.4 cm^{-1}. The triple zeta with polarization (TZP) gave the same values as DZP. The frequencies as well as the bond lengths in the TZ2P are found to be 273.9 pm and 161.9 cm^{-1}. The QZ4P gave 276 pm and 161.9 cm^{-1} for the pyramidal bond length and the vibrational frequency, respectively. The square shaped Ag4 clusters has a vibrational frequency of 140.7 cm^{-1} and the length of the square is 273.9 pm when single zeta wave function is used. The double zeta wave function gave almost the same values as the single zeta. The cluster Ag_5 forms a ring as well as a pyramid. In the five sided ring, the bond length is 272.3 pm and the vibrational frequency is 140.9 cm^{-1}. The double zeta wave function gave the same value as the single zeta. In the case of double zeta with polarization, the bond length is 271.6 pm whereas the frequency is 131.4 cm^{-1}. The TZP values are 271.7 pm for the five sided bond length and the vibrational frequency is 131.26 cm^{-1}. The TZ2P gave 264.1 pm for the bond length and 147.5 cm^{-1} for the frequency. The QZ4P values are 264.2 pm and 147.3 cm^{-1}, respectively. The clusters Ag_5 in the pyramidal form gave two strong bonds. First a square of four atoms is formed with bond distance 286.6 pm. Then on top one more atom is placed which is at a distance of 276.6 pm from each of the four atoms. The vibrational frequencies are 69.2 cm^{-1} (2 values),

Table 1. The vibrational frequencies of the Ag_5 pyramid by using DZP wave functions and degeneracies.

S. No.	Frequency (cm^{-1})	Intensity km/mol	Degeneracy
1	64.6	0.488	2
2	81.8	2.273	1
3	139.7	0.146	2
4	169.8	1.683	1

87.2 cm^{-1} (one strong value), 146.1 cm^{-1} (2 weak values) and 178.9 cm^{-1} (one strong value). The DZ values are same as those of SZ. The DZP values are 286.7 pm for the square bond length and 274.8 pm for the on top atom. The frequencies, intensities and degeneracies are given in Table 1 along with a serial number (S. No.).

The Ag_6 ring in single zeta wave function has a bond length of 270.8 pm and a strong vibration at 131.9 cm^{-1} with degeneracy 2 and weak lines at 114.1, 165.7, 167.6 and 172.1 cm^{-1}. In the case of DZP, the bond length changed to 270.1 pm which is only a minor change compared with the unpolarized single zeta function. However, in the case of DZP, the vibrational frequencies (intensities) are changed to 103.6 (0.03), 122.5 (2.8), 124.2 (2.77), 154.1 (0.004), 155.8 (0.004), 160.4 (0.007) cm^{-1}(arb. units). It is clear that there is a strong ring oscillation as about 123 cm^{-1}.

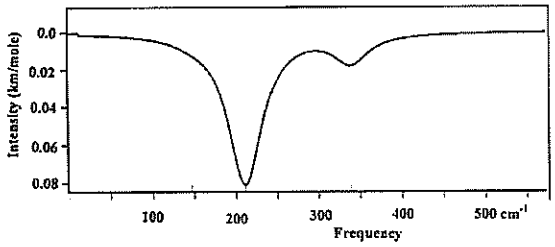

Figure 1. The vibrational spectrum of $AgSe_2$ calculated from first principles showing two strong vibrations.

THE AgSe CLUSTERS

The $AgSe_2$ has Se-Ag bond length 260.3 pm and Se-Se bond length 237.2 pm when single zeta function is used. The frequencies (intensities) are 146.8 (0.16), 2113 (6.31), 238.5 (1.18) cm^{-1} (arb. units). The double zeta wave functions give Se-Ag distance 265.4 pm and Se-Se distance 251.8 pm and frequencies (intensities) 129.4 (1.74), 176.8 (8.05), 266.9 (0.73) cm^{-1}(km/mol). The DZP gave Se-Ag distance 262.2 pm, Se-Se distance 240.5 pm and frequencies (intensities) of 139.7 (1.23), 177.5 (7.9), 292.3 (0.24) cm^{-1}(km/mol). The vibrational spectrum of $AgSe_2$ calculated from the first principles is shown in Figure 1.

The Ag_3Se has a single Se in the centre of a triangle, which is built from three Ag atoms. The Ag-Se bond length is 256.0 (picometer) when single zeta (SZ) is used. In the case of a triangular structure Ag-Se-Ag angle is 120 degrees so that a single distance defines the location of all of the four atoms. In the DZP, the bond length changed to 252.2 pm. The vibrational frequencies (intensities) are given in Table 2.

We show a picture of the charge density in Figure 2.

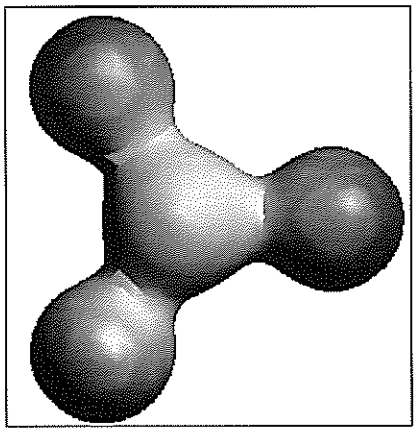

Figure 2. A picture of the charge density of Ag_3Se by using SZ wave functions.

Table 2. The vibrational frequencies and intensities of Ag_3Se in single zeta (SZ) as well as double zeta with polarization (DZP) wave function for Ag_3Se.

S. No.	Frequency cm^{-1} (SZ)	Intensity km/mol	Degeneracy	Frequency cm^{-1} (DZP)	Intensity (DZP)
1	28.63	1.85	2	31.2	1.95
2	51.59	10.14	1	56.5	8.71
3	223.71	0.66	2	217.7	0.16

Journal of Science and Technology in the Tropics (2007) 3: 129-133

(a) The Ag_2Ge_2 has the Ag-Ge distance of 251.5 pm, Ge-Ag-Ge angle of 88 degrees and Ag-Ge-Ag angle of 92 degrees when single zeta wave function is used. The frequencies (intensities) are 184.4 cm^{-1} (4.75) and 201.9 cm^{-1} (7.48) when double zeta wave function is used, the bond length comes out to be 264.0 pm, Ge-Ag-Ge angle 62.5 degrees and Ag-Ge-Ag angle comes out to be 121.3 degrees. The frequencies (intensities) are 107.2 cm^{-1} (0.135), 201.6 cm^{-1} (8.2). The double zeta with polarization gave Ag-Ge bond length of 261.8 pm, Ge-Ag-Ge angle of 61.1 degree and Ag-Ge-Ag angle of 118.9 degrees. The frequencies (intensities) in the double zeta with polarization are 100.37 (0.25) and 196.3 (6.71).

(b) The Ag_2Ge has Ag-Ge distance of 258.5 pm and Ag-Ge-Ag angle 71.7 degrees. The vibrational frequencies with SZ are 67.1 (0.005), 168.3 (0.272) and 215.02 (0.227). The DZ values are Ag-Ge distance 258.3 pm and bond angle 71.6 degrees. The frequencies (intensities) are 67.1 (0.004), 169.05 (0.277) and 215.7 (0.227). The values calculated for DZP wave function are Ag-Ge bond distance 253.4 pm and bond angle Ag-Ge-Ag is 74.5 degrees. The vibrational frequencies and intensities are 58.2 (0.006), 175.15 (0.255) and 215.2 (0.244). The TZP functions gave Ag-Ge bond distance 254.1 pm and bond angle Ag-Ge-Ag of 74.1 degrees. The vibrational frequencies for the TZP are 59.5 (0.004), 172.45 (0.243), 213.1 (0.253), cm^{-1} (km/mol). A charge density plot of Ag_2Ge is shown in Figure 3.

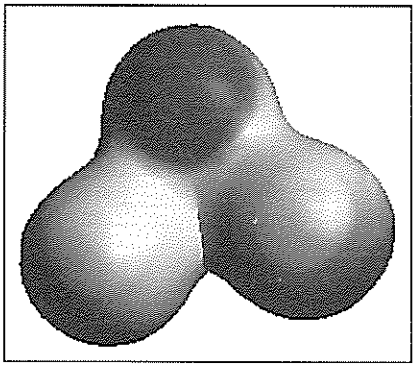

Figure 3. A picture of charge density of Ag_2Ge calculated from single zeta wave functions.

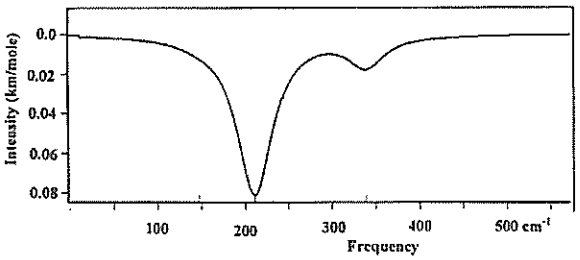

Figure 4. The vibrational spectrum of Ag_3Ge_3 hexagon calculated by using the first principles with SZ wave functions.

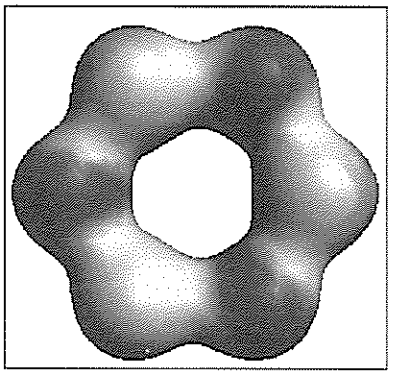

Figure 5. The charge density plot of Ag_3Ge_3 by using SZ wave functions.

(c) The Ag_3Ge with Ag_3 on the corners of a triangle and Ge in the center gives Ge-Ag bond length of 255.2 pm and Ag-Ge-Ag angle of 120 degrees as it should be for the center of an equilateral triangle. The vibrational frequencies (intensities) are 22.6 (1.26) two values, 117.4 (12.9) one value and 227.9 (0.034) two values when DZ is used. For DZP, Ge-Ag bond distance is 251.7 pm and Ag-Ge-Ag angle is 120 degrees as it should be for a triangle. The frequencies (intensities) are 38.8 (0.026) two values, 124.2 (0.000001) one value and 226.2 (2.43) two values, cm^{-1} (km/mole).

(d) The system Ag_3Ge_3 is hexagonal with alternate Ag and Ge atoms with Ge-Ag distance 246.4 pm. The SZ vibrational spectrum is shown in Figure 4.

The calculated frequencies (intensities) are 22.4 (1.125) two values, 101.2 (1.87) one value, 202.62 (7.65) two values, 258.8 (0.07) two values when SZ wave functions are used. When DZ wave function is used the bond length Ge-Ag comes out to be 254.0 pm and the frequencies (intensities) [degeneracies] are, 64.1 (0.037)

[1], 168.5 (5.22) [2], 224.8 (2.51) [2] cm^{-1} (km/mole). The DZP bond length is 250 pm and the frequencies (intensities) [degeneracies] are 61.2 (0.005) [1], 168.6 (4.331) [2], 222.02 (3.045) [2], cm^{-1} (km/mole). The charge density of Ag_3Ge_3 is shown in Figure 5.

COMPARISON OF CALCULATED VALUES WITH EXPERIMENTAL RAMAN SPECTRA

We show in Figure 6 the experimental Raman spectra of glassy $GeSe_2$ and glassy $Ag_4Ge_3Se_9$. The experimental work has been done by Dejus *et al.* [14].

The Ag-$GeSe_2$ has a strong Raman time at 205 cm^{-1} and another at 221 cm^{-1}. There are some weak lines, which are not identified. When silver is added the 221 cm^{-1} goes inside the 200 cm^{-1} line and hence becomes difficult to resolve, but there is a broad line at 200 cm^{-1}. There is a continuum below 100 cm^{-1} and small oscillations are hidden within the noise. In our calculations, it is clear that there is absorption near 215 cm^{-1} in Ag_2Ge (SZ), which is near the experimental value of 221 cm^{-1}. The continuum below 100 cm^{-1} is due to particle size but Ag_2Ge has a mode at 67 cm^{-1}. The Raman spectra require a change in polarizability upon shining by light. This change in polarizability is not associated with all of the vibrations. Therefore, there are more modes in the vibrational spectra than in Raman.

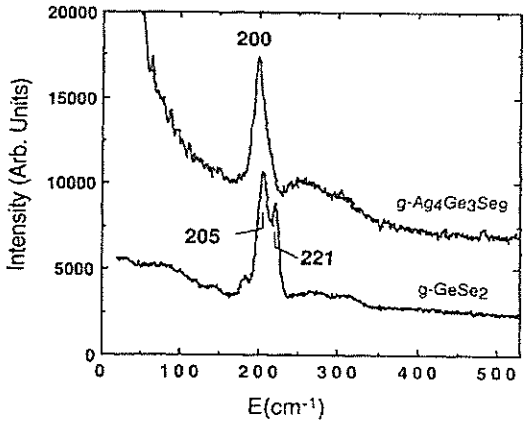

Figure 6. The experimental Raman spectra of glassy GeSe2 and Ag4Ge3Se9.

CONCLUSIONS

We have performed extensive ab initio calculations of clusters of atoms constituting Ag and Ge atoms. The calculated values of the vibrational frequencies show that Ag_2Ge is formed in the glass. The calculations also show that in Ag metal, Ag_3 is the smallest cluster formed which is of the size of 0.277 nm.

Acknowledgments – We are grateful to the Malaysian Academy of Sciences, Scientific Advancement Fund Allocation (SAGA), for financial support. The University of Malaya for kind encouragements and to Dr J. A. Van Gisbergen for kindly providing ADF, which is used in the present study. We also wish to express our gratefulness to Dr. Roger Dejus of the Argonne National Laboratory, Argonne, Il, for his kind permission(email dated June 5, 2007) to use his experimental Raman spectra.

REFERENCES

1. Choi H. and Yu P.Y. (2001) *Phys. Rev. B* **63:** 235210.
2. Rau C., Armand P., Pradel A., Varsamis C.P.E., Kamitsos E.I., Granier D., Ibanez A. and E. Philippot E. (2001) *Phys. Rev. B* **63:** 184204.
3. Carini G., Cutroni M., Fontana A., Mariotto G. and Rocca F. (1984) *Phys. Rev. B* **29:** 3567.
4. Benassi P., Fontana A. and Rodrigues P.A.M. (1991) *Phys. Rev. B* **43:** 1756.
5. Phillips J.C. (1981) *J. Non-Crst. Solids* **43:** 37.
6. Thorpe M.F. (1983) *J. Non-Cryst. Solids* **57:** 355.
7. Wang J.Y., Wells J., Georgiev D.G., Boolchand P., Jackson K. and Micoulat M. (2001) *Phys. Rev. Lett.* **87:** 185503.
8. Devi V.R., Madhavi M.B., Srihari E.L., Shrivastava K.N. and Boolchand P. (2005) *J. Non-Cryst. Solids* **351:** 489.
9. Devi V.R. and Shrivastava K.N. (2004) *Chem. Phys. Lett.* **396:** 238.
10. Kassim H.A., Jalil I.A., Yusof N., Devi V.R. and Shrivastava K.N. (2007) *J. Non-Cryst. Solids* **353:** 111.
11. Kassim H.A., Jalil I.A., Yusof N., Devi V.R. and Shrivastava K.N. (2007) *Phys. Stat. Solid (C)* **4:** 570.
12. Sherrill C.D., Leininger M.L., Van Huis T.J. and Schaefer H.F. (1998) *J. Chem. Phys.* **108:** 1040.
13. Valeev E.F. and Schaefer III, H.F. (1998) *J. Chem. Phys.* **108:** 7197.
14. Dejus R.J., Le Poire D.J., Susman S., Volin K.J. and Price D.L. (1991) *Phys. Rev.* B **44:** 11705.

gamergate is the top-ranked individual [4, 11]. In contrast, such aggressive behaviour was rarely observed in *P. leeuwenhoeki* colonies with reproductive females. It is noteworthy why some species make a dominance hierarchy based on aggressive behaviour while the others do not show such aggression in the presence of reproductive females, even though all three species mentioned above have similar colony size. A knowledge of many other ponerine species with gamergates is needed for the answer. As in other ponerine ants [e.g. 11-13], workers of *P. leeuwenhoeki* showed aggressions in the absence of reproductive females. The frequency of aggressions was drastically decreased in a few days after orphaning, and the alpha worker subsequently laid eggs. Furthermore, virgin workers under gamergate-present condition showed typical policing behaviour: they attacked the workers with developed ovaries. These observations indicate that workers recognized the ovary development of nestmate as shown in the gamergate species *Dinoponera quadriceps* [14], *Gnamptogenys menadensis* [15], and *Diacamma* sp. [16]. The recognition mechanism is another important topic for the study on the biology of this ant species.

Acknowledgements – We thank Sk. Yamane for identification, and T. Matsumoto for kind help on this research. This work was supported by Grants-in-Aid for Scientific Research from Monbshou [No. 08041136 (leader, T. Matsumoto)] and JSPS [A, No. 11691130, and B, No. 14405036 (leader, F. Ito)], a grant for young scientist from JSPS (A. Gotoh), and a grant from University of Malaya FRGS[FP034/2006A] (leader, R. Hashim).

REFERENCES

1. Ito F. and Ohkawara K. (1994) Spermatheca size differentiation between queens and workers in primitive ants: relationship with reproductive structure of colonies. *Naturwissenschaften* **81**: 138-140.
2. Peeters C. (1997) Morphologically "primitive" ants: comparative review of social characters, and the importance of queen-worker dimorphism. *In* Choe J. and Crespi B. (eds) *The Evolution of Social Behavior in Insects and Arachnids,* pp 372-391. Cambridge Univ. Press.
3. Peeters C. and Ito F. (2001) Colony dispersal and the evolution of queen morphology in social Hymenoptera. *Annual Review of Entomology* **46**: 601-630.
4. Ito F. (1993) Functional monogyny and dominance hierarchy in the queenless ponerine ant *Pachycondyla* sp. in West Java, Indonesia. *Ethology* **95**: 126-40.
5. Ito F. (1999) Male behavior and regulation of worker mating in the ponerine ant *Pachycondyla (Bothroponera)* sp. (Hymenoptera : Formicidae). *Journal of Insect Behavior* **12**: 193-198.
6. Monnin T and Peeters C. (2007) How many gamergates is an ant queen worth? *Naturwissenschaften* (in press).
7. Blatrix R. and Jaisson P. (2000) Optimal gamergates in the queenright ponerine ant *Gnamptogenys striatula* Mayr. *Insectes Sociaux* **47**: 193-197.
8. Peeters C. and Hölldobler B. (1995) Reproductive cooperation between queens and their mated workers: the complex life history of an ant with a valuable nest. *Proceedings of the National Academy of Sciences of the United states of America* **92**: 10977-10979.
9. Gobin B., Peeters C. and Billen J. (1998) Colony reproduction and arboreal life in the ponerine ant *Gnamptogenys menadensis* (Hymenoptera: Formicidae). *Netherland Journal of Zoology* **48: 53-63.**
10. Hamilton W.D. and May R.M. (1977) Dispersal in stable habitats. *Nature* **269:** 578-81.
11. Ito F. and Higashi S. (1991) A linear dominance hierarchy regulating reproduction and polyethism in the queenless ponerine ant *Pachycondyla sublaevis*. *Naturwissenschaften* **78**: 80-82.
12. Gobin B, Peeters C. and Billen J. (2001) Dominance interactions regulate worker mating in the polygynous ponerine ant *Gnamptogenys menadensis*. *Ethology* **107**: 495-508.
13. van Walsum E., Gobin B., Ito F. and Billen J. (1998) Worker reproduction in the ponerine ant *Odontomachus simillimus*. *Sociobiology* **32**: 427-440.
14. Monnin T and Peeters C. (1999) Dominance hierarchy and reproductive conflicts among subordinates in a monogynous queenless ant. *Behavioral Ecology* **10**: 323-332.
15. Gobin B., Billen J. and Peeters C. (1999) Policing behaviour towards virgin egg-layers in a polygynous ponerine ant. *Animal Behaviour* **58**: 1117-1122.
16. Tsuji K., Egashira K. and Hölldobler B. (1999). Regulation of worker reproduction by direct physical contacts in the ant *Diacamma* sp. from Japan. *Animal Behavior* **58:** 337-343.

Journal of Science and Technology in the Tropics (2007) **3**: 69-74

Construction of fusion and non-fusion expression plasmids of the complete NS4 gene of the HCV 1b genotype

Xun Meng and Chu Yonglie
Department of Microbiology and Immunology, Xi'an Jiaotong University, 710061 Shaanxi, P.R. China
(Email: sallyxun201@yahoo.com)

Received 03.12.2006; accepted 02.10.2007

Abstract A region encompassing the coding sequences of the nonstructural protein NS4 of the HCV genotype 1b was amplified by nested-PCR from the plasmid pHCV17 which contained a DNA copy of the HCV1b genome. The DNA fragments were cloned into the fusion expression vector pET28a (+) and the non-fusion expression vector pBV220. The recombinant plasmids were transformed into *E. coli* BL21 (DE3) and DH5α strains respectively. The PCR products and the recombinant plasmids were analyzed by DNA sequencing. The results of sequencing confirmed the correct construction of fusion and non-fusion expression plasmids for the complete NS4 gene of HCV 1b. Comparison of the DNA sequence with NCBI database showed significant similarity to a number of other NS4 genes of HCV genotypes. A phylogenetic tree was constructed for the NS4 gene.

Keywords hepatitis C virus (HCV) – nonstructural gene NS4 – Nest-PCR – recombinant fusion plasmid – recombinant non-fusion plasmid

INTRODUCTION

The hepatitis C virus is a single-stranded RNA virus with a genome approximately 9,400 nucleotides in length [1]. The genome consists of a single, large open reading frame (ORF). This ORF encodes a single polyprotein composed of 3000 amino acids (aa) [2-4] that is processed into several polypeptides, including a capsid protein (core), two envelope proteins (El and E2), and nonstructural proteins (NS2, NS3, NS4a, NS4b, NS5a, and NS5b) [5, 6]. The nonstructural NS4 protein plays an important role in the viral life-cycle and in the development of an immune response to HCV. The NS4A protein acts as a cofactor for the NS3 serine protease cleaving the precursor polyprotein into NS3/NS4A, NS4A/NS4B and NS4B/NS5A proteins [7-9]. The functions of NS4B are still unknown; however, it may be important in viral replication and assembly [10, 11]. Information regarding the fine antigenic structure of the native NS4 protein is necessary to improve diagnostic methods, to develop effective anti-HCV reagents and vaccines and to better understand the pathogenetic mechanisms of the liver cell damage. In this paper, we describe the construction of fusion and non-fusion expression plasmids for the complete NS4 gene of HCV 1b. These plasmids will be very useful for future study of the NS4 gene and HCV.

MATERIALS AND METHODS

Strains, plasmids and culture conditions

The bacterial strains and plasmids used in this study are listed in Table 1. *Escherichia coli* strains were grown at 37 °C in Luria-Bertani medium. Antibiotics were added at the following concentrations when required: 100 μg of ampicillin per mL and 50μg of kanamycin per mL.

PCR template

In previous work from this laboratory, a recombinant plasmid was constructed by RT-PCR from a local HCV-infected patient's serum and designated pHCV17. The plasmid of pHCV17 contains the complete genome of the HCV 1b genotype. In this study, pHCV17 was used as the template to amplify the complete NS4 gene.